

ABSTRACT

Title of dissertation: USING THE HIGGS
TO PROBE NATURALNESS

Christopher Bruce Verhaaren,
Doctor of Philosophy, 2016

Dissertation directed by: Zackaria Chacko
Department of Physics

The extreme sensitivity of the mass of the Higgs boson to quantum corrections from high mass states, makes it ‘unnaturally’ light in the standard model. This ‘hierarchy problem’ can be solved by symmetries, which predict new particles related, by the symmetry, to standard model fields. The Large Hadron Collider (LHC) can potentially discover these new particles, thereby finding the solution to the hierarchy problem. However, the dynamics of the Higgs boson is also sensitive to this new physics. We show that in many scenarios the Higgs can be a complementary and powerful probe of the hierarchy problem at the LHC and future colliders.

If the top quark partners carry the color charge of the strong nuclear force, the production of Higgs pairs is affected. This effect is tightly correlated with single Higgs production, implying that only modest enhancements in di-Higgs production occur when the top partners are heavy. However, if the top partners are light, we show that di-Higgs production is a useful complementary probe to single Higgs production. We verify this result in the context of a simplified supersymmetric

model.

If the top partners do not carry color charge, their direct production is greatly reduced. Nevertheless, we show that such scenarios can be revealed through Higgs dynamics. We find that many color neutral frameworks leave observable traces in Higgs couplings, which, in some cases, may be the only way to probe these theories at the LHC. Some realizations of the color neutral framework also lead to exotic decays of the Higgs with displaced vertices. We show that these decays are so striking that the projected sensitivity for these searches, at hadron colliders, is comparable to that of searches for colored top partners. Taken together, these three case studies show the efficacy of the Higgs as a probe of naturalness.

USING THE HIGGS TO PROBE NATURALNESS

by

Christopher Bruce Verhaaren

Dissertation submitted to the Faculty of the Graduate School of the
University of Maryland, College Park in partial fulfillment
of the requirements for the degree of
Doctor of Philosophy
2016

Advisory Committee:
Professor Zackaria Chacko, Chair/Advisor
Professor Kaustubh Agashe
Professor Sarah Eno
Professor Alice Mignerey
Professor Raman Sundrum

© Copyright by
Christopher Bruce Verhaaren
2016

Dedication

To Hilary

Acknowledgments

It is futile to try and include all those who have contributed to the completion of this work, however I will make the attempt. On the academic side, I owe a great debt to my adviser, Zackaria Chacko. He has kept me busy, giving me continual opportunities to learn new skills and explore new ideas. He has shown interest not only for our work together, but also for other aspects of my life.

Other members of the Maryland Center for Fundamental Physics have played similar, though scaled down, roles. In particular Kaustubh Agashe, Raman Sundrum, and Ted Jacobson have done much to shape the way I think about physics. Others, including Keith Dienes, Rabi Mohapatra, Paulo Bedaque, and Sarah Eno have been patient with my questions and supportive of my work. I am also grateful to Tom Cohen for much good advice over the years, and for all the fun I had as his TA in the Manhattan Project class.

Many graduate students and post-docs have had similar influence, including those I have been lucky enough to collaborate with. Their patience with my questions and kind corrections are greatly appreciated. They include, Prateek Agrawal, David Curtin, Anton de la Fuente, Sungwoo Hong, Rashmish Mishra, Simon Riquelme, Prashant Saraswat, Daniel Stolarski, Antony Speranza, Yuhsin Tsai, and Luca Vecchi. Apologies to the many I have left out.

Outside the university, I am continually grateful to my wife Hilary. What she has been able to do with so little for so long is truly amazing. Her support, and correction, has been essential to my reaching this point. I also depend on the

refreshment and love I receive from Jack, Juliet, and Tabitha. Their excitement for life, learning, and for just being with their Dad provides needed relief in difficult times.

My parents have been another constant source of support. Their own experiences of what graduate school is like has given needed empathy and encouragement. The support of Hilary's parents, less familiar with this strange life choice, is made all the more meaningful by their trust that I somewhat know what I'm doing. I hope they turn out to be correct.

Many other friends have made the time sweeter here in Maryland. Thanks to all.

Table of Contents

List of Tables	vii
List of Figures	viii
List of Abbreviations	x
1 Introduction	1
1.1 Naturalness	5
1.1.1 Neutral Naturalness	12
1.2 Using the Higgs to Probe Naturalness	13
2 Higgs Pair Production	16
2.1 Collider Phenomenology	21
2.2 EFT Modifications to di-Higgs Production	24
2.3 Heavy Stop Modifications: Low Energy Theorem	28
2.4 Light Stop Modifications: Full Loop Calculation	31
3 Models of Neutral Naturalness	43
3.1 Mirror Twin Higgs	44
3.2 Folded Supersymmetry	48
3.3 Quirky Little Higgs	51
4 Higgs Couplings Predictions	58
4.1 Mirror Twin Higgs	58
4.2 Folded-SUSY	66
4.2.1 Raising the MSSM Higgs Mass with an Extra $U(1)_X$	67
4.2.2 Higgs Decays to Photons	71
4.3 Quirky Little Higgs	75
5 Exotic Higgs Decays	81
5.1 Mirror Glueballs	86
5.1.1 Spectrum	87
5.1.2 Mirror Gluon Coupling to a SM-like Higgs Boson	94

5.1.3	Mirror Glueball Lifetime	97
5.1.4	Exotic Higgs Decays	98
5.1.5	Estimating 0^{++} production	100
5.2	Sensitivity of Exotic Higgs Decays	104
5.2.1	Geometrical Signal Estimates	105
5.2.2	Estimated Sensitivity of Searches	107
6	Conclusion	122
	Bibliography	126

List of Tables

3.1	Schematic ‘theory space’ of symmetry based solutions to the hierarchy problem.	44
5.1	Extent of detector volumes for geometrical signal estimates, modeled on the ATLAS detector.	107
5.2	Triggers for displaced vertex searches of exotic Higgs decays to mirror glueballs.	110
5.3	Summary of explored displaced vertex searches for exotic Higgs decays to mirror glueballs.	111
5.4	ATLAS detector regions with sensitivity to displaced vertices.	112

List of Figures

1.1	Leading standard model correction to the Higgs self-energy.	7
2.1	Leading gluon fusion to di-Higgs diagrams in the Standard Model. . .	16
2.2	Effective vertices in non-resonant gluon fusion to di-Higgs production.	17
2.3	Di-Higgs production cross section in EFT.	27
2.4	Invariant mass spectrum for di-Higgs events at the LHC14 for bench- mark points.	33
2.5	Percentage corrections to single and double Higgs production at 14 TeV as a function of soft masses.	35
2.6	Percentage corrections to single and double Higgs production at 100 TeV as a function of soft masses.	36
2.7	Percentage corrections to single and double Higgs production at 14 TeV as a function of A -terms.	37
2.8	Percentage corrections to single and double Higgs production at 100 TeV as a function of A -terms.	38
2.9	Percentage corrections to single and double Higgs production at 14 TeV as a function of mixing angle and light stop mass.	39
2.10	Percentage corrections to single and double Higgs production at 100 TeV as a function of mixing angle and light stop mass.	40
3.1	Cancellation of top-loop divergence in the Mirror Twin Higgs model.	48
3.2	Cancellation of top-loop divergence in Folded-SUSY model.	49
3.3	Top-loop divergences in Little Higgs model.	53
3.4	Leading divergent diagram in Little Higgs model.	54
3.5	Cancellation of top-loop divergence in Little Higgs model.	55
4.1	Predicted Higgs couplings in the Mirror Twin Higgs model.	64
4.2	Predicted Higgs to $\gamma\gamma$ decays in Folded-SUSY.	73
4.3	Contribution to the logarithmic divergence in Folded-SUSY from the stop mixing term.	75
4.4	Predicted Higgs coupling deviations in the Quirky Little Higgs model.	78
5.1	Spectrum of glueballs in pure SU(3) theory.	88

5.2	Expected mass of the lightest glueball in Folded-SUSY.	90
5.3	Expected mass of the lightest glueball in Twin Higgs type models. . .	91
5.4	Estimates of the lifetime of the lightest glueball.	99
5.5	Ratio of mirror to SM strong couplings and the Higgs branching ratio into glueballs.	100
5.6	Plot of the parameter encapsulating mirror hadronization, κ	103
5.7	Geometrical signal estimates for the number of Higgs to glueball ($h \rightarrow$ $0^{++}0^{++}$) detection events.	108
5.8	Contours of excludable (or discoverable) values of $\log_{10} \kappa$	114
5.9	Projected sensitivities of the displaced decay searches expressed model- independently as limits on the exotic Higgs decay branching ratio $\text{Br}(h \rightarrow XX)$ as a function of proper lifetime.	115
5.10	Comparison of jet triggers.	118
5.11	Summary of discovery potential from exotic Higgs decays at LHC run 1, LHC14 with 300 fb^{-1} , HL-LHC and 100 TeV.	121

List of Abbreviations

BSM	Beyond the Standard Model
DM	Dark Matter
DV	Displaced Vertex
EFT	Effective Field Theory
eV	electron Volt
keV, MeV, GeV, TeV	kilo-, Mega-, Giga-, Tera-electron Volts
EW	Electroweak
EWSB	Electroweak Symmetry Breaking
FSUSY	Folded Supersymmetry
FTH	Fraternal Twin Higgs
GUT	Grand Unified Theory
H.c.	Hermitian conjugate
HCAL	Hadronic Calorimeter
IT	Inner Tracker
KK	Kaluza-Klein
LEP	Large Electron-Positron
LET	Low Energy Theorem
LHC	Large Hadron Collider
LO	Leading Order
MS	Muon System
MSSM	Minimal Supersymmetric Standard Model
MTH	Mirror Twin Higgs
NGB	Nambu-Goldstone Boson
NLO	Next to Leading Order
NN	Neutral Naturalness
PDF	Parton Distribution Function
pNGB	pseudo-Nambu-Goldstone Boson
QCD	Quantum Chromodynamics
QED	Quantum Electrodynamics
QFT	Quantum Field Theory
QLH	Quirky Little Higgs
RGE	Renormalization Group Equation
SM	Standard Model
SUSY	Supersymmetry
TH	Twin Higgs

Chapter 1: Introduction

We demonstrate understanding of nature’s structure through prediction and verification. Over time, this process is self correcting. Experiment may corroborate an idea, but more precise measurements often reveal deviations from the initial model. Then, the model is refined and must be tested against a new set of predictions, and so it goes.

A useful case study of this process is the sequence of atomic models. With the benefit of hindsight, many past models appear simplistic. But only from our unfair access to more data. We know a model that more perfectly explains phenomena unknown to the past.¹ To learn from the pattern of the past we cannot judge by the data of the present.

That atoms even existed was debated for many years. Dalton’s quantitative theory motivated the utility of atoms in chemistry [2–4], and over time they become widely accepted by chemists. Such physicists as Clausius [5,6], Maxwell [7–10], and Boltzmann [11–13] used the atomic hypothesis of hard spheres obeying Newtonian mechanics to obtain much of thermal physics. However, even these successes were

¹It seems appropriate to include this caution about how we treat the intellectual achievements of others: “It is a rare mind indeed that can render the hitherto non-existent blindingly obvious. The cry ‘I could have thought of that’ is a very popular and misleading one, for the fact is that they didn’t, and a very significant and revealing fact it is too.” [1]

insufficient to convince some skeptics, including Ernst Mach [14, 15] and the future Noble Laureate in chemistry Wilhelm Ostwald [16, 17]. The critics finally relented as recently as 1905 with Einstein's explanation of Brownian motion [18], which relied crucially on physical atoms.²

Before even this vindication of the atomic hypothesis, J.J. Thomson had discovered the electron [20]. These particles were correctly surmised to be a constituent. Consequently, before it could finally take its place as an accepted model, the notion of atoms as unbreakable hard spheres had to be corrected.

Thomson's own atomic model drew upon the known facts about atoms: they contain electrons and are electrically neutral. To balance their negative electric charge, Thompson embedded the point-like electrons in a diffuse, positively charged fluid [21]. This fit the established facts and made new predictions of atomic structure.

Rutherford set out to verify Thomson's model in his famous gold foil experiment, carried out by Geiger and Marsden [22]. By projecting α -particles at a thin gold foil and observing their deflection as they passed through, he hoped to substantiate Thomson's ideas. Instead of only small angle deflections, however, they measured wide angle α -particle scattering that was inconsistent with Thomson's construction [23]. This led to Rutherford's own 'solar system' model of the atom, with a small dense positively charged nucleus at its center and the electrons orbiting about its edge.

Such a configuration, however, is at odds with classical electrodynamics. The

²A discussion as to whether or not Mach ever accepted physical atoms is given in [19].

orbiting, and hence accelerating, electrons should quickly radiate all their energy and collide with the nucleus. Thus, for Rutherford's atom to match experiments probing atomic lengths, unknown dynamics had to be postulated to keep atoms stable.

Niels Bohr made the crucial jump toward understanding atomic physics [24–26]. Using Planck's quantum hypothesis [27] and Einstein's physical photon explanation of the photoelectric effect [28], Bohr supposed that electron orbits might be stable if they could only radiate discrete amounts of energy. This atomic model was simplistic, assuming circular electron orbits, and somewhat ad hoc in its rules. However, these simple rules explained the Balmer series of Hydrogen spectra [29] and correctly predicted the Rydberg constant [30] in terms of atomic parameters.

Bohr's rules were fantastically successful in explaining the spectrum of the Hydrogen atom, but no other. When applied to Helium, or any other atom they disagreed with experiment. More complete formulations of Quantum Mechanics by Heisenberg [31] and Schrödinger [32–35] did much to explain Bohr's rules and led to successful analyses of many other atomic and molecular systems.

However, increasingly sophisticated scrutiny of atomic spectra showed clear deviations from this first quantum mechanical understanding. This led to the inclusion of spin [36] and fully relativistic quantum mechanics [37–39]. Eventually, quantum field theory (QFT), quantum electrodynamics (QED) in particular, was used to explain the small shift in the Hydrogen spectrum discovered by Lamb [40]. In half a century, the interplay between theory and experiment, in modeling and testing, transformed our perception of the atom from a hard sphere to roiling quan-

tum fields.

This review of atomic models should remind ourselves how scientific understanding progresses. The present experimental facts motivate a self-consistent construction to ‘explain’ them. This framework, without fail, makes predictions (not always recognized at the outset) beyond the present data. New experiments are implemented to test the predictions. This examination leads to corrections, whether small or large, to the model and the cycle continues.

Indeed, what we today call the Standard Model of particle physics took decades of back and forth between experiment and modeling. Eventually it was recognized that the weak nuclear force had a vector-like interaction with matter [41, 42]. This indicated that this force could be described by a Yang-Mills [43, 44] gauge theory. However, the limited range of the weak force meant that the mediators of the force had to be massive [45–47], unlike the massless photon of electromagnetism. It was unclear, however, how to incorporate these massive vectors in a self-consistent way.

The crucial step toward overcoming these problems was realizing that the massive vectors we measure at experimental energies need not be fundamentally massive. Initially massless vectors may obtain a mass at low energies when a scalar field develops a vacuum expectation value (VEV) [48–51]. This process does not require that the scalar field be elementary, but this simplest construction makes a good first model of electroweak (EW) interactions [52, 53].

This most basic guess has since taken its place within the Standard Model (SM) of particle physics. In some ways the choice of an elementary Higgs field (the name acquired by this scalar) echoes Bohr’s circular electron orbits. It captures the

essential behavior, and is simple to analyze.

From another view, an elementary Higgs is like Rutherford's orbiting electrons. In that case, the stability of the electron orbits appeared at odds with electrodynamics. Our understanding of classical physics makes such a construction theoretically uncomfortable. Similarly, our understanding of scalar fields in QFT makes us suspicious of a light SM Higgs.

1.1 Naturalness

The paradigm of effective field theory (EFT) is both powerful and perceptive. Effective theories focus on the degrees of freedom relevant to the physical process being considered, freeing the analysis from less important effects. This involves removing particles and interactions that play a subdominant role. Such a modification of the QFT implies there is a scale, often denoted Λ , above which the EFT cannot be trusted to give accurate results. The energy scales above and below Λ are often called ultraviolet (UV) and infrared (IR) in analogy to the electromagnetic spectrum, and a model of high energy physics that reduces to the low energy EFT is called a UV completion.

For instance, in many condensed matter systems the low energy degrees of freedom are insensitive to the details of the molecular lattice they move through. The interactions among these modes are encapsulated by an EFT involving only these low energy states, and exhibit similarities across many distinct lattices. This simpler model makes very successful, and universal, predictions for processes at

energies below the scale of the lattice spacing a , or $\Lambda \sim a^{-1}$. Above Λ the details of the lattice are important, and the EFT should not be used.

Now, suppose there were tiny particle physicists living on one of these lattices. The first experiments such physicists would perform would be at low energy, and therefore insensitive to the details of the lattice. A tiny theorist might construct a model of these interactions, but without knowledge of higher energy, only the EFT would be verifiable. The physicists might suppose the EFT to be fundamental, or they might not. As the experiments pushed to higher energies the deviations from the EFT, those specific to whatever lattice their world consisted of, would begin to appear.

Our Standard Model of particle physics must be an EFT. The SM cannot explain the dark matter (DM) observed gravitationally throughout the universe. The SM cannot explain the asymmetry between baryons and anti-baryons. The SM says nothing about gravitational interactions. There must be more going on, making the SM and EFT below some scale associated with the new particles needed to explain these phenomena. Hopefully, the LHC will continue to reveal the nature of our vacuum, just as the tiny lattice bound physicists strive to determine which lattice they live on.

What does this have to do with the SM Higgs? Scalar masses are generically sensitive to very high scales. The SM Higgs is sensitive to at least the highest scales in the EFT. This can be seen most clearly in the one loop contribution to the Higgs' self energy (see Fig. 1.1), which is quadratically sensitive to Λ .³ This was noticed

³All Feynman diagrams drawn with the FEYMP package [54]

$$h \text{ --- } \lambda_t \text{ --- } \text{loop}(t) \text{ --- } \lambda_t \text{ --- } h \quad \sim \frac{3\lambda_t^2}{8\pi^2} \Lambda^2$$

Figure 1.1: The contribution to the Higgs self-energy due to the top quark. Because of the top’s large coupling to the Higgs, this process is the most sensitive to new physics scales Λ .

explicitly when embedding the SM in grand unified theories (GUTs) [55, 56]. In that case, the Higgs mass was naturally at the GUT scale $\sim 10^{16}$ GeV. Without a mechanism to protect its mass, we also expect Planck scale, $M_{\text{Pl}} \sim 10^{19}$ GeV, effects related to gravity to set the Higgs a mass close to M_{pl} .⁴ This is often referred to as the hierarchy problem.

In 2012 the Higgs boson was discovered at the Large Hadron Collider (LHC) [57, 58]. The mass of the Higgs is about 125 GeV [59], some 17 orders of magnitude below the Planck mass. As pointed out in 1979, the SM can only produce this hierarchy of scales by choosing parameters to cancel, not exactly but precisely to one part in 10^{34} [60]. Such a tuning of parameters is termed ‘unnatural.’

Note that the idea of naturalness is somewhere between a matter of aesthetics and a logical necessity. We cannot simply apply the Sherlockian adage that “When you have excluded the impossible, whatever remains, however improbable, must be the truth” [61–64]. We do not know why nature has the structure it does, many varieties appear possible, but not chosen. This resonates with the response

⁴In this dissertation we use units with c the speed of light and \hbar Planck’s constant divided by 2π equal to unity.

to Sherlock from another English detective about a hundred years later. Speaking of Sherlock’s advice, Dirk Gently declares [65]

“I reject that entirely. The impossible often has a kind of integrity to it that the merely improbable lacks. How often have you been presented with an apparently rational explanation of something that works in all respects other than one, which is that it is hopelessly improbable?...The first idea merely supposes that there is something we don’t know about...[t]he second, however, runs contrary to something...we do know about. We should therefore be very suspicious of it and all its specious rationality.”

The point is that we are exploring the great unknown of nature’s structure. We deem something impossible when it contradicts experimental results, but there are a wide variety of possible extensions of the SM that do not contradict current data. Therefore, we judge by qualities somewhat less ironclad than logical impossibility. If, however, one takes impossibility as the limit of vanishing probability, then the chance of 1 in 10^{34} is close to impossible. Or, to use Dirk’s words, a light SM Higgs is “hopelessly improbable.”

The success of the naturalness principle, as defined by ’t Hooft [66], in former particle physics questions has been outlined in, for instance, [67].⁵ These include some retrodictions related to the mass of the electron [68, 69] and the mass splitting of the charged and neutral pions [70]. However, the mass of the charm quark

⁵’t Hooft’s definition is sometimes called technical naturalness.

was (correctly) predicted [71] by combining naturalness arguments with the GIM mechanism [72].

If the Higgs is not an elementary scalar, but a composite of tightly bound fermions [60, 73, 74], then its mass is generically set by the strength of the binding force. This compositeness scale is the cut off Λ of the SM EFT. Tying the Higgs mass to this new force leads to experimental consequences like seeing other composite states with mass similar to the Higgs. In addition, signals of the Higgs non-point-like structure should become visible in the properties of the weak force carriers. The Large Lepton-Positron (LEP) collider, which discovered these force carriers, also studied them in great detail. Their results indicate that the scale of Higgs compositeness must be significantly larger than the mass of the Higgs.

An elementary Higgs may be naturally light if it is protected by a symmetry. The most studied possibility is supersymmetry (SUSY) [75]. This structure relates bosons and fermions, giving them identical masses. Consequently, scalars in SUSY models can inherit the mass protection enjoyed by chiral fermions. This prevents the Higgs mass from getting large quantum corrections. Effects from the top quark, for instance, are exactly canceled by contributions from the top squarks (or stops), scalar particles related, by SUSY, to the top quark.

There are other symmetries that can keep scalars light. In theory of the strong nuclear force, quantum chromodynamics (QCD), for instance, the pion is a composite particle with mass an order of magnitude below the compositeness scale of about 1 GeV. This is because the pion is a pseudo-Nambu-Goldstone boson (pNGB) of chiral symmetry breaking. In a similar way, the Higgs, as a composite

or as an elementary particle, could be the pNGB of some symmetry, making it a ‘Little Higgs’ [76–79]. The signals of these scenarios are new states related to the SM particles by the protecting symmetry.

Modern composite frameworks take advantage of this pNGB idea; for a review see [80]. There are many symmetries that might keep the Higgs light, and each gives their own particular experimental signature. Unexpectedly, some of these models [81–83] are intimately related, through the AdS/CFT correspondence [84–86], to geometric frameworks [87, 88] that address Higgs naturalness.

Whether the Higgs is elementary or composite, if a symmetry keeps it light, new partner states must appear. Because the top quark gives the largest correction to the Higgs’ mass, the so-called ‘top partners’ should have masses below about 1 TeV in a natural theory. Other SM particles give smaller corrections, so naturalness allows them to be somewhat heavier. This is why searches for top partners is a focus of the LHC program. So far, however, no top partners have been found.

However, there is still room for these top partners, even if they are light. In SUSY for example, the stops could be stealthy and nearly degenerate with the top quark [89–94], or part of a compressed spectrum such that it is heavy but approximately degenerate with the particle it decays to [95–103], though these possibilities are coming under increased scrutiny [94, 96, 101, 104–110]. The stops might decay into other light SUSY particles (like the scalar partner of the tau lepton [111, 112]), or decay via baryon number violating R -parity violation [113–115] where LHC searches are just starting to become sensitive [116–120]. Because top partners can be hidden in various exotic decay modes, complementary indirect searches may play a crucial

role in their discovery.

The most obvious indirect probe is Higgs production through gluon fusion. This loop level process is affected by new colored states that couple to the Higgs. So far, this production mode has seem consistent with the SM [121, 122]. Another indirect search is the production of Higgs boson pairs. The leading production mechanism for these pairs is also sensitive to new colored particles that couple to the Higgs. In addition, the SM di-Higgs rate exhibits a cancellation near threshold, which these new particles can spoil. Therefore, if top partners carry SM color, they may affect the di-Higgs rate more than single Higgs production. This topic is explored in Chapter 2, see also [123]. While the more detailed analysis has been completed for SUSY, the qualitative results apply to generic colored top partners.

As the constraints on colored top partners increase, it may seem that naturalness is not a good guide [124]. However, the lack of colored symmetry partners can also be seen as a clue to nature’s structure. It is something like the ‘curious incident of the dog in the night-time’ [125]. Once, when Sherlock’s case appeared to have no way forward, Holmes seemed confident it was nearly solved. This prompted the following exchange,

“Is there any point to which you would wish to draw my attention?”

“To the curious incident of the dog in the night-time.”

“The dog did nothing in the night-time.”

“That was the curious incident.”

In like manner, a lack colored top partners at the LHC may indicate that the sym-

metry partners are not colored. Because the top quark is colored, it was historically assumed that its symmetry partner would also be colored. However, if the protecting symmetry does not commute with SM color, then the top partners can be color neutral. These scenarios are manifestations of neutral naturalness.

1.1.1 Neutral Naturalness

Neutral naturalness (NN) is the name given to symmetry based solutions to the hierarchy problem whose partner particles do not carry SM color.⁶ The first and prototypical realizations of this framework are the Mirror Twin Higgs (MTH) [129] and Folded SUSY (FSUSY) models [130].⁷

Theories like the MTH [132–136] are completely neutral to all SM gauge forces. This framework has been reduced to the minimally required field content in the Fraternal Twin Higgs (FTH) [137] and generalized systematically in the orbifold Higgs [138, 139]. As they stand these are effective models with a low cutoff, around 5-10 TeV, but many possibilities have been explored to UV complete them. These include supersymmetric [140–142], Randall-Sundrum [143], or composite Higgs [144–146] setups. These UV completions offer new experimental signals [147] as well as possible connections to flavor [148].

Because the SM and Mirror sectors may only connect through the Higgs, many of the experimental constraints on these models are cosmological. These include possible DM candidates [149–153], detectable gravitational waves [154, 155], and

⁶There are also ideas that address Higgs naturalness without compositeness or symmetry [126–128] and N-naturalness.

⁷The related Left-Right Twin Higgs [131] model predicts colored top partners.

connections to the SM neutrino sector [156, 157]. Finite temperature effects [158] and baryogenesis [159] are also being studied.

Other models produce top partners that are color neutral, but carry EW charge. FSUSY, including its deconstructed [160] and generalized [161] versions, is of this type, and so are the Quirky Little Higgs (QLH) [162] and Dark Top [163] models. In the Dark Top a hidden sector color group is broken and the top partner can make up the DM.

NN seems to require that top partners be charged under a hidden sector $SU(3)$ gauge group of similar strength to the SM. Some phenomenological studies have focused on the ‘quirky’ [164–166] nature of the top partners states [167–172]. But other striking signals of these constructions may also occur [173], including exotic Higgs decays to mirror glueballs [174].

Although specific models have not yet been constructed, qualitatively distinct NN models may be possible. Studies have been made of guaranteed signals of these more general possibilities and how to discover them at the LHC or a 100 TeV machine [175, 176]. It seems that almost all symmetry based naturalness can be detected by experiment in one way or another.

1.2 Using the Higgs to Probe Naturalness

The naturalness problem of the SM Higgs has been discussed for decades. However, now that the Higgs has been discovered we have a new angle on naturalness: the Higgs itself. In determining whether the Higgs is composite we now

investigate the Higgs' properties. If the Higgs is protected by a symmetry we know partner particles must couple to it, making the Higgs a guaranteed portal to the partner sector. In short, the Higgs is uniquely suited to assess its own naturalness.

An experimental program to examine the Higgs' properties has begun in earnest at the LHC. Naturalness, however, suggests that these studies may be a window to new particles and interactions. The exquisite sensitivity of its mass makes the Higgs *the* SM particle to point the way to what lies beyond.

This dissertation outlines several ways the Higgs can probe symmetry based solutions to the hierarchy problem. In so doing we follow the Higgs from the cradle to the grave, that is, from production to decay. Higgs production from and decays into SM states are used to test Higgs couplings. Deviations from the SM couplings signal something new, but the evidence is indirect. By exploring how the couplings change for specific extensions of the SM we can see patterns emerge.

Some loop induced production and decay channels are additionally sensitive to new physics. New states, like symmetry partners, can contribute to the process, changing its magnitude and often the differential distribution of its cross-section. As with the tree level Higgs couplings, understanding how these processes change when new particles are added gives particular benchmarks to look for in experiment.

Finally, the Higgs may have 'exotic' decays, meaning decays into particles beyond the SM. In some cases this merely leads to invisible decays, where the new particles are not detected. However, because the Higgs connects the two sectors, it may be that the hidden states can decay back into SM fields on detector length scales. Often these types of decays are suppressed by some large mass scale associated

with the hidden sector, and this can make the life times of the hidden states long. The experimental signal is therefore a displaced vertex, where the displacement is due to the hidden particle traveling some large distance before decaying into SM particles. Such processes do not occur in SM Higgs decays, making these signals loud declarations of new physics.

In Chapter 2 we consider the corrections to Higgs pair production due to colored top partners. This channel is accidentally small in the SM, making it a good place to look for deviations from SM expectations. We show, however, that the di-Higgs rate is closely tied to single Higgs production, making the likely deviations small, unless the top partners are light, making the model more natural. In this case, we show that di-Higgs production can probe top partners that single Higgs production does not see. Chapter 3 introduces case study models for neutral naturalness that span much of the possible phenomenology. Then, in Chapter 4 we determine the modifications of Higgs couplings to SM states in these models. We find that the LHC is not expected to have the necessary precision to probe NN through couplings alone. Next, in Chapter 5 we demonstrate how exotic decays of the Higgs can be used to discover or exclude NN at colliders the LHC and future colliders. This chapter demonstrates the impressive reach of these signatures, comparable to colored top partner searches, due to the displaced decays of hidden glueballs.

Chapter 2: Higgs Pair Production

One of the crucial experimental properties of the Higgs is its production modes and rates. These are intimately related to the tree level and loop level couplings of the Higgs to SM and BSM particles. In this chapter we consider the effects of symmetry partner particles on the production of Higgs boson pairs.

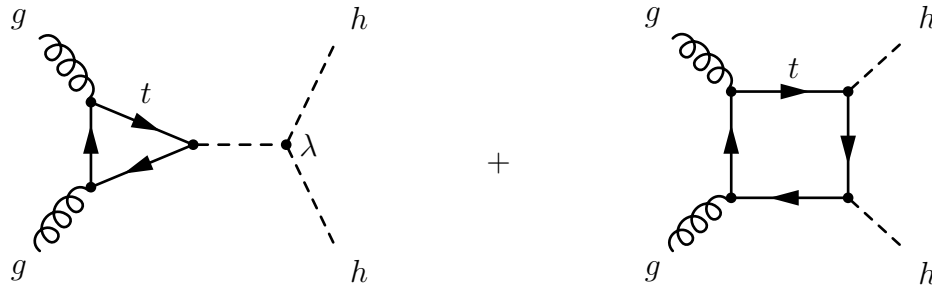


Figure 2.1: Leading gluon to di-Higgs diagrams in the Standard Model.

Like single Higgs production, the dominant di-Higgs production channel at the LHC is gluon fusion, which is depicted in Fig. 2.1. In the SM and its extensions, di-Higgs production probes a different combination of couplings and masses than other loop processes such as single Higgs production via gluon fusion. One could then imagine that, even if for some reason the hGG coupling were SM-like, there could be large deviations in di-Higgs production. This expectation is further motivated by the fact that in the SM the two diagrams of Fig. 2.1 interfere destructively making the SM di-Higgs production cross section smaller than the naive expecta-

tion [177–179].¹ It appears that typical BSM scenarios would spoil this cancellation, significantly modifying the di-Higgs rate. Indeed this is the case for models with modified electroweak sectors or where di-Higgs production is resonantly enhanced through heavy fields that decay to Higgs pairs.

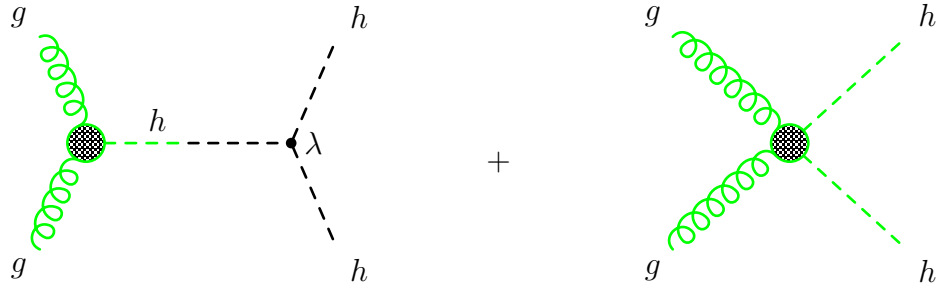


Figure 2.2: Gluon fusion to di-Higgs diagrams with EFT vertices. The green lines indicate the amplitudes focused on in this work. We refer to the diagrams on the left (right) as triangle (box) diagrams because of their topology in the SM.

In this Chapter we instead focus on another potential source of modifications: new colored fields that couple to the Higgs. Such fields are particularly motivated by simple symmetry solutions to the hierarchy problem. The top partners in such scenarios carry color charge and in the most natural realizations are not too heavy. We investigate how much these frameworks may modify di-Higgs production at the LHC and future hadron colliders by their impact on the momentum-dependent hGG and h^2GG vertices (shaded green in Fig. 2.2), while keeping the Higgs quartic coupling λ at its SM value. Throughout we refer to these as ‘non-resonant’ corrections.

As a first step, consider the EFT below some cutoff Λ for the Higgs-gluon couplings hGG and h^2GG . In general, integrating out new heavy $m \sim \Lambda$ colored

¹Throughout this work we refer to the diagrams on the left (right) of Fig. 2.2 as triangle (box) diagrams because of their topology in the SM.

fields that couple to the Higgs generates operators of the form

$$\left(\frac{c_1}{\Lambda^2}|H|^2 + \frac{c_2}{\Lambda^4}|H|^4 + \dots\right) G_{\mu\nu}G^{\mu\nu}, \quad (2.1)$$

where H is the Higgs doublet in the unbroken theory. In the broken theory, we expand the operators to quadratic order in the physical Higgs field h . By including the SM contribution, which we denote $c_{\text{SM}} \simeq \alpha_s/12\pi$, we obtain the effective operators

$$\begin{aligned} & \frac{h}{\sqrt{2}v} \left(c_{\text{SM}} + \frac{2c_1v^2}{\Lambda^2} + \frac{4c_2v^4}{\Lambda^4} + \dots \right) G_{\mu\nu}G^{\mu\nu} \\ & + \frac{h^2}{4v^2} \left(-c_{\text{SM}} + \frac{2c_1v^2}{\Lambda^2} + \frac{12c_2v^4}{\Lambda^4} + \dots \right) G_{\mu\nu}G^{\mu\nu}, \end{aligned} \quad (2.2)$$

where $v = 174$ GeV and the sign flip between single and double Higgs couplings in the SM has been included.

We now introduce a core observation from the first run of the LHC: modifications to the total single Higgs production rate are small. If the only BSM physics is new colored fields coupled to the Higgs, the cross section modifications must be $\lesssim \mathcal{O}(20\%)$ [121, 122], implying modifications to the hGG coupling of $\lesssim \mathcal{O}(10\%)$. A careful study of Eq. (2.2) reveals the implications of this observation for non-resonant di-Higgs production.

For heavy decoupling states, the usual rules of EFT apply. In particular, small corrections to single Higgs production imply $c_1v^2/\Lambda^2 \ll c_{\text{SM}}$ and we can safely ignore the higher order terms. Then, Eq. (2.2) implies that the corrections to the h^2GG coupling are small if corrections to hGG are small, as both are controlled by the same parameter combination $c_1v^2/\Lambda^2 \ll c_{\text{SM}}$. Thus, we expect similar suppression in the non-resonant contributions to both diagrams in Fig. 2.2.

The cancellation that occurs in the SM is due to the non-decoupling nature of the fermions that run in the loop, as their mass increases so does their coupling to the Higgs. Unlike the SM fermions, decoupled non-resonant new physics generically exhibits constructive interference between the triangle and box diagrams. Therefore, non-resonant corrections to di-Higgs production may spoil the SM cancellation, increasing corrections beyond single Higgs production. But, from Eq. (2.2) we see that this happens at order v^4/Λ^4 , so it is a small effect.

Quite generally then, the constraint that the hGG coupling be SM-like implies that models with only colored, non-resonant, BSM states have fairly SM-like di-Higgs rates where the EFT is valid. Clearly, this scenario's best chance for large deviations from the SM di-Higgs rate is that the new particles are somewhat light so that an EFT analysis is inapplicable. In this case models must be checked individually. This chapter explores this possibility in the context of scalar top partners (stops) in a simplified supersymmetric extension of the SM.

Supersymmetry is attractive because it provides a solution to the hierarchy problem, provides simple dark matter candidates, and unifies the gauge couplings. In natural SUSY models one expects stops with masses below the TeV scale. Such stops have been searched for directly at colliders, but these searches depend strongly on the superpartner spectrum and specific decay modes of the stop. The bounds on stops decaying to a top and neutral LSP are approaching the TeV scale when the LSP is light [180–183], and are expected to get stronger with future LHC data [184, 185]. The bounds on very light stops, with masses in the 100 - 200 GeV range are much more difficult to evade. Possibilities do exist, however, many of which are

mentioned in Sec. 1.1. Because stops can be hidden in various exotic decay modes, complementary indirect bounds on top squarks are a crucial tool in the exploration of weak scale SUSY.

Indirect probes of stops include modifications to the W mass [186, 187], corrections to Higgs production rates and branching ratios [188, 189] in loop processes, Higgs kinematic distributions [190, 191] especially at high p_T , effects on Higgs wavefunction renormalization [175, 192], and stop-onium resonances [104, 193–195]. Stronger constraints could be obtained with future colliders [196, 197]. Because these probes of new physics are indirect, if a deviation is found it will be difficult to solve the inverse problem: what is the nature of the new physics that modifies a particular observable? Therefore, it is very important to explore as many different complementary probes as possible.

Higgs pair production has been studied in the Minimal Supersymmetric Standard Model (MSSM) [198, 199], with [200, 201] exploring the effects of scalars in loops. In this chapter we use stops as a concrete and well motivated example to show that small deviations in single Higgs gluon fusion makes it very difficult to generate large enhancements in double Higgs production from non-resonant contributions alone. We show this in the context of EFT, with stops using low energy theorems [202–205] (LETs), and with a full one-loop calculation [200, 201]. Despite these considerations, we do find that current Higgs data allow small, tuned, regions of parameter space with $\mathcal{O}(1)$ deviations in the di-Higgs total cross section.

In the following section, we survey the experimental and phenomenological literature on di-Higgs production at hadron colliders. Despite significant uncertainty,

these motivate sensitivity benchmarks for this study. In Sec. 2.2, we analyze generic (and decoupling) heavy physics contributions to di-Higgs production using EFT, while in Sec. 2.3 we analyze heavy stops in the non-decoupling regime using LETs. Finally in Sec. 2.4 we do the full one-loop calculation necessary for the case of light stops. In this case, we find regions of parameter space where di-Higgs production has potentially observable modifications at the LHC and a 100 TeV machine which are nonetheless consistent with single Higgs production constraints from Run 1.

2.1 Collider Phenomenology

We begin by reviewing the prospects to measure the di-Higgs channel at the LHC and future hadron colliders. Due to its importance in understanding electroweak symmetry breaking, di-Higgs production is a well studied channel. The SM di-Higgs production rate was calculated long ago [206, 207], and at LHC energies the gluon fusion channel (see Fig. 2.1) dominates [208]. This process was computed at leading order (LO) [198, 208] and next-to-leading order (NLO) in the heavy top limit [209], with more recent computations including higher orders in $1/m_t$ [210–212], parton shower effects [213], and virtual corrections [214]. There are also computations of di-Higgs plus one jet [215–217] and vector boson fusion (di-Higgs plus two jets) [218]. Calculations continue to improve, but due to the difficulty of the final state, the uncertainty in projecting the collider reach in this channel is dominated by experimental challenges.

With Run 1 data, ATLAS has released a search for non-resonant di-Higgs

in the $bb\gamma\gamma$ channel [219] setting a limit three orders of magnitude above the SM prediction.² There are also resonant searches in the $4b$ channel from CMS [220, 221] and ATLAS [222, 223], and in the $bb\gamma\gamma$ [224] and the multi-lepton/photon channel [225] from CMS and $bb\tau\tau$ and $\gamma\gamma WW$ from ATLAS [226], all of which have cross section limits that are $\mathcal{O}(\text{pb})$, while the pair production cross section in the SM at 8 TeV is $\mathcal{O}(\text{fb})$. Both ATLAS [227, 228] and CMS [229, 230] have recently released 13 TeV searches, and with the incoming data these are expected to improve. Future projections depend very strongly on estimations of experimental efficiencies and systematics. Preliminary studies for high luminosity LHC at ATLAS [231] and CMS [232] in the $bb\gamma\gamma$ channel and CMS in the $bbWW$ [233] show a marginal sensitivity to observing pair production with $3,000 \text{ fb}^{-1}$ at 14 TeV, but studies are ongoing.

There are phenomenological studies that are more optimistic about the reach, but their sensitivity estimates vary greatly, even among those considering the same channels. For the most studied channel, $bb\gamma\gamma$ [234–239] significance estimates span from about 2σ to 6σ . Other channels, including $bb\tau\tau$ [215, 235, 240], $bbWW$ [215, 235, 241], and $4b$ [215, 242, 243] have similar qualitative variance in the observability of these channels. Therefore, we take uncertainty benchmarks of 30% and 60% for observing deviations from the total SM rate, but ultimately more study will be needed to determine the true sensitivity of future searches.

It is important to note, however, that di-Higgs modifications from stops also

²This search sees a 2.4σ excess, but as we will see below, this excess cannot be explained by new particles running in loops.

lead to a modified spectrum in the di-Higgs invariant mass m_{hh} or p_T . Thus, to obtain the strongest possible limit one would ideally perform an analysis that is sensitive to not only the total cross section but also the spectrum, especially features at higher center of mass energies. Such an analysis would depend heavily on the final state which is being observed. Therefore, instead of a full shape analysis for a specific final state we consider two invariant mass bins to demonstrate the importance of considering the spectrum.

If loops of new particles, such as stops, are responsible for a modification to the di-Higgs total rate, then other di-Higgs production channels will have SM-like rates and can be used to disentangle new physics scenarios. Vector boson fusion is a large component of di-Higgs plus two jets. This channel has been studied [218, 235, 244] but because of the small cross section, it is quite challenging at the LHC. Higgs pair production in association with $\bar{t}t$ is another challenging channel [245, 246], but perhaps a combination of these channels in conjunction with improvements in collider analysis could yield sensitivity in the future. Di-Higgs production has also been explored for BSM physics, both in the context of EFTs [238, 239, 247–250], as well as specific new physics models [179, 198–201, 205, 251–269].

Planning is underway for higher energy hadron colliders where the larger cross section for Higgs pair production may dramatically improve measurement prospects. The details of any putative collider and detector are still largely uncertain, but there have been several phenomenological studies of this process. The $bb\gamma\gamma$ [238, 270], $4W$ [271], and $bb + \text{leptons}$ (and possibly also photon or missing energy) [272] all appear to be promising ways to measure di-Higgs production at a 100 TeV collider.

We also consider modifications to di-Higgs production due to stops for a 100 TeV proton-proton collider, taking precision benchmarks of 10% and 20% on the rate.

Finally, as we have emphasized, it is useful to compare $gg \rightarrow hh$ to $gg \rightarrow h$. The fitted rates for single Higgs production in gluon fusion, normalized to the SM value, are $0.85^{+0.19}_{-0.16}$ at CMS [121] and $1.23^{+0.23}_{-0.20}$ at ATLAS [122], so we take the current bound to be 20%. These bounds will improve in the future, but ultimately will be systematics limited because of uncertainties in the SM prediction as well as experimental complications. With $3,000 \text{ fb}^{-1}$, the expected error on the coupling is 3-5% [273], so we take the ultimate expected error on the rate (twice the error on the coupling) to be 10%.

2.2 EFT Modifications to di-Higgs Production

In this section, we consider the generic effects of new heavy colored particles on di-Higgs production from an EFT perspective. When integrated out, these states will induce the effective operators presented in the introduction in Eq. (2.2). We can then write the relevant couplings contributing to di-Higgs production as

$$\begin{aligned} & \frac{\alpha_s}{12\sqrt{2}\pi v} (1 + \kappa_1^h + \kappa_2^h + \dots) h G_{\mu\nu}^a G^{\mu\nu a} \\ & - \frac{\alpha_s}{48\pi v^2} (1 + \kappa_1^{hh} + \kappa_2^{hh} + \dots) h^2 G_{\mu\nu}^a G^{\mu\nu a} - \frac{m_h^2}{2v} h^3. \end{aligned} \quad (2.3)$$

Here we have defined the relative coupling shifts induced by the higher dimension operators defined in Eq. (2.1),

$$\kappa_1^h = -\kappa_1^{hh} = c_1 \frac{24\pi}{\alpha_s} \frac{v^2}{\Lambda^2}, \quad (2.4)$$

$$\kappa_2^h = -3\kappa_2^{hh} = c_2 \frac{48\pi}{\alpha_s} \frac{v^4}{\Lambda^4}. \quad (2.5)$$

We would like to understand the extent to which these coupling shifts can modify the di-Higgs production rate while being consistent with the observed SM-like single Higgs production.

The total di-Higgs production cross section can be written as

$$\sigma(pp \rightarrow hh) = \int_{\tau_h}^1 d\tau \frac{d\mathcal{L}}{d\tau} \hat{\sigma}(\tau s), \quad (2.6)$$

where the gluon parton luminosity is defined as

$$\frac{d\mathcal{L}}{d\tau} = \int_{\tau}^1 \frac{dx}{x} f_g(x, Q) f_g(\tau/x, Q),$$

and $f_g(x, Q)$ is the gluon parton distribution function (PDF), with factorization scale Q . Throughout this paper we use the MSTW [274–276] PDFs when calculating the hadronic differential cross sections, with renormalization and factorization scales set to the invariant mass of the di-Higgs system. The LO partonic cross section in Eq. (2.6) is given by

$$\hat{\sigma}(\hat{s}) = \frac{\alpha_s^2 \hat{s} \beta_h}{2^{15} 3^2 \pi^3 v^4} |A(\hat{s})|^2, \quad (2.7)$$

with $\beta_h = (1 - 4m_h^2/\hat{s})^{1/2}$. From the couplings in Eq. (2.3), the function $A(\hat{s})$ is given by

$$A(\hat{s}) = \frac{3m_h^2}{\hat{s} - m_h^2} (1 + \kappa_1^h + \kappa_2^h + \dots) - (1 + \kappa_1^{hh} + \kappa_2^{hh} + \dots). \quad (2.8)$$

Consider the case in which the new heavy colored states decouple from the Higgs as their mass is raised. This happens when EWSB gives a subleading contribution to their mass. In this case, there is a separation of scales, $v \ll \Lambda$, and the EFT expansion in Eq. (2.2) is a useful one. The dimension 6 operator dominates over the dimension 8 (and higher) operators, $c_1 v^2 / \Lambda^2 \gg c_2 v^4 / \Lambda^4$ and there is a well-defined relation between the single and double Higgs production rate via gluon fusion in terms of the parameter κ_1^h : $\kappa_1^h = -\kappa_1^{hh}$. In Fig. 2.3 we plot the ratio of the di-Higgs production cross section to the SM prediction as a function of the hGG coupling shift κ_1^h . As the Run 1 Higgs results restricts $|\kappa_1^h| < 10\%$, we observe that an enhancement or suppression of the di-Higgs production rate of order 30% is still allowed by the data within the context of the EFT. In this case, one can easily understand the origin of the enhancement (suppression) when κ_1^h is negative (positive) by examining the interference between the box and triangle diagrams (see Fig. 2.2) via the function $A(\hat{s})$ in Eq. (2.8). For instance, when κ_1^h is negative, the smaller triangle amplitude is suppressed, while $\kappa_1^{hh} = -\kappa_1^h$ is positive and the dominant box amplitude is enhanced. This implies that the interference between the amplitudes is reduced in comparison to the SM and the di-Higgs rate is enhanced.

There are two qualitatively distinct cases to consider. In the first new heavy colored states do not decouple from the Higgs as their mass is raised. This occurs if the new states obtain a substantial portion of their mass from EWSB. In the language of the EFT, each operator in Eq. (2.2) is of similar size and thus the expansion is not useful from a practical point of view. This type of non-decoupling behavior is of course very familiar from the top quark contribution to the hGG and

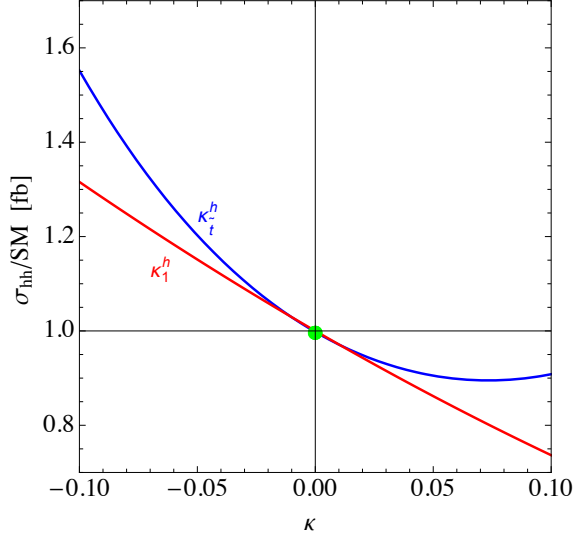


Figure 2.3: Di-Higgs production cross section relative to the SM value as a function of hGG coupling deviation in an EFT dominated by the leading dimension six operator (red, κ_1^h) computed in Sec. 2.2, and for heavy stops using the LET (blue, κ_t^h) computed in Sec. 2.3. The coupling deviation κ is taken in range $[-0.1, 0.1]$ as suggested by the LHC Run 1 Higgs data.

$hhGG$ couplings. In this case it is instead necessary to specify the model for the new heavy colored states and apply the LETs [202–205], as seen for light stops in Sec. 2.3.

Finally, when the new states are light enough neither the EFT nor LET descriptions are valid. In the case of di-Higgs production, this occurs when the masses of the new states in the loop are similar to the characteristic invariant mass of the di-Higgs system under consideration. In this situation it is necessary to specify the model under consideration and compute the full one loop contribution to di-Higgs production. This is carried out for light stops in Sec. 2.4.

2.3 Heavy Stop Modifications: Low Energy Theorem

For the remainder of this chapter we specialize to the case of stops in supersymmetry, which provides a well-motivated, concrete example of new colored particles with significant couplings to the Higgs. As is well known, the MSSM requires two Higgs doublets. However, motivated by the lack of evidence for new scalars and the fact that the Higgs production and decay rates are measured to be near the SM value, we take the 125 GeV Higgs to be the lightest neutral scalar boson and work in the decoupling limit. For the light stops that we consider in this work, we typically cannot obtain the 125 GeV Higgs mass in the MSSM. However, there are many possible scenarios that raise the Higgs mass including, for example, the NMSSM (for a review see [277, 278]) or non-decoupling D -terms [279, 280] an example of which is given in Chap 3. Therefore, we assume the SM Higgs potential, particularly the triple Higgs coupling, to focus on the stop contributions.

We begin by describing our conventions for the stop sector. The stop mass matrix is given by

$$\mathcal{M}_t^2 = \begin{pmatrix} m_{LL}^2 & m_{LR}^2 \\ m_{LR}^2 & m_{RR}^2 \end{pmatrix}, \quad (2.9)$$

where we have defined

$$\begin{aligned} m_{LL}^2 &= m_{Q_3}^2 + y_t^2 v_u^2 + \tilde{\Delta}_Q (v_d^2 - v_u^2), \\ m_{RR}^2 &= m_{U_3}^2 + y_t^2 v_u^2 + \tilde{\Delta}_U (v_d^2 - v_u^2), \\ m_{LR}^2 &= y_t (A_t v_u - \mu v_d) \equiv m_t X_t, \end{aligned} \quad (2.10)$$

with $\tilde{\Delta}_Q = \frac{1}{2}(\frac{1}{2}g^2 - \frac{1}{6}g'^2)$, $\tilde{\Delta}_U = \frac{1}{2}(\frac{2}{3}g'^2)$. We also take $\sqrt{v_u^2 + v_d^2} = v = 174$ GeV and

define $\tan \beta \equiv v_u/v_d$. This matrix can be diagonalized, with eigenvalues m_1 and m_2 satisfying $m_2 > m_1$, by performing a rotation of the basis by the angle θ defined by

$$\cos 2\theta = \frac{m_{LL}^2 - m_{RR}^2}{m_2^2 - m_1^2}, \quad \sin 2\theta = -\frac{2m_t X_t}{m_2^2 - m_1^2}. \quad (2.11)$$

In this section we examine the generic corrections to the di-Higgs production rate in the limit that the stops are heavy in comparison to the typical di-Higgs invariant mass. As alluded to in the previous section, the stops can in general exhibit non-decoupling behavior as their masses are raised if the X_t parameter is also raised in a correlated fashion. This is analogous to the case of the top quark in the SM. Because of this potential non-decoupling behavior, we apply the LET [202–205] to derive the couplings of the Higgs to gluons induced by stops. The starting point is the stop threshold contribution to the running of α_s . After canonical normalization of the gluon field, we obtain the following effective Lagrangian:

$$\mathcal{L} \supset \frac{\alpha_s b_0^c}{16\pi} [\log \det \mathcal{M}_{\tilde{t}}^2] G_{\mu\nu} G^{\mu\nu}, \quad (2.12)$$

where $b_0^c = \frac{1}{6}$ is the QCD beta function coefficient for stops.

Using Eq. (2.12) we determine the couplings of the Higgs h to gluons generated from stops by expanding around v_u and v_d in the Higgs fluctuations. Including the dominant SM top quark contribution, we arrive at the following effective Lagrangian describing the Higgs couplings to gluons:

$$\mathcal{L} = \frac{\alpha_s}{12\sqrt{2}\pi v} (\kappa_t^h + \kappa_{\tilde{t}}^h) h G_{\mu\nu} G^{\mu\nu} - \frac{\alpha_s}{48\pi v^2} (\kappa_t^{hh} + \kappa_{\tilde{t}}^{hh}) h^2 G_{\mu\nu} G^{\mu\nu}. \quad (2.13)$$

The coefficients $\kappa_t^h, \kappa_{\tilde{t}}^h$ ($\kappa_t^{hh}, \kappa_{\tilde{t}}^{hh}$) encode the top quark (stop) contributions to the

hGG and h^2GG couplings. In particular, for the stop contribution we have

$$\begin{aligned}\kappa_t^h &\equiv \frac{v}{8} \left(c_\alpha \frac{\partial}{\partial v_u} - s_\alpha \frac{\partial}{\partial v_d} \right) \log \det \mathcal{M}_t^2, \\ \kappa_t^{hh} &\equiv -\frac{v^2}{8} \left(c_\alpha^2 \frac{\partial^2}{\partial v_u^2} + s_\alpha^2 \frac{\partial^2}{\partial v_d^2} - 2s_\alpha c_\alpha \frac{\partial^2}{\partial v_u \partial v_d} \right) \log \det \mathcal{M}_t^2.\end{aligned}\tag{2.14}$$

Here $c_\alpha = \cos \alpha$ and $s_\alpha = \sin \alpha$ encode the mixing between the light and heavy CP-even Higgs bosons by an angle α . Neglecting the small contributions from D -terms ($g, g' \rightarrow 0$) and taking the decoupling limit ($\alpha \rightarrow \beta - \pi/2$) we obtain

$$\begin{aligned}\kappa_t^h &= \frac{1}{4} \frac{m_t^2 (m_1^2 + m_2^2 - X_t^2)}{m_1^2 m_2^2}, \\ \kappa_t^{hh} &= -\frac{m_t^4}{m_1^2 m_2^2} \left\{ 1 + \frac{(m_1^2 + m_2^2 - X_t^2)}{4m_t^2} - \frac{(m_1^2 + m_2^2 - X_t^2)^2}{2m_1^2 m_2^2} \right\} \\ &= \kappa_t^h (8 \kappa_t^h - 1) - \frac{m_t^4}{m_1^2 m_2^2},\end{aligned}\tag{2.15}$$

where in the final step we have written κ_t^{hh} in terms of κ_t^h . These stop-induced contributions are to be compared to the top quark contributions, which in the decoupling limit are $\kappa_t^h = \kappa_t^{hh} = 1$. Therefore, the parameters κ_t^h and κ_t^{hh} measure the relative coupling shift from the SM values in an analogous way to the EFT coupling shifts defined in the previous section. We see from the last line in Eq. (2.16) that a definite correlation exists between the $hhGG$ and the hGG couplings, and in the limit of heavy stops, $m_{1,2} \gg m_t$, the $hhGG$ coupling shift is fully determined by κ_t^h .

As emphasized above, the Run 1 data probe deviations in the hGG coupling at the 10% level, $|\kappa_t^h| \lesssim 10\%$. We use this constraint to estimate the allowed size of the corrections to the di-Higgs rate from heavy stops by using Eq. (2.16). We find that $\mathcal{O}(50\%)$ corrections are possible when the hGG coupling is smaller than its SM value by about 10%, see Fig. 2.3. The behavior is easily understood by

examining the couplings κ_t^h and κ_t^{hh} and accounting for the interference between the two diagrams depicted in Fig. 2.2. For instance, when κ_t^h is negative the s -channel Higgs exchange amplitude is slightly suppressed compared to its SM value, while the larger-in-magnitude contact diagram is mildly enhanced (since κ_t^{hh} is positive when κ_t^h is negative, assuming the stops are heavy). Therefore, the interference between the diagrams is less effective leading to the enhanced rate in this region, shown in Fig. 2.3.

The figure also shows the importance of the non-decoupling behavior by comparing the EFT and LET calculations. Large A -terms mean the stops can get a large fraction of their mass from EWSB even if they are relatively heavy. This leads to different and potentially larger effects in di-Higgs production. Therefore, if a deviation is observed but no on-shell states are discovered, the size of the deviation could disentangle different types of decoupling vs non-decoupling new physics scenarios.

2.4 Light Stop Modifications: Full Loop Calculation

Finally, we consider the effects of light stops on the di-Higgs rate, which requires a full one loop analysis. To calculate the parton-level single Higgs and di-Higgs production cross sections we implemented the SM+Stops model described above into the FEYNARTS package [281, 282] and employed the FEYNARTS, FORMCALC, and LOOPTOOLS suite of packages [281, 282] to calculate the amplitudes and evaluate loop functions. We used the MSTW [274–276] PDFs when calculating the hadronic

differential cross sections, with renormalization and factorization scales set to the invariant mass of the di-Higgs system. For the spectra in Fig. 2.4 we use constant K-factors to normalize our LO result to the NLO results in [235]. However, to the order we are working in, the K-factors cancel out in all other plots as only ratios of the BSM rate with the SM rate are shown. We have also cross checked our results using the full one-loop MSSM computations of Refs. [200, 201], finding good agreement.³

We begin by examining some benchmark models and their effect on the di-Higgs invariant mass spectra. In the SM, the amplitude for di-Higgs production vanishes at threshold because of a cancellation between the top box diagram and a triangle diagram that utilizes the triple Higgs coupling [177–179], and this is true for any field content as long all masses are acquired via the Higgs vacuum expectation value. Therefore, the invariant mass distribution in the SM is very small near threshold and grows to a peak near $m_{hh} \sim 2m_t$, as we see in Fig. 2.4. Generic new physics that mediates one-loop di-Higgs production will spoil this cancellation, so light colored particles can lead to large deviations near threshold. We demonstrate this for some benchmark cases in Fig. 2.4.

Benchmark A has $m_1 = 325$ GeV, $m_2 = 500$ GeV, $\sin \theta = 0.4$: it has both

³We differ in the writing of the function F_3 defined in equation (B.2) of [201]:

$$\begin{aligned}
F_3(s, t, h_1, h_2, m_{\tilde{q}_i}^2, m_{\tilde{q}_j}^2) = & -s(t + m_{\tilde{q}_i}^2)C_{iii}^{00}(s) + sm_{\tilde{q}_i}^2 C_{jjj}^{00}(s) - tt_1 C_{ijj}^{h_1 0}(t) - tt_2 C_{ijj}^{h_2 0}(t) \\
& + (t^2 - h_1 h_2)C_{iji}^{h_1 h_2}(s) - 2stm_{\tilde{q}_i}^2 D_{jjj}^{h_1 h_2 00}(s, t) \\
& + \left[st^2 - 2t_1 t_2 m_{\tilde{q}_i}^2 + s(m_{\tilde{q}_i}^2 - m_{\tilde{q}_j}^2)^2 \right] D_{ijj}^{h_1 h_2 00}(s, t) \\
& + \frac{s}{2} \left[p_T^2(m_{\tilde{q}_i}^2 + m_{\tilde{q}_j}^2) + (m_{\tilde{q}_i}^2 - m_{\tilde{q}_j}^2)^2 \right] D_{ijj}^{h_1 0 h_2 0}(t, u) + (t \leftrightarrow u). \quad (2.17)
\end{aligned}$$

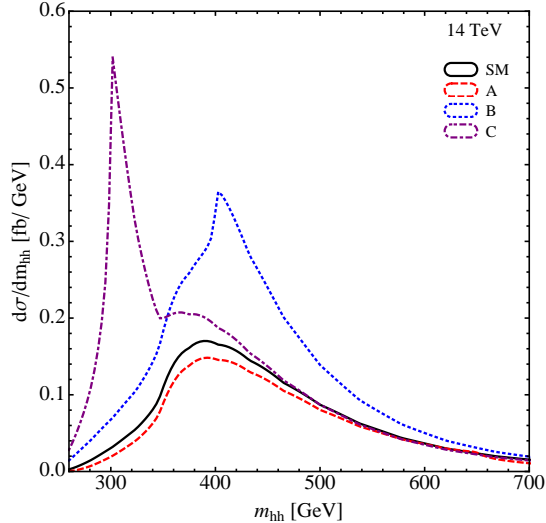


Figure 2.4: Invariant mass spectrum for di-Higgs events at the LHC14. We show spectra for the SM, which peaks at $\sim 2m_t$, and the benchmark points: A) Both stops near the weak scale and current constraints satisfied, $m_1 = 325$ GeV, $m_2 = 500$ GeV, $\sin \theta = 0.4$, B) One stop heavy, current constraints satisfied and a large enhancement of di-Higgs production through tuning of the mixing angle, $m_1 = 200$ GeV, $m_2 = 1000$ GeV, $\sin \theta = 0.223$, C) One stop light and single Higgs production constraints *not* satisfied, $m_1 = 150$ GeV, $m_2 = 1000$ GeV, $\sin \theta = 0$.

stops light but the mixing angle is such that the rate of $gg \rightarrow h$ is only enhanced by $\sim 15\%$ and the $h \rightarrow \gamma\gamma$ rate is within 5% of the SM value. This is a typical case where even having light stops the di-Higgs spectrum looks SM-like, and the total rate is $\sim 86\%$ of the SM; a modification unobservable at the LHC. This also illustrates the effect found in Fig. 2.3 that the sign of the modification in single production is anti-correlated with that of the di-Higgs rate. Benchmark B has one light stop and one heavy stop, $m_1 = 200$ GeV, $m_2 = 1000$ GeV, $\sin \theta = 0.223$, with the mixing angle carefully tuned to give a large enhancement in the di-Higgs rate while still being allowed by single Higgs data. The largest enhancement in the

spectrum occurs around 400 GeV where the lighter stop in the loop can go on-shell. The total di-Higgs rate is enhanced by $\sim 70\%$, the single Higgs rate is reduced by $\sim 20\%$, and the di-photon modification is small.

In benchmark C we show the generic but excluded case with one light stop: $m_1 = 150$ GeV, $m_2 = 1000$ GeV, $\sin\theta = 0$. Here the cancellation in the matrix element at threshold discussed in the introduction is spoiled and there is a large cross section enhancement at low invariant mass. The total cross section is enhanced by $\sim 90\%$, but the single Higgs rate is also enhanced by $\sim 80\%$.

We now discuss the expected modifications to the di-Higgs production rate as a function of more general stop sector parameters. Throughout we consider corrections to single Higgs and di-Higgs production. We will also consider two bins of di-Higgs invariant mass: $260 < m_{hh} < 350$ GeV and $260 < m_{hh} < 2000$ GeV. The first region is motivated because for light stops, the di-Higgs invariant mass spectrum can deviate significantly from the SM prediction for $m_{hh} < 2m_t$, as illustrated in Fig. 2.4. Thus, although the total number of signal events may be smaller, when constraining new non-resonant contributions to di-Higgs production it may help to focus on di-Higgs invariant mass bins close to the threshold for production as this is where corrections are likely to be greatest. We also consider the full invariant mass regime to make contact with previous phenomenological studies.

In this section we consider corrections at 14 TeV and 100 TeV. The total di-Higgs production cross section increases substantially when going from 14 to 100 TeV, which is essentially due to the increased gluon luminosity. This is the main reason that sensitivity to di-Higgs production improves significantly with a 100 TeV

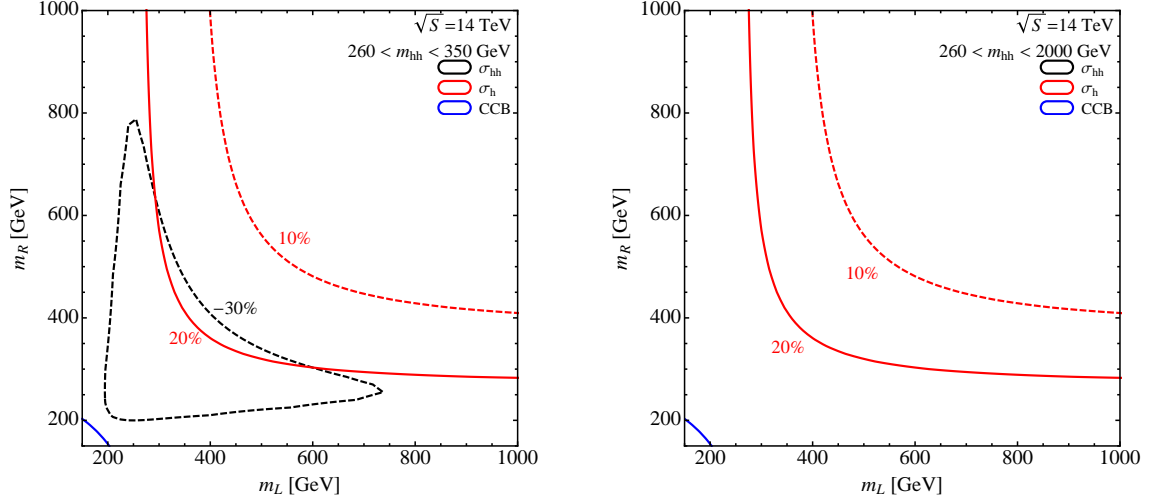


Figure 2.5: Percentage corrections to the single Higgs (red) and di-Higgs (black) production cross sections at $\sqrt{s} = 14$ TeV in a low energy bin with invariant masses $260 < m_{hh} < 350$ GeV (left) and a wide bin with $260 < m_{hh} < 2000$ GeV (right). For the wide energy bin the corrections fall below the benchmark sensitivity for all soft masses shown. Both stop soft masses are varied independently and the A -terms are set to zero. The masses on the axes are the physical masses of the left- and right-handed stops. Small differences between left and right-handed stops due to different D -term couplings can be seen. We also show blue contours of the approximate color-breaking vacuum constraint described in Sec. 2.4.

proton-proton collider when compared to the LHC. However, for light stops the *ratio* of cross section modifications to the SM cross section remains roughly the same for both colliders. The reason for this is that although the total gluon luminosity in both cases is significantly different, the gradient of the gluon luminosity with respect to parton center of mass energy is not significantly different in the region of interest for di-Higgs production. Thus, when integrating over the PDFs the increased gluon luminosity is roughly a constant factor, especially in the low invariant mass bin. Therefore, when the ratio of total cross section with stops to the total SM cross section is taken this factor essentially drops out. Therefore, the fractional corrections

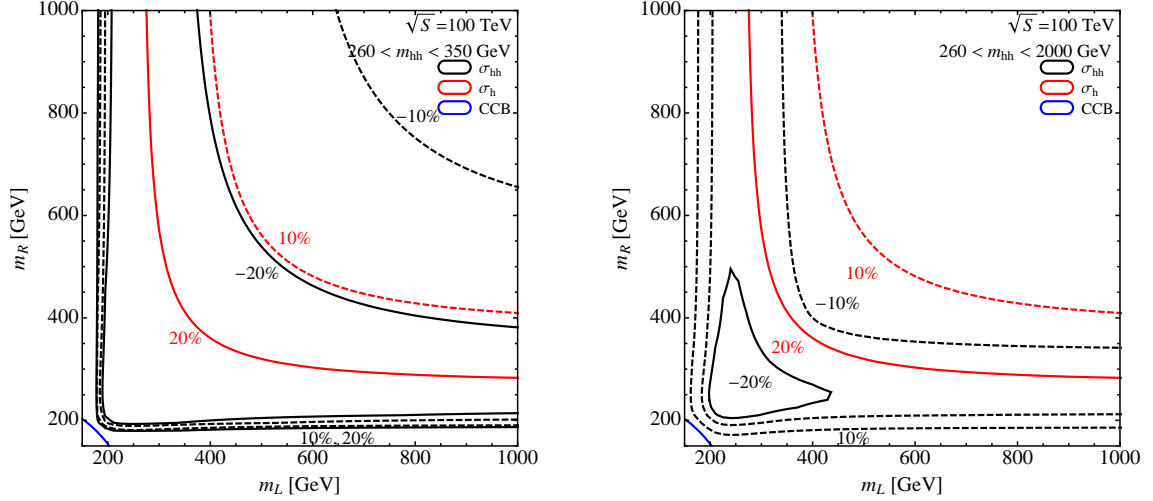


Figure 2.6: Same as Fig. 2.5 but for $\sqrt{S} = 100$ TeV.

are very similar at 14 and 100 TeV. This does not persist when the stops are heavy and features in the invariant mass distribution appear at large m_{hh} where the gluon luminosity between 14 and 100 TeV is significantly different. In this case, however, the corrections are typically smaller than the expected sensitivity. Thus, for the fractional corrections to the total cross section the 14 TeV results are also roughly illustrative of the 100 TeV result, although the expected sensitivity is increased at higher center of mass energy, so it should be kept in mind that contours of different di-Higgs cross section are appropriate in this case.

In general the stop parameter space can be described by three physical parameters, such as the two stop mass eigenvalues m_1, m_2 , and the mixing angle, or alternatively the two soft masses \tilde{m}_L, \tilde{m}_R and the mixing parameter X_t . To plot the corrections a projection down to a two-dimensional subspace is necessary. Results for a variety of projections for the full loop calculation are shown in Figs. 2.5 through 2.10. In Figs. 2.5 and 2.6 the stop mixing X_t -terms are set to zero and only

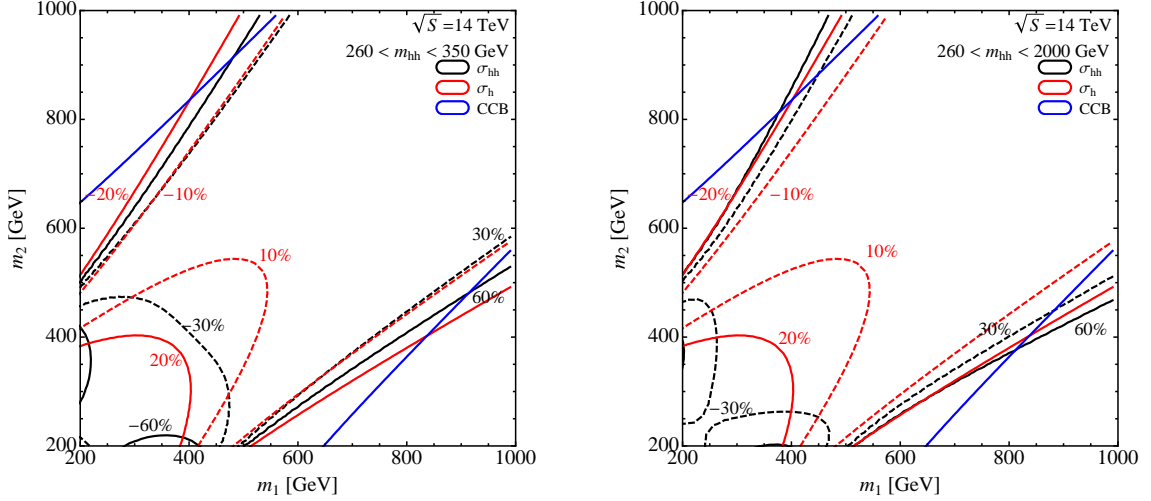


Figure 2.7: As in Fig. 2.5 with the exception that both stop soft masses are set equal and the A -terms are varied. In both cases regions which lead to a $\sim -20\%$ change in the single production rate typically imply a $\sim 30\%$ change in the pair production rate. The approximate color breaking vacuum constraint shown in blue is relevant for large mass splittings due to the large X_t -terms.

the physical mass eigenvalues are varied. In Figs. 2.7 and 2.8 the two soft masses are set equal, $\tilde{m}_L = \tilde{m}_R$, and varied and the X_t -term is also varied. The results are shown in the basis of physical masses. In Figs. 2.9 and 2.10 we fix the mass eigenvalue of the heavy stop to a benchmark value and then vary the light stop mass and the stop mixing angle.

In all figures a consistent picture emerges. Usually, cases with observable deviations in the di-Higgs production rate also have observable deviations in the single Higgs production rate. Furthermore, in the ‘blind spot’ region where the single Higgs corrections are small the di-Higgs corrections are also typically suppressed unless both stops are quite light, consistent with our EFT analysis. Thus, when indirectly constraining light stops, where the EFT expectation does not apply, which

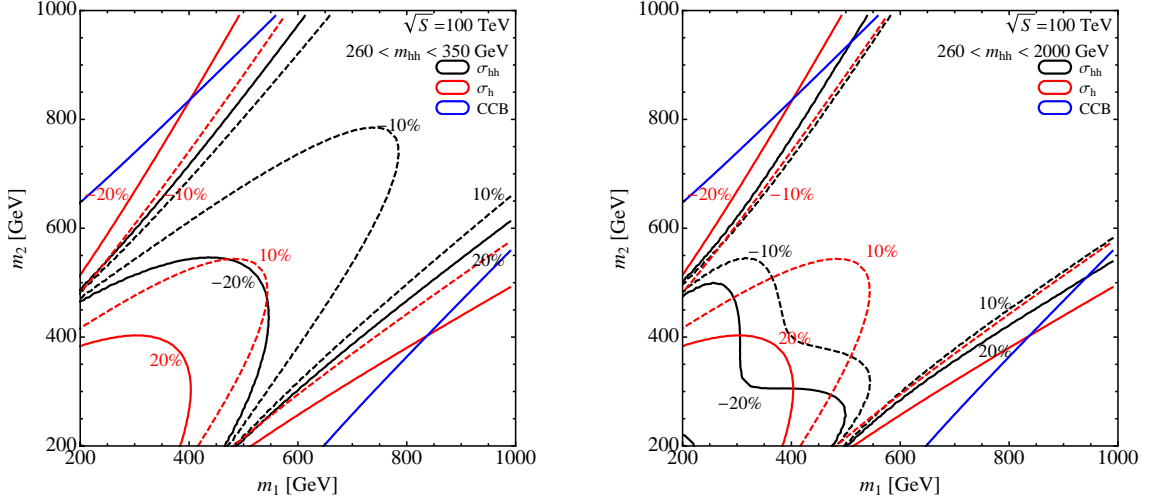


Figure 2.8: Same as Fig. 2.7 but for $\sqrt{S} = 100$ TeV.

may have evaded direct detection at the LHC, the single Higgs production and di-Higgs production processes are highly complementary. The strongest indirect constraints, especially for light stops, would arise from the combination of the two. Furthermore, Figs. 2.5 through 2.10 suggest that tuned regions of parameter space may remain after LHC8 in which observable non-resonant stop contributions to di-Higgs deviations may still arise at LHC14.

It is also interesting that, as advertised previously, in Figs. 2.7 through Fig. 2.10 it is clear that deviations relative to the SM may be significantly larger in low invariant mass bins than they are for the total cross section. However, due to the smaller signal rate, the statistics will be lower in the low mass bin than for the total cross section. Thus, in a collider analysis aimed at indirectly constraining stop squarks it may be necessary to study a number of invariant mass cuts to determine the optimal constraint.

Finally, in Figs. 2.9 and 2.10 it is clear that if both stops are light the stan-

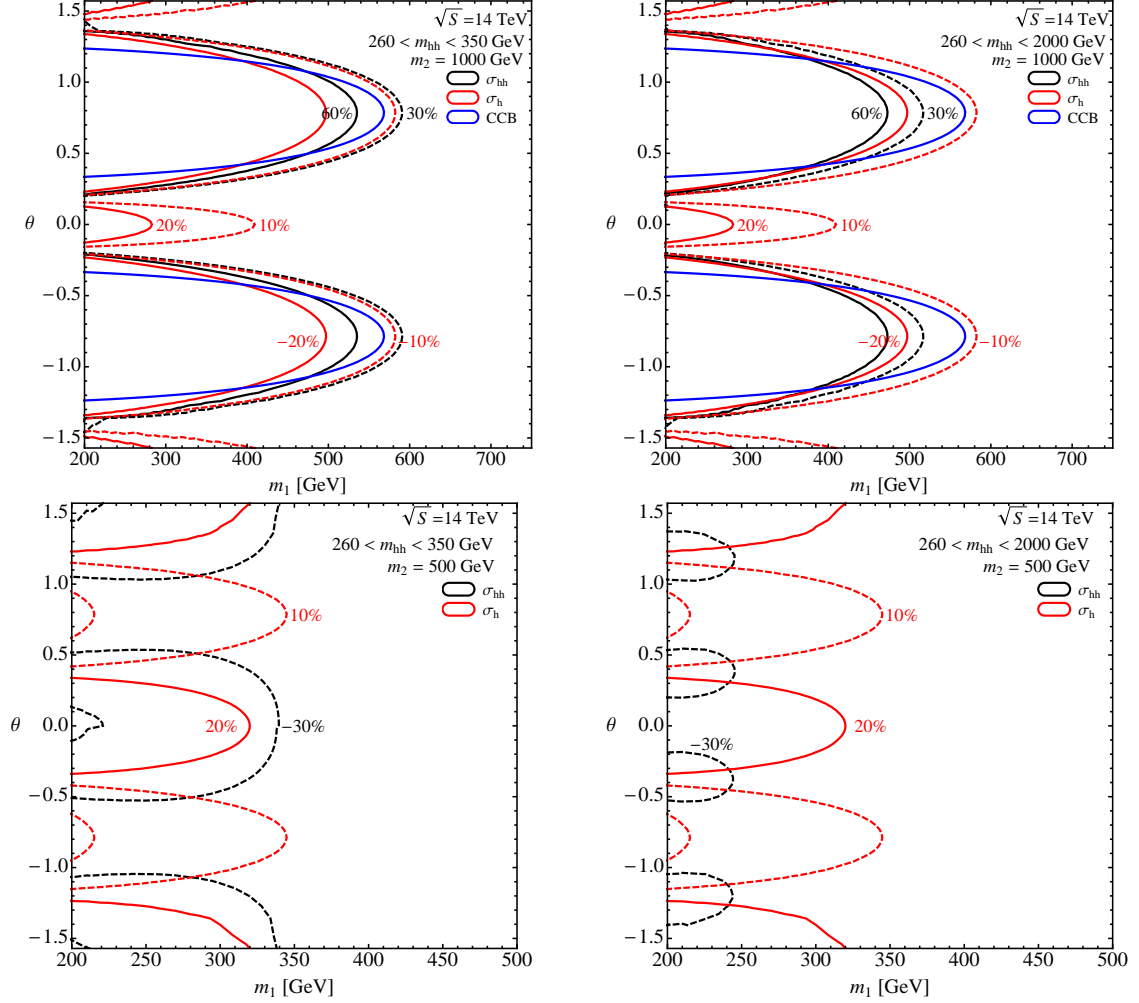


Figure 2.9: As in Fig. 2.5 with the exception that the heavy stop mass is fixed at 1000 GeV (upper panels) and 500 GeV (lower panels) and the light stop mass and mixing angle are varied.

standard ‘blind spot’ in stop contributions to single Higgs productions may be closed by constraining di-Higgs production. This is consistent with our EFT discussion, as even when the stop loop contributions to the hGG coupling have been tuned to precisely zero there will remain contributions to the h^2GG coupling coming from a dimension-8 operator. Therefore, the h^2GG coupling in the blind spot will typically be $\mathcal{O}(m_t^4/m_1^2 m_2^2)$. Hence, if we face the unfortunate situation that both stops

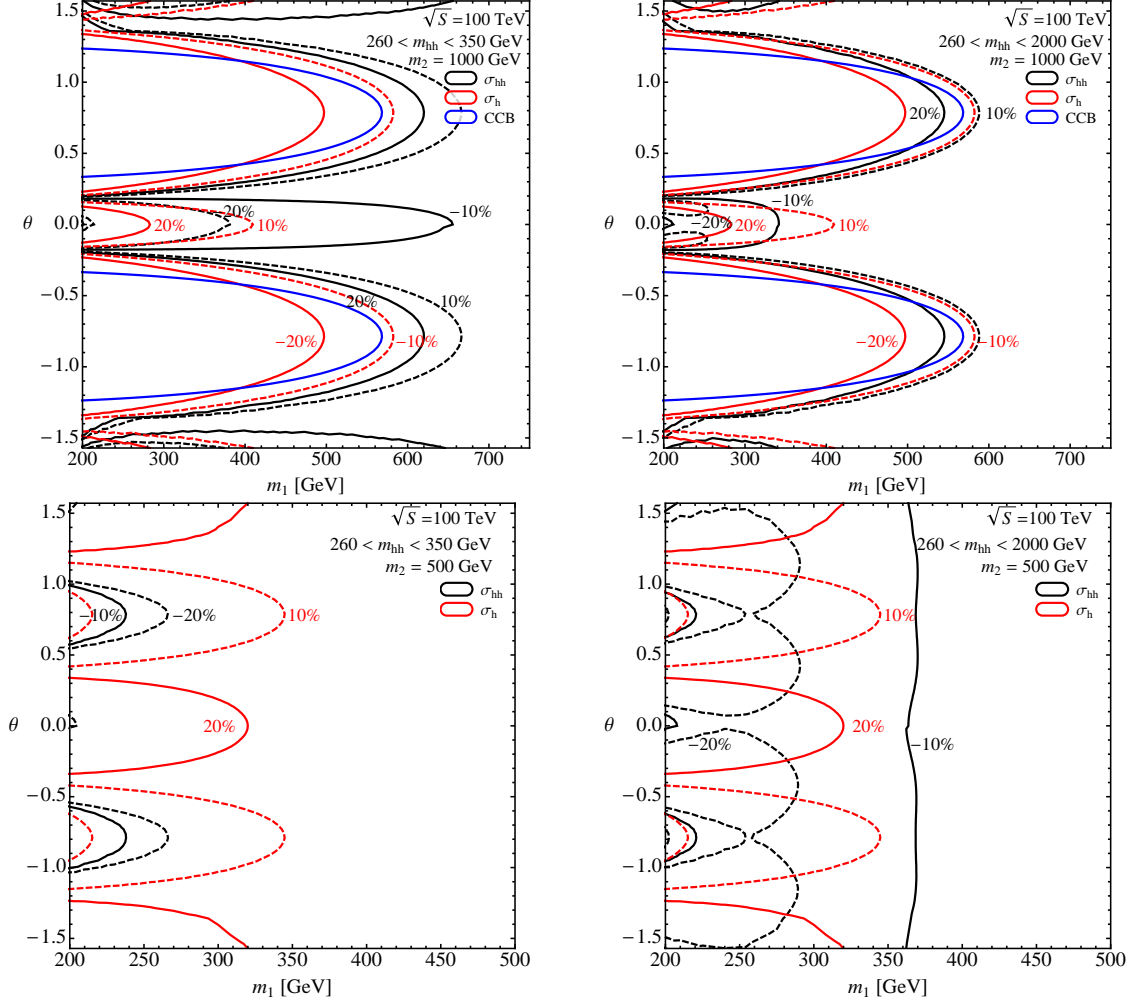


Figure 2.10: Same as Fig. 2.9 but for $\sqrt{S} = 100$ TeV.

are light and hGG deviations are absent due to a pernicious cancellation between stop loop contributions to the hGG coupling, it may still be possible to indirectly constrain this scenario through di-Higgs production measurements at the LHC.

Additional Indirect Constraints

There are other indirect constraints on stops. We briefly comment on how they compare to the constraints and predictions considered previously. The most relevant of these constraints comes from very large A -terms. These can generate

charge- or color-breaking vacua in the scalar potential that are deeper than the EW vacuum [283–293]. One can approximate the maximum allowed A -term by considering a D -flat direction in field space where $\langle H_u \rangle = \langle \tilde{t}_L \rangle = \langle \tilde{t}_R \rangle$, and requiring that all minima in that direction have positive vacuum energy. This leads to the condition [283–287]

$$A_t^2 < 3 (m_{H_u}^2 + |\mu|^2 + m_{Q_3}^2 + m_{U_3}^2) . \quad (2.18)$$

In the decoupling limit, $m_{H_u}^2 + |\mu|^2 = -m_h^2/2$ where m_h is the physical Higgs mass. We can take the small μ or large $\tan \beta$ limit which sets $A_t = X_t$. This allows us to plot the bound from Eq. (2.18) in Figs. 2.5 through 2.10.

We stress that Eq. (2.18) is a very crude approximation for the stability bound on the A -terms. In order to accurately compute the bound, one must take into account loop contributions [294,295], tunneling effects [296–298], and properly account for cosmological history [299]. There now exist sophisticated computer codes [300] which can compute bounds in various different supersymmetric models [301–303]. Other groups have recently considered the effect of the 125 GeV Higgs on these bounds [304–307]. A full computation of the vacuum stability of our scenario is beyond the scope of this work, so we use Eq. (2.18) to give a rough sense of where those bounds would lie.

Precision EW observables can also be used as constraints [308]. One particularly important example is the ρ -parameter, which measures the splitting of electroweak multiplets. This constraint depends sensitively on the mass of the right handed sbottom as well as the mixing in the sbottom sector, and because of this

additional model dependence we do not show the constraint on our figures. We find that generically the ρ -parameter gives weaker constraints than vacuum stability.

In this chapter we have explored the impact of new colored states coupled to the Higgs particle on the production of Higgs boson pairs. Such states are motivated by naturalness, with prime examples being top-partners. Therefore, di-Higgs production is a one way to use the Higgs to explore naturalness.

This class of non-resonant new physics can in principle lead to significant modifications to di-Higgs production. In most cases, however, the current experimental constraints on single Higgs production in the gluon fusion channel limit the extent to which the di-Higgs rate can deviate from the SM prediction. This can easily be seen in the case of heavy new colored states from an EFT analysis. The case of new light colored states requires a more detailed specification of the model and a full one loop calculation of the di-Higgs rate. We have performed such an analysis for the case of stops in supersymmetry, finding that modifications are typically small, but that tuned regions with $\mathcal{O}(1)$ enhancements to the cross sections exist.

This result demonstrates that future di-Higgs measurements could be used to place indirect constraints on the presence of light stops if they have somehow otherwise evaded detection at the LHC. However, these modifications are likely to be modest given the present constraints on single Higgs production. Thus, if large modifications in the di-Higgs production rate were observed this work would suggest that they are more likely to come from resonant new physics, or modifications of the weak sector and/or Higgs self-coupling, rather than from non-resonant contributions from new colored fields coupled to the Higgs.

Chapter 3: Models of Neutral Naturalness

In this chapter we introduce three specific constructions that span much of the NN model-space: Mirror Twin Higgs [129], Folded-SUSY [130], and Quirky Little Higgs [162]. The fact that they are motivated by naturalness means that the top partners are expected to be close to the EW scale, \lesssim TeV. However, because they are color neutral, the production rates are small at the LHC. This makes the Higgs among the strongest probes of these scenarios. However, the details vary from cases to case as we see below and explore in the following chapters.

The sense in which the models we focus on span the NN ‘theory space’ is shown Table 3.1. The top partners in symmetry based solutions to the hierarchy problem are separated by their spin and the charges they share with the SM.¹ The most familiar models, like SUSY or pNGB models, predict top partners that carry all SM charges. However, NN models may have only EW charges or none at all. The models we outline in this chapter span the different spin choices of EW charged top partners. In addition, we outline the Twin Higgs model, but cannot describe a completely neutral framework with scalar top partners as none have yet been discovered. As mentioned in the introduction, the Higgs portal may be the only

¹There also exist spin 1 top partner models [309, 310].

	Scalar	Fermion
QCD & EW	SUSY	pNGB Higgs / RS
EW	Folded-SUSY	Quirky Little Higgs
None	???	Twin Higgs

Table 3.1: Schematic ‘theory space’ of symmetry based solutions to the hierarchy problem. The top partner’s representation under the Lorentz Group vary by column while the charges it shares with the SM vary with row.

robust probe of such a model. However, there may be some other requirement of the construction that provides additional avenues for discovery.

3.1 Mirror Twin Higgs

The MTH model assumes a mirror copy of the complete SM, called the twin sector, along with a Z_2 symmetry that exchanges each SM particle with the corresponding twin. In addition, the Higgs sector of the theory is assumed to respect an approximate global symmetry, which may be taken to be either $SU(4)\times U(1)$ or $O(8)$. This global symmetry is not exact, being explicitly violated by the SM Yukawa couplings, and the SM EW gauge interactions. In particular, a subgroup of this global symmetry is gauged, and contains the $SU(2)\times U(1)$ electroweak interactions of the SM, and of the twin sector. The SM Higgs doublet emerges as a light pNGB when the global symmetry is spontaneously broken. Even though the gauge and Yukawa interactions explicitly violate the global symmetry, the discrete Z_2 symmetry ensures the quadratically divergent contributions to the Higgs mass cancel at one-loop order.

The next step is to understand the cancellation of the quadratic divergences in this model. We first consider the case where the breaking of the global symmetry, which for concreteness we take to be $SU(4) \times U(1)$, is realized by a weakly coupled Higgs sector. The $SU(2) \times SU(2) \times U(1)$ subgroup of $SU(4)$ and the additional $U(1)$ are gauged giving rise to the electroweak interactions in the SM and twin sectors. We use the labels A and B to denote the SM and twin sectors respectively. Then, under the action of the discrete Z_2 symmetry, the labels A and B are interchanged, $A \leftrightarrow B$. In this notation, H_A represents the SM Higgs doublet and H_B the twin doublet. The field H , defined as

$$H = \begin{pmatrix} H_A \\ H_B \end{pmatrix}, \quad (3.1)$$

is chosen to transform as the fundamental representation under the global $SU(4)$ symmetry. The $SU(4)$ invariant potential for H takes the form

$$m^2 H^\dagger H + \lambda (H^\dagger H)^2. \quad (3.2)$$

If the parameter m^2 is negative, the $SU(4) \times U(1)$ symmetry is spontaneously broken to $SU(3) \times U(1)$ and there are 7 massless NGBs in the spectrum. Depending on the alignment of the VEV, several of these NGBs will be eaten. If, however, the VEV of H lies along H_B , the SM Higgs doublet H_A will remain massless.

The gauge and Yukawa interactions give rise to radiative corrections that violate the global symmetry and generate a mass for H_A . We focus on the top Yukawa coupling, which takes the form

$$\lambda_A H_A q_A t_A + \lambda_B H_B q_B t_B. \quad (3.3)$$

These interactions generate quadratically divergent corrections to the Higgs potential at one loop order. The corrections take the form

$$\Delta V = \frac{3}{8\pi^2} \Lambda^2 \left(\lambda_A^2 H_A^\dagger H_A + \lambda_B^2 H_B^\dagger H_B \right), \quad (3.4)$$

where Λ is the UV cutoff. The Z_2 symmetry, however, ensures $\lambda_A = \lambda_B \equiv \lambda$ so that

$$\Delta V = \frac{3\lambda^2}{8\pi^2} \Lambda^2 \left(H_A^\dagger H_A + H_B^\dagger H_B \right) = \frac{3\lambda^2}{8\pi^2} \Lambda^2 H^\dagger H. \quad (3.5)$$

Thus, this contribution respects the global symmetry and cannot contribute to the mass of the NGBs. The leading contributions to the SM Higgs potential therefore arise from terms which are only logarithmically divergent. Consequently, there are no quadratically divergent contributions to the Higgs mass at one loop order.

The discussion so far has been restricted to the case when the breaking of the global symmetry is realized by a weakly coupled Higgs sector. However, the cancellation is independent of the specifics of the UV completion and depends only on the symmetry breaking pattern. To see this we consider the low energy EFT for the light degrees of freedom, in which the symmetry is realized nonlinearly. We parametrize the pNGB degrees of freedom in terms of fields $\Pi^a(x)$ that transform nonlinearly under the broken symmetry. For the purpose of writing interactions, it is convenient to define an object H which transforms linearly under $SU(4) \times U(1)$,

$$H = \begin{pmatrix} H_A \\ H_B \end{pmatrix} = \exp\left(\frac{i}{f}\Pi\right) \begin{pmatrix} 0 \\ 0 \\ 0 \\ f \end{pmatrix}. \quad (3.6)$$

Here f is the symmetry breaking VEV, and Π is given, in unitary gauge where all the B sector NGBs have been eaten by the corresponding vector bosons, by

$$\Pi = \left(\begin{array}{ccc|c} 0 & 0 & 0 & h_1 \\ 0 & 0 & 0 & h_2 \\ 0 & 0 & 0 & 0 \\ \hline h_1^* & h_2^* & 0 & 0 \end{array} \right). \quad (3.7)$$

The discrete Z_2 symmetry continues to interchange H_A and H_B . Expanding the exponential we obtain

$$H = \begin{pmatrix} \mathbf{h} \frac{if}{\sqrt{\mathbf{h}^\dagger \mathbf{h}}} \sin\left(\frac{\sqrt{\mathbf{h}^\dagger \mathbf{h}}}{f}\right) \\ 0 \\ f \cos\left(\frac{\sqrt{\mathbf{h}^\dagger \mathbf{h}}}{f}\right) \end{pmatrix} \quad (3.8)$$

where $\mathbf{h} = (h_1, h_2)^\text{T}$ is the Higgs doublet of the SM

$$H_A = \mathbf{h} \frac{if}{\sqrt{\mathbf{h}^\dagger \mathbf{h}}} \sin\left(\frac{\sqrt{\mathbf{h}^\dagger \mathbf{h}}}{f}\right) = i\mathbf{h} + \dots, \quad (3.9)$$

$$H_B = \begin{pmatrix} 0 \\ f \cos\left(\frac{\sqrt{\mathbf{h}^\dagger \mathbf{h}}}{f}\right) \end{pmatrix} = \begin{pmatrix} 0 \\ f - \frac{1}{2f} \mathbf{h}^\dagger \mathbf{h} + \dots \end{pmatrix}. \quad (3.10)$$

Now consider again the Z_2 symmetric top quark sector, Eq. (3.3). To quadratic order in \mathbf{h} this takes the form

$$i\lambda_t \mathbf{h} q_A t_A + \lambda_t \left(f - \frac{1}{2f} \mathbf{h}^\dagger \mathbf{h} \right) q_B t_B. \quad (3.11)$$

From this Lagrangian, we can evaluate the radiative contributions to the Higgs mass parameter. The contributing diagrams are shown in Fig. 3.1.

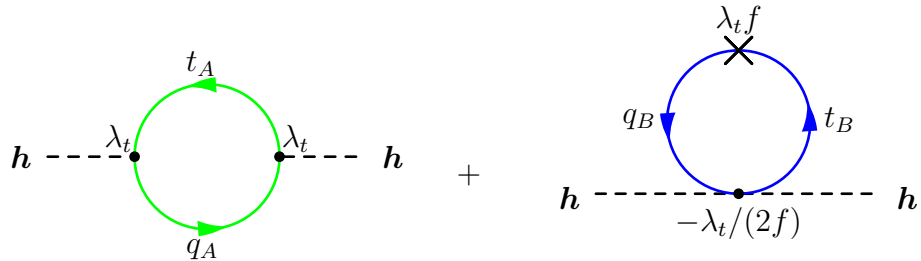


Figure 3.1: Cancellation of quadratic divergences in the Mirror Twin Higgs model. The cancellation holds when the top and its partner are charged under different $SU(3)$ s.

Evaluating these diagrams we find that the quadratic divergence arising from the first diagram is exactly canceled by that of the second. The first and second diagrams have been colored differently to emphasize that the particles running in the two loops carry different $SU(3)$ charges. The first loop has the SM top quarks which carry SM color. The particles running in the second loop, however, are twin top quarks charged under twin color, not SM color.

We also note the recent minimal incarnation of this model, the Fraternal Twin Higgs [137]. Rather than the full doubling of the SM, this model only includes the third generation in the mirror sector. In such a model, the lightest mirror states may be glueballs of $SU(3)_B$, depending on the mass of the mirror bottom quark.

3.2 Folded Supersymmetry

SUSY is perhaps the best known solution to the hierarchy problem. In supersymmetric theories every known particle is related by the symmetry to another particle with a different spin, called its superpartner. The gauge quantum numbers of each particle and its corresponding superpartner are identical. In supersymmetric

extensions of the SM, the quadratically divergent contributions to the Higgs mass from loops involving the SM particles are canceled by new diagrams involving the superpartners.

In the case of the top quark, whose left and right components belong to the $SU(2)$ doublet q and $SU(2)$ singlet u , the corresponding scalar partners are the scalar stops, which we label by \tilde{q} and \tilde{u} . Supersymmetric extensions of the SM generally contain two Higgs doublets, one labeled H_u which gives mass to the up-type quarks and another, labeled H_d , which gives mass to the down-type quarks and leptons. Both H_u and H_d have fermionic superpartners, the Higgsinos. In supersymmetric theories, the one loop quadratically divergent contributions to the up-type Higgs mass associated with the top Yukawa coupling are canceled by diagrams involving the stops. The relevant couplings take the form

$$(\lambda_t H_u q u + \text{H.c.}) + \lambda_t^2 |\tilde{q} H_u|^2 + \lambda_t^2 |\tilde{u}|^2 |H_u|^2 . \quad (3.12)$$

These interactions lead to radiative corrections to the up-type Higgs mass from the diagrams shown in Fig. 3.2.

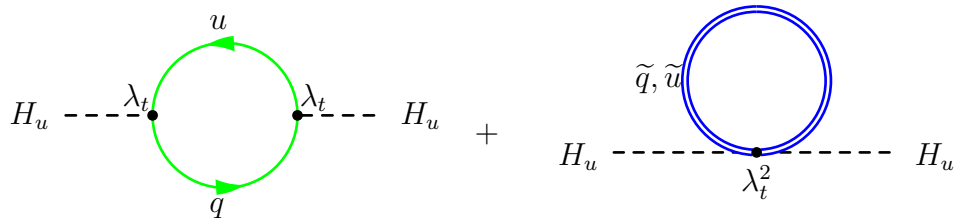


Figure 3.2: Cancellation of quadratic divergences in the Folded SUSY model. This divergence is canceled even if the top and stop transform under different color groups.

From the form of the interaction in Eq. (3.12), we see that for the cancellation

to go through, the left-handed stop \tilde{q} must carry charge under the $SU(2)$ gauge interactions of the SM. At the diagrammatic level, however, the cancellation does not depend on whether the stops transform under SM color.

In Folded Supersymmetric theories the cancellation of the one loop quadratic divergences associated with the top Yukawa coupling takes place exactly as in the diagrams above, but the top and its scalar partners, labeled “folded stops” or “F-stops”, are charged under different color groups. While the fermions transform under the familiar SM color group, now labeled $SU(3)_A$, the scalars transform under a separate hidden color group, labeled $SU(3)_B$. The electroweak quantum numbers of the F-stops are identical to those of the corresponding SM fermions. This scenario can be realized in a 5D supersymmetric construction, with the extra dimension compactified on S^1/Z_2 (see [160] for an alternative UV completion). A combination of boundary conditions and discrete symmetries ensures that the spectrum of light states includes the SM particles and the scalar folded superpartners (“F-spartners”) that cancel the quadratic divergences arising from the couplings of SM fermions to the up- and down-type Higgs bosons. The gauginos are projected out by the boundary conditions, and are not part of the low energy spectrum. The slepton and EWino spectrum is the same as in the MSSM, with soft masses given by the scale of the extra dimension in the minimal model.² The interactions of the top quarks and the F-stops with the up-type Higgs have exactly the same form as in (3.12), and

²Note that there is no tuning associated with splitting the folded squarks from the gauginos. In the extra dimensional construction the folded squarks have zero mass tree level; the scale of their soft masses is given by gauge (and Higgs for the third generation) interactions, see [130] for the explicit soft masses. Thus, the squarks are generally lighter than the gauginos by the gauge coupling squared divided by a loop factor.

the cancellation of quadratic divergences between the fermion and scalar diagrams happens in exactly the same way.

The F-stops are not charged under SM color, which drastically reduces their production cross section at hadron colliders compared to colored stops in standard SUSY theories. However, because they still carry EW charge, Large Electron-Positron (LEP) collider limits require that they be heavier than ~ 100 GeV. The lightest states in the mirror sector are therefore the $SU(3)_B$ glueballs, which can be produced in decays of the SM-like Higgs and lead to the discovery signature discussed in Chapter 5.

Direct production of the F-squarks in Drell-Yan-like processes and subsequent annihilation through quirky dynamics may yield additional discovery signatures [167], including $W\gamma$ resonances at the LHC [311]. Possible glueball signals from these processes are discussed in [172].

3.3 Quirky Little Higgs

In Little Higgs models the Higgs doublet emerges as a pNGB whose mass is protected against one loop quadratic divergences by collective symmetry breaking. To understand how this mechanism operates, consider the Simplest Little Higgs model [79]. In this theory the $SU(2)_L \times U(1)_Y$ gauge symmetry of the SM is embedded in the larger gauge group $SU(3)_W \times U(1)_X$. All the states in the SM that are doublets under $SU(2)_L$ are now promoted to triplets. The Higgs sector for this theory is assumed to respect a larger approximate global $[SU(3) \times U(1)]^2$ symmetry,

of which the gauged $SU(3)_W \times U(1)_X$ is a subgroup. This approximate global symmetry, which is explicitly violated by both the gauge and Yukawa interactions, is broken to $[SU(2) \times U(1)]^2$, which contains $SU(2)_L \times U(1)_Y$ of the SM as a subgroup. The SM Higgs doublet is contained among the uneaten pNGBs that emerge from this symmetry breaking pattern, and its mass is protected against large radiative corrections.

The symmetry breaking pattern may be realized using two scalar triplets of $SU(3)_W$, which we denote by ϕ_1 and ϕ_2 . If the tree level potential for these scalars, $V(\phi_1, \phi_2)$ is of the form

$$V(\phi_1, \phi_2) = V_1(\phi_1) + V_2(\phi_2) , \quad (3.13)$$

then this sector possesses an $[SU(3) \times U(1)]^2$ global symmetry. When ϕ_1 and ϕ_2 acquire VEVs f_1 and f_2 , this symmetry is broken to $[SU(2) \times U(1)]^2$. For simplicity we assume that the two VEVs are equal, so that $f_1 = f_2 = f$. However, this is not required for the mechanism to work. Of the 10 resulting NGBs, 5 are eaten while the remaining 5 contain the SM Higgs doublet.

The next step is to understand how the cancellation of quadratic divergences associated with the top Yukawa coupling arises in this theory. The top sector takes the form

$$\lambda_1 \phi_1 Q t_1 + \lambda_2 \phi_2 Q t_2 , \quad (3.14)$$

where Q represents the $SU(3)$ triplet containing the third generation left-handed quarks, while t_1 and t_2 are $SU(3)$ singlets that carry the same electroweak charge as the right-handed top quark in the SM. These interactions do not respect the full

$[\text{SU}(3) \times \text{U}(1)]^2$ global symmetry but only the gauged $\text{SU}(3)_W \times \text{U}(1)_X$ subgroup. As a consequence, the potential for ϕ_1 and ϕ_2 will receive corrections, and the 5 uneaten NGBs will acquire a mass. However, this radiatively generated contribution to the mass is not quadratically, but only logarithmically divergent.

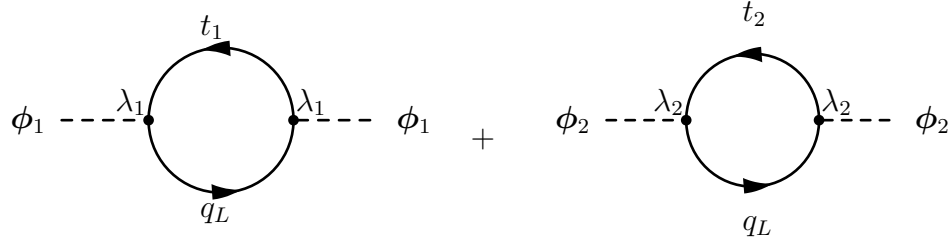


Figure 3.3: Quadratic divergences from the top sector of the Littlest Higgs model.

The diagrams that can potentially lead to quadratically divergent contributions to the masses of the pNGBs are shown in Fig. 3.3. The divergent parts of these graphs are given by

$$\frac{3}{8\pi^2} \Lambda^2 \lambda_1^2 \phi_1^\dagger \phi_1 + \frac{3}{8\pi^2} \Lambda^2 \lambda_2^2 \phi_2^\dagger \phi_2. \quad (3.15)$$

However, we see that these terms respect the full global $\text{SU}(3) \times \text{SU}(3)$ symmetry and so cannot contribute to the mass of the pNGBs. This is not a coincidence, but a consequence of collective symmetry breaking. To see this, note that in Eq. (3.14) if either of the λ_i is set to zero then the Lagrangian for the top sector recovers the full $\text{SU}(3) \times \text{SU}(3)$ global symmetry and all the resulting NGBs are all massless. Therefore, the global symmetry is violated only in the presence of both λ_1 and λ_2 , which collectively break the symmetry. Therefore, any correction to the pNGB masses can only arise from a diagram that includes both λ_1 and λ_2 . There are, however, no such quadratically divergent diagrams. The lowest order diagram that

corrects the potential and contains both λ_1 and λ_2 is the box diagram, shown in Fig. 3.4, which is only logarithmically divergent.

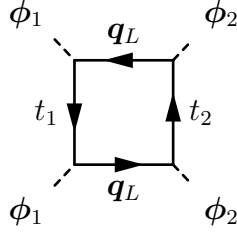


Figure 3.4: Logarithmically divergent contribution to the Higgs potential. This contribution vanishes unless both λ_1 and λ_2 are nonzero.

We can show that this protection mechanism depends only on the symmetry breaking pattern of the model and is independent of the details of the dynamics that breaks the symmetry. To do this, we parametrize the uneaten pNGBs, in unitary gauge, by a set of fields $\pi(x)$. It is convenient to construct from the $\pi(x)$ two objects ϕ_1 and ϕ_2 that transform linearly under the full broken $SU(3) \times SU(3)$ symmetry.

$$\varphi_1 = e^{i\Pi/f} \begin{pmatrix} 0 \\ 0 \\ f \end{pmatrix}, \quad \varphi_2 = e^{-i\Pi/f} \begin{pmatrix} 0 \\ 0 \\ f \end{pmatrix}, \quad (3.16)$$

with the relevant degrees of freedom encapsulated by

$$\Pi = \left(\begin{array}{cc|c} 0 & 0 & \mathbf{h} \\ 0 & 0 & \\ \hline \mathbf{h}^\dagger & & 0 \end{array} \right). \quad (3.17)$$

The Lagrangian for the top sector then takes the form

$$\frac{\lambda_1}{\sqrt{2}} \varphi_1^\dagger Q t_1 + \frac{\lambda_2}{\sqrt{2}} \varphi_2^\dagger Q t_2. \quad (3.18)$$

Expanding to quadratic order in \mathbf{h} and making the definitions

$$t^c \equiv i \left(\frac{\lambda_1}{\sqrt{\lambda_1^2 + \lambda_2^2}} t_2 - \frac{\lambda_1}{\sqrt{\lambda_1^2 + \lambda_2^2}} t_1 \right), \quad (3.19)$$

$$T^c \equiv \frac{\lambda_2}{\sqrt{\lambda_1^2 + \lambda_2^2}} t_2 + \frac{\lambda_1}{\sqrt{\lambda_1^2 + \lambda_2^2}} t_1 \quad (3.20)$$

this becomes

$$\mathbf{h} q (\lambda_t t^c + \lambda_T T^c) + m_T T T^c \left(1 - \frac{1}{2f^2} \mathbf{h}^\dagger \mathbf{h} \right). \quad (3.21)$$

Here we have defined

$$\lambda_t = \frac{\sqrt{2}\lambda_1\lambda_2}{\sqrt{\lambda_1^2 + \lambda_2^2}}, \quad \lambda_T = i \frac{\lambda_2^2 - \lambda_1^2}{\sqrt{2}\sqrt{\lambda_1^2 + \lambda_2^2}}, \quad m_T = \frac{f}{\sqrt{2}} \sqrt{\lambda_1^2 + \lambda_2^2}. \quad (3.22)$$

The diagrams contributing to the Higgs mass, see Fig. 3.5, demonstrate the cancellation of quadratic divergences. Notice that because q couples to both t^c and T^c that the top partner must transform under the same SU(3) as the top. Thus, the two loops have been given the same color. If, however, there is some symmetry that forces $\lambda_1 = \lambda_2$ then the coupling λ_T of q to T^c vanishes and the cancellation goes through even if t^c and T^c transform under different SU(3) color groups.

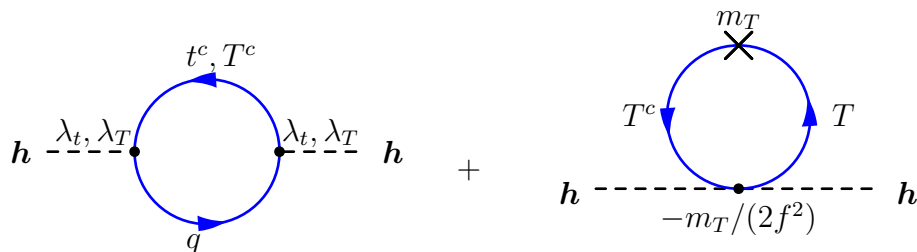


Figure 3.5: Cancellation of quadratic divergences in the Littlest Higgs model. The two fermions must transform under the same SU(3) unless $\lambda_1 = \lambda_2$.

In Quirky Little Higgs models the one loop quadratic divergences generated by the top quark are canceled exactly as in the diagrams shown above, but the fermionic

top partners T and T^c do not transform under the SM color group, $SU(3)_c$. These partners are instead charged under a different $SU(3)$, labeled as $SU(3)_B$. However, the electroweak quantum numbers of the quirks are the same as those of their SM partners. In this construction, all the fermions that are charged under $SU(3)_B$ have masses much above the scale where the gauge group gets strong. As a consequence, the system exhibits quirky dynamics.

Quirky Little Higgs models can be realized in a 5 dimensional space with the extra dimension compactified on S^1/Z_2 . The breaking of the $SU(3)_W \times U(1)_X$ gauge group down to the SM is realized by boundary conditions and separately by a scalar field Φ that transforms as a triplet under $SU(3)_W$. The 5 dimensional theory also possesses an $SU(6)$ gauge symmetry that is broken down to the SM $SU(3)_A$ color group and to $SU(3)_B$ by boundary conditions. This construction allows the third generation quark doublet q and the top partner T to emerge as zero modes from the same bulk multiplet, but transforming under different color groups. The Higgs doublet is contained among the pNGBs that emerge from Φ after the breaking of the $SU(3)_W \times U(1)_X$ symmetry. The interactions in Eq. (3.21) arise from couplings of Φ to the multiplets that contain the top quarks and the top partners. The $SU(6)$ gauge symmetry ensures the equality of the couplings in Eq. (3.21) that is necessary to enforce the cancellation of the quadratic divergence.

As in FSUSY, the quadratic corrections to the Higgs mass of the SM fermions are canceled by partners charged under a different $SU(3)$, but carry the same electroweak charges. This means that they can be produced directly at colliders and give rise to phenomenology similar to FSUSY, including glueball signatures [172].

The most significant difference is that the top partners are fermions, which leads to deviations in the couplings of the Higgs to SM particles. In short, the Higgs is the persistent channel for discovering these models.

Chapter 4: Higgs Couplings Predictions

Any structure that seeks to protect the Higgs mass from large quantum corrections by way of a symmetry predicts new particles that couple strongly to the Higgs. The complete framework may also predict couplings between the Higgs and SM fields that differ from the SM results. Projections for the full high luminosity LHC run (3000 fb⁻¹) [273] show that the Higgs invisible branching fraction will be probed down to about 10%. The precision for the signal strengths in the cleanest Higgs channels, ZZ , WW , and $\gamma\gamma$, is projected to be around 5%.

4.1 Mirror Twin Higgs

In order to understand the implications of the MTH model for Higgs production and decays, we first determine the couplings of the Higgs to the states in the low energy theory. We employ the nonlinear model defined in Eq. (3.8) and choose the unitary gauge in the visible sector with $h_1 = 0$ and $h_2 = (v + \rho)/\sqrt{2}$ to obtain

$$H_A = \begin{pmatrix} 0 \\ if \sin\left(\frac{v + \rho}{\sqrt{2}f}\right) \end{pmatrix}, \quad H_B = \begin{pmatrix} 0 \\ f \cos\left(\frac{v + \rho}{\sqrt{2}f}\right) \end{pmatrix}. \quad (4.1)$$

The couplings of the weak gauge bosons to the Higgs originate from

$$|D_\mu^A H_A|^2 + |D_\mu^B H_B|^2 \quad (4.2)$$

where the $D^{A,B}$ denote the covariant derivative employing the A, B gauge bosons.

Expanding out the kinetic terms we find

$$\begin{aligned} \frac{1}{2} \partial_\mu \rho \partial^\mu \rho + \left[\frac{f^2 g^2}{2} W_{A\mu}^+ W_A^{\mu-} + \frac{f^2 g^2}{4 \cos^2 \theta_W} Z_{A\mu} Z_A^\mu \right] \sin^2 \left(\frac{v + \rho}{\sqrt{2} f} \right) \\ + \left[\frac{f^2 g^2}{2} W_{B\mu}^+ W_B^{\mu-} + \frac{f^2 g^2}{4 \cos^2 \theta_W} Z_{B\mu} Z_B^\mu \right] \cos^2 \left(\frac{v + \rho}{\sqrt{2} f} \right). \end{aligned} \quad (4.3)$$

From this we obtain the masses of the W^\pm and Z gauge bosons in the visible and twin sectors and their couplings to the Higgs, ρ . We find that

$$m_{W_A}^2 = \frac{f^2 g^2}{2} \sin^2 \left(\frac{v}{\sqrt{2} f} \right), \quad m_{W_B}^2 = \frac{f^2 g^2}{2} \cos^2 \left(\frac{v}{\sqrt{2} f} \right). \quad (4.4)$$

The masses of the Z bosons are related to those of the W s by the usual factor of $\cos \theta_W$. Notice that the VEV of the Higgs in the SM, $v_{EW} = 246$ GeV, is related to the parameters v and f of the MTH model by the relation

$$v_{EW} = \sqrt{2} f \sin \left(\frac{v}{\sqrt{2} f} \right) \equiv \sqrt{2} f \sin \vartheta. \quad (4.5)$$

From this expression, which defines the angle ϑ , we see that v and v_{EW} become equal in the $v \ll f$, or equivalently $\vartheta \ll 1$, limit.

In the absence of any effects that violate the Z_2 symmetry, minimization of the Higgs potential requires $v_{EW} = f$, so that the state ρ is composed of visible and hidden sector states in equal proportions. In order to avoid the experimental limits on this scenario, it is desirable to create a hierarchy between these scales so that $v_{EW} < f$. This is most simply realized by a soft explicit breaking of the Z_2 symmetry. This allows the gauge and Yukawa couplings to remain the same across the A and B sectors, so that the cancellation of quadratic divergences remains intact.

We can expand out Eq. (4.3) to obtain the couplings of the Higgs to the electroweak gauge bosons

$$\begin{aligned} \frac{1}{2} \partial_\mu \rho \partial^\mu \rho + \left[m_{W_A}^2 W_{A\mu}^+ W_A^{\mu-} + \frac{m_{Z_A}^2}{2} Z_{A\mu} Z_A^\mu \right] \left(1 + 2 \frac{\rho}{v_{\text{EW}}} \cos \vartheta + \dots \right) \\ + \left[m_{W_B}^2 W_{B\mu}^+ W_B^{\mu-} + \frac{m_{Z_B}^2}{2} Z_{B\mu} Z_B^\mu \right] \left(1 - 2 \frac{\rho}{v_{\text{EW}}} \tan \vartheta \sin \vartheta + \dots \right). \end{aligned} \quad (4.6)$$

We see that the couplings of ρ to the W and Z differ by a factor of $\cos \vartheta$ from the SM prediction.

We now turn to the top quark sector (3.3). Expanding this in the unitary gauge we find

$$\begin{aligned} \lambda_t \left[i f q_A t_A \sin \left(\frac{v + \rho}{\sqrt{2} f} \right) + f q_B t_B \cos \left(\frac{v + \rho}{\sqrt{2} f} \right) \right] \\ = i \frac{\lambda_t v_{\text{EW}}}{\sqrt{2}} q_A t_A \left[1 + \frac{\rho}{v_{\text{EW}}} \cos \vartheta \right] + \lambda_t f q_B t_B \cos \vartheta \left[1 - \frac{\rho}{v_{\text{EW}}} \tan \vartheta \sin \vartheta \right] \end{aligned} \quad (4.7)$$

where for simplicity we have not differentiated the components in the SU(2) doublets. We also see that the mass of the top quark's mirror twin partner is

$$m_T = \lambda_t f \cos \vartheta = m_t \cot \vartheta. \quad (4.8)$$

We can now determine the implications of the MTH model for Higgs production and decays. We have seen that the tree level couplings of ρ to the visible sector fermions and bosons are simply altered by a factor $\cos \vartheta$ relative to the SM. Since the new particles in the model carry no SM charges, the radiatively generated couplings of the Higgs to gluons and photons are modified relative to the SM by exactly the same factor. It follows that all production cross sections are modified by the square of this factor,

$$\sigma(pp \rightarrow \rho) = \cos^2 \vartheta \sigma_{\text{SM}}(pp \rightarrow h), \quad (4.9)$$

where h is the SM Higgs boson. There is a similar relation for decays of the Higgs into A sector particles,

$$\Gamma(\rho \rightarrow A_i) = \Gamma^{\text{SM}}(h \rightarrow \text{SM}_i) \cos^2 \vartheta, \quad (4.10)$$

where the subscript i labels particle species. In addition, ρ will decay into B sector particles that are light enough. A factor of $\sin \vartheta$ accompanies couplings of ρ to twin sector states, relative to the corresponding SM interactions. We define the fraction δ as

$$\delta = \frac{\Gamma(\rho \rightarrow B)}{\Gamma^{\text{SM}}(h) \sin^2 \vartheta}. \quad (4.11)$$

In the limit that the states in the twin sector have the same masses as their visible sector partners, $\delta = 1$. Away from this limit, δ is expected to differ from unity due to kinematic effects. The total Higgs width in the MTH model is given by

$$\Gamma(\rho) = \Gamma^{\text{SM}}(h) [\cos^2 \vartheta + \delta \sin^2 \vartheta]. \quad (4.12)$$

Employing the expressions $\Gamma_{\text{BR}}^{\text{SM}}(h \rightarrow \text{SM}_i)$ and $\Gamma_{\text{BR}}(\rho \rightarrow A_i)$ to denote the branching fractions into the same particle species i we obtain

$$\frac{\sigma(pp \rightarrow \rho) \Gamma_{\text{BR}}(\rho \rightarrow A_i)}{\sigma_{\text{SM}}(pp \rightarrow h) \Gamma_{\text{BR}}^{\text{SM}}(h \rightarrow \text{SM}_i)} = \frac{\cos^2 \vartheta}{1 + \delta \tan^2 \vartheta} = \frac{1}{\left(1 + \delta \frac{m_t^2}{m_T^2}\right) \left(1 + \frac{m_t^2}{m_T^2}\right)}. \quad (4.13)$$

As explained earlier, in the case when the Z_2 symmetry is only softly broken, the gauge and Yukawa couplings are the same in the visible and twin sectors. This allows us to obtain expressions for the masses of the particles in the twin sector, and predict δ . The masses of the B sector particles are related to those in the A sector by

$$m_B = m_A \cot \vartheta, \quad (4.14)$$

and so for $f \gg v$ the B sector masses are significantly larger than those of the A sector. The B sector particles couple to ρ with the same coupling as in the SM, but modified by the factor $-\sin\vartheta$.

The leading order relation for SM Higgs decays to fermions f is given by

$$\Gamma(h \rightarrow f\bar{f}) = \frac{N_c}{16\pi} m_h \lambda_f^2 \left(1 - 4 \frac{m_f^2}{m_h^2}\right)^{3/2}, \quad (4.15)$$

where λ_f is to be evaluated at the Higgs mass. For decays into gauge bosons we use [312]

$$\Gamma(h \rightarrow VV^*) = \frac{3m_h}{32\pi^3} \frac{m_V^4}{v_{\text{EW}}^4} \delta_V R_T \left(\frac{m_V^2}{m_H^2}\right), \quad (4.16)$$

where $\delta'_W = 1$, $\delta'_Z = \frac{7}{12} - \frac{10}{9} \sin^2 \theta_W + \frac{40}{9} \sin^4 \theta_W$, and

$$R_T(x) = \frac{3(1 - 8x + 20x^2)}{\sqrt{4x - 1}} \cos^{-1} \left(\frac{3x - 1}{2x^{3/2}}\right) - \frac{1 - x}{2x} (2 - 13x + 47x^2) - \frac{3}{2} (1 - 6x + 4x^2) \ln x, \quad (4.17)$$

when the mass of the vector is less than the mass of the Higgs. By suitably modifying these expressions, we can obtain the width of the Higgs into twin fermions and twin electroweak gauge bosons. The Higgs may also decay into twin gluons g_B :

$$\Gamma(\rho \rightarrow g_B g_B) = \frac{\alpha_s^2 m_h^3}{72\pi^3 v^2} \left| \frac{3}{4} \sum_q A_F \left(\frac{4m_q^2}{m_h^2}\right) \right|^2 \quad (4.18)$$

with A_F defined in Eq. (4.45). The sum is over the twin quarks, but is dominated by the twin top.

We use these formulas in conjunction with the factor of $\sin^2\vartheta$ to determine δ

as a function of m_t/m_T :

$$\begin{aligned}
\delta = & \sum_j \Gamma_{\text{BR}}^{\text{SM}}(h \rightarrow f_j \bar{f}_j) \left[\frac{1 - 4 \frac{m_{f_j}^2 m_T^2}{m_h^2 m_t^2}}{1 - 4 \frac{m_{f_j}^2}{m_h^2}} \right]^{3/2} + \sum_j \Gamma_{\text{BR}}^{\text{SM}}(h \rightarrow V_j V_j^*) \frac{R_T \left(\frac{m_{V_j}^2 m_T^2}{m_h^2 m_t^2} \right)}{R_T \left(\frac{m_{V_j}^2}{m_h^2} \right)} \\
& + \Gamma_{\text{BR}}^{\text{SM}}(h \rightarrow gg) \frac{\left| A_F \left(\frac{4m_T^2}{m_h^2} \right) \right|^2}{\left| A_F \left(\frac{4m_t^2}{m_h^2} \right) \right|^2} \tag{4.19}
\end{aligned}$$

In our analysis, we take into account the decay modes of ρ into the twin sector bottom and charm quarks, and into the tau and muon leptons. We use the Higgs widths reported in [313].

Using these results we can determine the rate of Higgs events into any SM state and the branching fraction into twin sector states. We plot these results in Fig. 4.1. The blue line represents the rate of Higgs events into SM final states in the softly broken MTH model normalized to the SM. The green line denotes the branching fraction of the Higgs into the twin sector particles. A key observation is that the MTH model predicts a relation between the Higgs invisible branching fraction and the modification to standard model rates. In a more minimal construction like the FTH, this can vary somewhat, but even in that case the dominant decay channels, to twin bottoms and taus, contribute to the invisible width, but the detailed value will be different. The SM coupling modifications, however, do not depend on the mass of the twin sector particles.

The corrections to the Higgs couplings in the MTH model relative to the SM are constrained by precision electroweak measurements. In theories where the Higgs emerges as a pNGB, its couplings to the fermions and gauge bosons are generally

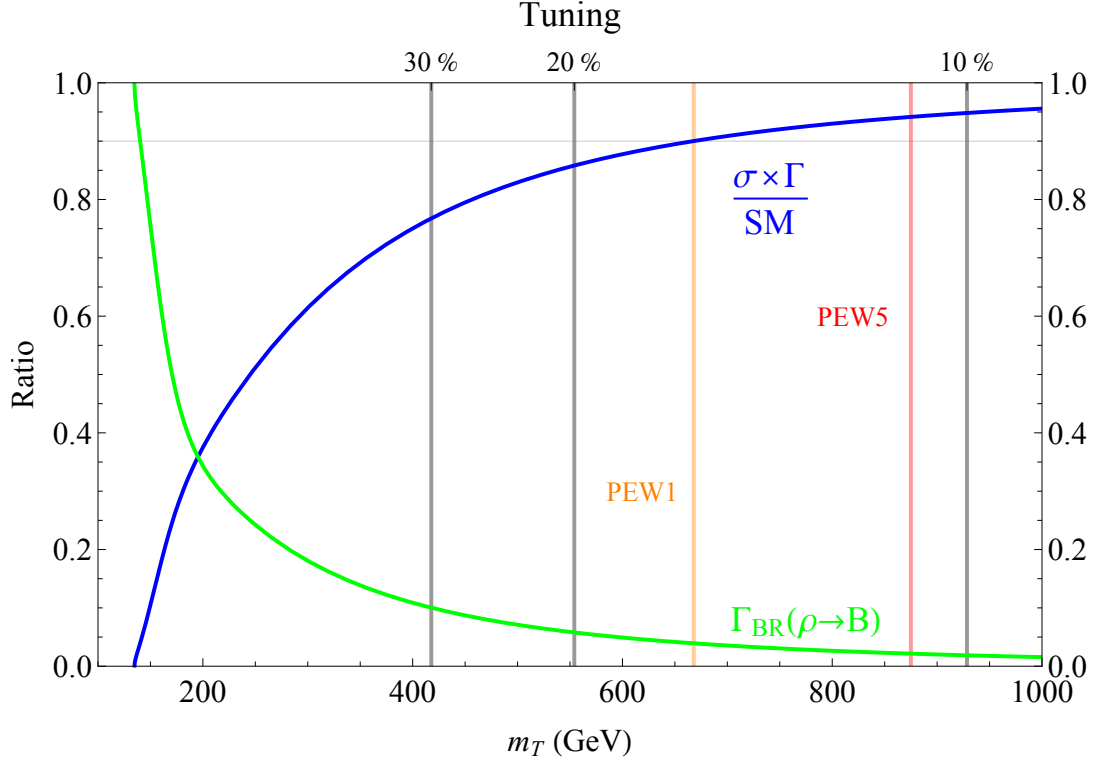


Figure 4.1: In blue, a plot of the rate of Higgs events into SM states normalized to the SM. The green line is the invisible branching ratio of the Higgs into mirror twin particles. The vertical orange and red lines are the 95% confidence bound from precision electroweak (PEW) constraints for a 1 and 5 TeV cutoff respectively.

smaller than in the SM. In [314] precision electroweak constraints were applied to the MCHM4 model [82], which, like MTH, modifies the Higgs couplings to all the vector bosons and fermions by a universal factor. Their bound on ϵ , where $\sqrt{1 - \epsilon^2} = \cos \vartheta$, also applies to the MTH model in a strongly coupled UV completion, and can be translated into a bound on the top partner mass. Their analysis was carried out assuming a cutoff $\Lambda = 3$ TeV. In general, however, the leading contributions to the oblique parameters go like

$$\alpha T \sim -\epsilon^2 \ln \left(\frac{\Lambda}{m_Z} \right), \quad \alpha S \sim \epsilon^2 \ln \left(\frac{\Lambda}{m_Z} \right), \quad (4.20)$$

where m_Z is the mass of the Z boson. For ϵ sufficiently small we expect these parameters to dominate the analysis. In that case we may translate the bound on ϵ at Λ to a bound on ϵ' at Λ' by

$$\epsilon^2 \ln \left(\frac{\Lambda}{m_Z} \right) = \epsilon^2 \left(1 + \frac{\ln \left(\frac{\Lambda}{\Lambda'} \right)}{\ln \left(\frac{\Lambda'}{m_Z} \right)} \right) \ln \left(\frac{\Lambda'}{m_Z} \right) \equiv \epsilon'^2 \ln \left(\frac{\Lambda'}{m_Z} \right). \quad (4.21)$$

The 2σ bound on ϵ' can be translated into a limit on the top partner mass. In Fig. 4.1 we denote bound corresponding to a 1 and 5 TeV cutoff by the vertical orange and red lines respectively.

Finally, we estimate the tuning Δ_m of the Higgs mass parameter m^2 as a function of the top partner mass as a measure of the naturalness of the MTH model.

We use the formula

$$\Delta_m = \left| \frac{2\delta m^2}{m_h^2} \right|^{-1} \quad (4.22)$$

to estimate the tuning. We have denoted the quantum corrections to the Higgs mass parameter as δm^2 and the physical Higgs mass as $m_h = 125$ GeV.

The diagrams in Fig. 3.1 lead to

$$|\delta m^2| = \frac{3\lambda_t^2 m_T^2}{8\pi^2} \ln \left(\frac{\Lambda^2}{m_T^2} \right), \quad (4.23)$$

up to finite effects. We take the cutoff Λ to be 5 TeV. In Fig. 4.1 we have denoted the top partner masses corresponding to 30%, 20%, and 10% tuning.

The results of Fig. 4.1 should be compared to our expectations for the precision at which the LHC will be able to constrain these couplings. Projections for the full high luminosity LHC run (3000 fb^{-1}) [273] show that the Higgs invisible branching fraction will be probed down to about 10%. The precision for the signal strengths in

the cleanest Higgs channels, ZZ , WW , and $\gamma\gamma$, is projected to be around 5%. The visible signal strengths are thus a stronger constraint on the model and can probe a level of tuning of about 10% (although combining several channels may improve this sensitivity). The sensitivity at the end of Run II is only slightly worse. We conclude that models that are tuned at the level of one part in ten may be able to escape detection at the LHC.

4.2 Folded-SUSY

In general, the low energy spectrum of FSUSY contains two Higgs doublets. Our analysis in this section will focus on the limit when one of the doublets is much lighter than the other, so that the corrections to the Higgs phenomenology primarily arise from the effects of the F-stops. In our discussion we follow the conventions of Haber [315]. In particular, we take $v_{\text{EW}} = \sqrt{v_d^2 + v_u^2} = 246$ GeV where v_u and v_d are the VEVs of the up-type and down-type Higgs fields respectively. The ratio of the up-type and down-type Higgs VEV is parametrized in terms of an angle β such that $\tan \beta = v_u/v_d$.

It is well known that in order to obtain a mass of 125 GeV for the light Higgs h^0 the MSSM is driven into a constrained parameter space with very heavy stops, resulting in significant tuning. This issue carries over to the folded SUSY construction. One of several possible ways to alleviate this constraint is to add another $U(1)_X$ gauge symmetry to the MSSM whose D -term contribution to the Higgs quartic increases the Higgs mass [279].

4.2.1 Raising the MSSM Higgs Mass with an Extra $U(1)_X$

Suppose we add a $U(1)_X$ gauge symmetry, with coupling g_X , to the MSSM which is then spontaneously broken. This affects the Higgs mass, the scalar masses, and the Higgs couplings to the scalars. We focus on the stop sector and closely follow the work of [279].

All MSSM matter content is given equal charge under hypercharge and $U(1)_X$. In addition, the heavy scalar fields ϕ and ϕ^c , which spontaneously break the symmetry, carry charges $\pm q$ under the new $U(1)_X$ but are singlets under every other MSSM gauge group. These fields are part of chiral superfields Φ and Φ^c with superpotential

$$\mathcal{W} = \lambda S (\Phi\Phi^c - w^2) \quad (4.24)$$

and soft masses

$$m_\phi^2 (|\phi|^2 + |\phi^c|^2). \quad (4.25)$$

For $\lambda^2 w^2 > m_\phi^2$ and equal soft masses these scalars obtain identical nonzero VEVs $\langle\phi\rangle$. The $U(1)_X$ gauge field Z'_μ also gets a mass $m_{Z'} = 2qg_X\langle\phi\rangle$. For Z'_μ to be phenomenologically viable $m_{Z'}$ cannot be far above the scale of the soft masses [316].

The usual MSSM D -terms

$$\frac{g_L^2}{2} \left(\sum_{\text{MSSM}} \phi_i^* q_i \sigma^a \phi_i \right)^2 + \frac{g_Y^2}{2} \left(\sum_{\text{MSSM}} \phi_i^* q_i \phi_i \right)^2 \quad (4.26)$$

(with the q_i denoting the charge of the i th field with respect to the appropriate gauge symmetry) are joined by

$$\frac{g_X^2}{2} \left(\sum_{\text{MSSM}} \phi_i^* q_i \phi_i + q|\phi|^2 - q|\phi^c|^2 \right)^2. \quad (4.27)$$

When ϕ and ϕ^c have masses much higher than the weak scale we can integrate them out. This generates the leading D -terms

$$\frac{g_L^2}{2} \left(\sum_{\text{MSSM}} \phi_i^* q_i \sigma^a \phi_i \right)^2 + \frac{g_Y^2 + \hat{s}^2}{2} \left(\sum_{\text{MSSM}} \phi_i^* q_i \phi_i \right)^2 \quad (4.28)$$

where

$$\hat{s}^2 = g_X^2 \left(1 + \frac{m_{Z'}^2}{2m_\phi^2} \right)^{-1} \frac{v_{\text{EW}}^2}{4m_Z^2}. \quad (4.29)$$

After integrating out the ϕ fields the tree level Higgs quartic becomes

$$\frac{1}{8} \left[g_L^2 + g_Y^2 + g_X^2 \left(1 + \frac{m_{Z'}^2}{2m_\phi^2} \right)^{-1} \right] (|H_u|^2 - |H_d|^2). \quad (4.30)$$

This effective enhancement of the hypercharge D -term raises the tree level Higgs mass to

$$m_{h^0}^2 = m_Z^2 \cos^2 2\beta (1 + \hat{s}^2). \quad (4.31)$$

The D -term contributions to the Higgs-stop couplings and the stop masses are similarly modified, as shown below.

This method, while not the unique way to raise the Higgs mass, serves to illustrate that models of this type may have only moderate tuning from the top sector. For concreteness we pick g_X such that the Higgs mass, including one loop effects from the top and stops, is 125 GeV. For $m_{Z'} = 4$ TeV and $m_\phi = 5$ TeV a perturbative g_X can be chosen to give the correct Higgs mass.

In the limit that only one Higgs doublet is light, its tree level couplings to the fermions and gauge bosons are necessarily of the same form as in the SM, up to small corrections. Therefore, we need only determine the couplings of the Higgs to

the F-stops. The stop mixing matrix is given by

$$\begin{pmatrix} M_{\tilde{Q}}^2 + m_t^2 + m_Z^2 \left(\frac{1}{2} - \frac{2}{3}s_W^2 - \frac{1}{6}\hat{s}^2 \right) \cos 2\beta & m_t(A_t - \mu \cot \beta) \\ m_t(A_t - \mu \cot \beta) & M_{\tilde{U}}^2 + m_t^2 + m_Z^2 \frac{2}{3} \cos 2\beta (s_W^2 + \hat{s}^2) \end{pmatrix} \quad (4.32)$$

where $\sin \theta_W \equiv s_W$, $m_t = \lambda_t v_{\text{EW}} \sin(\beta)/\sqrt{2}$.

Although the original incarnation of FSUY has $A_t = 0$, in our analysis we allow for the possibility that there may be more general constructions that admit nonvanishing A_t . Then the heavy stop \tilde{T} and the light stop \tilde{t} can be written as

$$\tilde{T} = \cos \alpha_t \tilde{q} + \sin \alpha_t \tilde{u} \quad (4.33)$$

$$\tilde{t} = -\sin \alpha_t \tilde{q} + \cos \alpha_t \tilde{u} \quad (4.34)$$

where

$$\cos 2\alpha_t = \frac{M_{\tilde{Q}}^2 - M_{\tilde{U}}^2 + m_Z^2 \cos 2\beta \left(\frac{1}{2} - \frac{4}{3}s_W^2 - \frac{5}{6}\hat{s}^2 \right)}{m_{\tilde{T}}^2 - m_{\tilde{t}}^2}, \quad \sin 2\alpha_t = \frac{2m_t(A_t - \mu \cot \beta)}{m_{\tilde{T}}^2 - m_{\tilde{t}}^2}. \quad (4.35)$$

and

$$\begin{aligned} m_{\tilde{T}, \tilde{t}}^2 &= \frac{1}{2} \left[M_{\tilde{Q}}^2 + M_{\tilde{U}}^2 + 2m_t^2 + \frac{1}{2}m_Z^2 \cos 2\beta (1 + \hat{s}^2) \right] \\ &\quad \pm \frac{1}{2} \sqrt{\left[M_{\tilde{Q}}^2 - M_{\tilde{U}}^2 + m_Z^2 \cos 2\beta \left(\frac{1}{2} - \frac{4}{3}s_W^2 - \frac{5}{6}\hat{s}^2 \right) \right]^2 + 4m_t^2(A_t - \mu \cot \beta)^2}. \end{aligned} \quad (4.36)$$

To ensure that the light stop \tilde{t} has non-negative mass the relation

$$\begin{aligned} m_t |A_t - \mu \cot \beta| &\leq \\ &\sqrt{\left[M_{\tilde{Q}}^2 + m_t^2 + m_Z^2 \left(\frac{1}{2} - \frac{2}{3}s_W^2 - \frac{1}{6}\hat{s}^2 \right) \cos 2\beta \right] \left[M_{\tilde{U}}^2 + m_t^2 + m_Z^2 \frac{2}{3} \cos 2\beta (s_W^2 + \hat{s}^2) \right]} \end{aligned} \quad (4.37)$$

must be satisfied.

We can then obtain the couplings of the heavy and light stop mass eigenstates to the light Higgs, $y_{\tilde{T}}h^0|\tilde{T}|^2$ and $y_{\tilde{t}}h^0|\tilde{t}|^2$. These are given by

$$y_{\tilde{T}} \equiv \frac{2}{v_{\text{EW}}} \left\{ m_t^2 + m_Z^2 \cos 2\beta \left[\frac{1}{4} + \frac{1}{4}\hat{s}^2 + \left(\frac{1}{4} - \frac{2}{3}s_W^2 - \frac{5}{12}\hat{s}^2 \right) \cos 2\alpha_t \right] + \frac{1}{2}m_t(A_t - \mu \cot \beta) \sin 2\alpha_t \right\}, \quad (4.38)$$

$$y_{\tilde{t}} \equiv \frac{2}{v_{\text{EW}}} \left\{ m_t^2 + m_Z^2 \cos 2\beta \left[\frac{1}{4} + \frac{1}{4}\hat{s}^2 - \left(\frac{1}{4} - \frac{2}{3}s_W^2 - \frac{5}{12}\hat{s}^2 \right) \cos 2\alpha_t \right] - \frac{1}{2}m_t(A_t - \mu \cot \beta) \sin 2\alpha_t \right\}. \quad (4.39)$$

We are now in a position to determine the Higgs phenomenology of this model. At tree level, the couplings of the Higgs to the fermions and to the W^\pm and Z gauge bosons are the same as in the SM model. Furthermore, since the F-stops carry no charge under SM color, the couplings of the Higgs to the gluons, which are generated at one loop, are also the same as in the SM. It follows that the Higgs production cross sections in the gluon fusion, associated production and vector boson fusion channels are largely unchanged from the SM predictions.

The Higgs decay widths into SM fermions, gluons and massive gauge bosons are also very close to the SM predictions. However, since the F-stops do carry electric charges, the rate of Higgs decays to two photons is affected. This can be used to constrain the model [189].

4.2.2 Higgs Decays to Photons

In the models we consider, the effects of new physics on Higgs production and decays often occur as simply a multiplicative factor relative the SM. In tree level processes this is a reflection of modified couplings between the Higgs and SM fields. Loop mediated processes, however, have more complicated corrections.

Because we are considering top partners which are not charged under color the gluon fusion and $h \rightarrow gg$ decay are affected in exactly the same way as tree level processes. When the top partner is electrically charged, however, the analysis of $h \rightarrow \gamma\gamma$ is more subtle.

At leading order the partial width of the Higgs to $\gamma\gamma$ is given by

$$\Gamma(h \rightarrow \gamma\gamma) = \frac{\alpha^2 m_h^3}{1024\pi^3} \left| \sum \mathcal{M} \right|^2 \quad (4.40)$$

where the amplitudes \mathcal{M} for each electrically charged vector, fermion, or scalar are given by

$$\mathcal{M}_V = \frac{g(m_V)}{m_V^2} Q_V^2 A_V(x_V), \quad (4.41)$$

$$\mathcal{M}_F = \frac{g(m_F)}{m_F^2} Q_F^2 A_F(x_F), \quad (4.42)$$

$$\mathcal{M}_S = \frac{g(m_S)}{m_S^2} Q_S^2 A_S(x_S). \quad (4.43)$$

In these definitions the Q s are the electrical charges in units of e , the charge of the proton and $g(m)$ is the coupling of the particle to the Higgs. The A functions are

given by

$$A_V(x) = -x^2 \left[\frac{2}{x^2} + \frac{3}{x} + 3 \left(\frac{2}{x} - 1 \right) \arcsin^2 \left(\frac{1}{\sqrt{x}} \right) \right], \quad (4.44)$$

$$A_F(x) = 2x^2 \left[\frac{1}{x} + \left(\frac{1}{x} - 1 \right) \arcsin^2 \left(\frac{1}{\sqrt{x}} \right) \right], \quad (4.45)$$

$$A_S(x) = -x^2 \left[\frac{1}{x} - \arcsin^2 \left(\frac{1}{\sqrt{x}} \right) \right] \quad (4.46)$$

where $x_i = 4m_i^2/m_h^2$ and is understood to be greater than one. The couplings g are defined by

$$\frac{g(m)}{m^2} = \frac{1}{m^2(v)} \frac{\partial m^2(v)}{\partial v} \quad (4.47)$$

where in the case of fermions the mass squared is taken to mean $|m(v)|^2$. Using these results we find the FSUSY result

$$\begin{aligned} \Gamma(h^0 \rightarrow \gamma\gamma) = \frac{\alpha^2 m_{h^0}^3}{1024\pi^3} & \left| \frac{2}{v_{\text{EW}}} A_V \left(\frac{4m_W^2}{m_{h^0}^2} \right) + \frac{2}{v_{\text{EW}}} \frac{4}{3} A_F \left(\frac{4m_t^2}{m_{h^0}^2} \right) \right. \\ & \left. + \frac{y_{\tilde{t}}}{m_{\tilde{t}}^2} \frac{4}{3} A_S \left(\frac{4m_{\tilde{t}}^2}{m_{h^0}^2} \right) + \frac{y_{\tilde{T}}}{m_{\tilde{T}}^2} \frac{4}{3} A_S \left(\frac{4m_{\tilde{T}}^2}{m_{h^0}^2} \right) \right|^2 \end{aligned} \quad (4.48)$$

where we have employed Eqs. (4.38) and (4.39) in the last two terms.

Having now accounted for all the decay modes we find the corrections to the total width are negligible. Therefore, we focus on only the diphoton channel. It can be seen from Eqs. (4.38), (4.39), and (4.48) that in general the stop loops will contribute with the same sign as the top loops and therefore lead to a reduction in the diphoton decay rate. If the mixing A_t is increased, however, the coupling of the Higgs to the light stop can change sign, and enhance the rate. We parametrize this difference from the SM value by

$$\delta = \frac{\Gamma(h^0 \rightarrow \gamma\gamma) - \Gamma^{\text{SM}}(h \rightarrow \gamma\gamma)}{\Gamma^{\text{SM}}(h \rightarrow \gamma\gamma)}. \quad (4.49)$$

Then, neglecting corrections to the overall Higgs width, we have

$$\frac{\sigma(pp \rightarrow h^0)\Gamma_{\text{BR}}(h^0 \rightarrow \gamma\gamma)}{\sigma_{\text{SM}}(pp \rightarrow h)\Gamma_{\text{BR}}^{\text{SM}}(h \rightarrow \gamma\gamma)} = 1 + \delta. \quad (4.50)$$

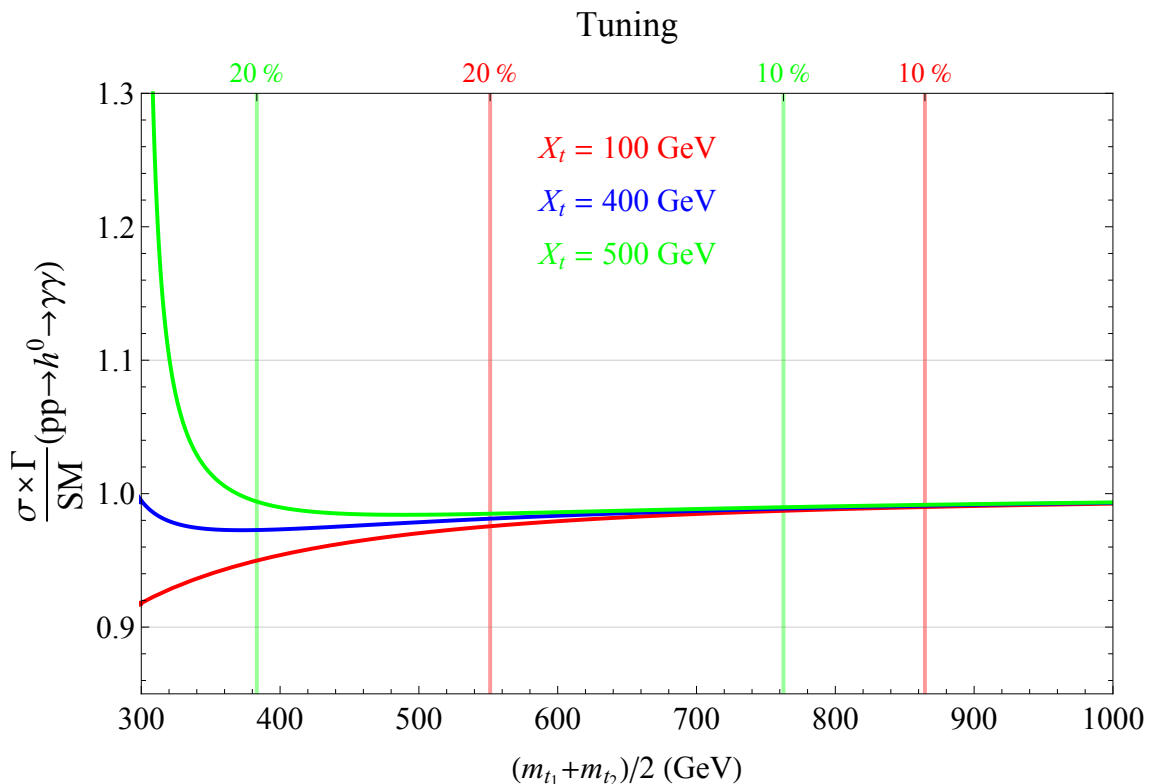


Figure 4.2: Plots of the total Higgs to diphoton rate normalized to SM value as function of the square averaged stop mass m_T^2 . The red, blue, and green lines correspond to mixing $A_t - \mu \cot \beta$ equal to 100, 400, and 500 GeV. We have taken the soft masses equal, $\tan \beta = 10$, and $\mu = -200$ GeV. Contours of tuning are also plotted. The color of the contour indicates the size of A_t for which it applies.

In Fig. 4.2 we plot the total rate of the $h^0 \rightarrow \gamma\gamma$ normalized to the SM value as a function of the square averaged stop mass $m_T^2 = \frac{1}{2}(m_{\tilde{T}}^2 + m_{\tilde{t}}^2)$. For definiteness we take the stop soft masses to be equal, $\mu = -200$ GeV, and choose $\tan \beta = 10$. The red, blue, and green lines correspond to mixing terms $A_t - \mu \cot \beta$ equal to 100, 400, and 500 GeV respectively. We see that for small mixing the rate is reduced

while for larger mixing the rate can be enhanced.

All numerical results, see Fig. 4.2, use the value of \hat{s} such that $m_{h^0} = 125$ GeV with stop loop corrections to the Higgs mass included [75]:

$$m_{h^0}^2 = m_Z^2 \cos^2 2\beta (1 + \hat{s}^2) + \frac{3\lambda_t^2 \sin^2 \beta}{2\pi^2} \left\{ m_t^2 \ln \left(\frac{m_{\tilde{T}} m_{\tilde{t}}}{m_t^2} \right) + \frac{\sin^2 2\alpha_t}{4} (m_{\tilde{T}}^2 - m_{\tilde{t}}^2) \ln \left(\frac{m_{\tilde{T}}^2}{m_{\tilde{t}}^2} \right) + \frac{\sin^4 2\alpha_t}{16m_t^2} \left[(m_{\tilde{T}}^2 - m_{\tilde{t}}^2)^2 - \frac{1}{2} (m_{\tilde{T}}^4 - m_{\tilde{t}}^4) \ln \left(\frac{m_{\tilde{T}}^2}{m_{\tilde{t}}^2} \right) \right] \right\} \quad (4.51)$$

where we have used the definition of $\sin 2\alpha_t$ from Eq. (4.35).

The tuning Δ_m of the Higgs mass parameter m^2 in this model differs only slightly from the MSSM case. As in the MTH model, we estimate the tuning as

$$\Delta_m = \left| \frac{2\delta m^2}{m_h^2} \right|^{-1} \quad (4.52)$$

where δm^2 represents the quantum corrections to the Higgs mass parameter and $m_h = 125$ GeV is the physical Higgs mass. In addition to the diagrams in Fig. 3.2, there is a logarithmic divergence due to stop mixing, as shown in Fig. 4.3. From these loops we find, for equal stop soft masses m_{soft} ,

$$|\delta m^2| = \frac{3\lambda_t^2}{16\pi^2} \left[2m_T^2 - 2m_t^2 - \frac{1}{2}m_Z^2 \cos 2\beta (1 + \hat{s}^2) + A_t^2 \right] \ln \left(\frac{\Lambda^2}{m_{\text{soft}}^2} \right) \quad (4.53)$$

where $\Lambda = 5$ TeV is the cutoff of the model. We have shown the tuning for various values of m_T^2 in Fig. 4.2. The color of each tuning contour corresponds to value of A_t used to generate the corresponding curve in the figure.

We see that the modifications to the Higgs couplings in FSUSY are very small, even when for very mild tuning. Therefore, precision Higgs couplings at the LHC

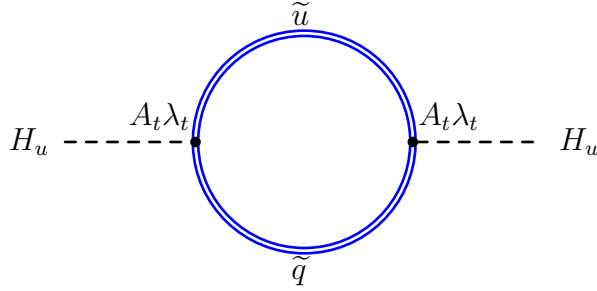


Figure 4.3: Contribution to the logarithmic divergence in FSUSY from the stop mixing term.

will not strongly constrain naturalness. In this framework, however, top and quark partners are charged under electroweak interaction and will be produced. This can lead to $W\gamma$ resonances [167, 311] and jets of mirror glueballs which can decay back through an off-shell Higgs to SM states [172].

4.3 Quirky Little Higgs

In the QLH model, when the scalar field Φ acquires a VEV, the $SU(3)_W \times U(1)_X$ gauge symmetry is broken down to $SU(2)_L \times U(1)_Y$ of the SM. We associate the SM-like Higgs doublet with some of the NGB modes that emerge from this breaking pattern. We parametrize the relevant degrees of freedom (neglecting the $SU(2)_W$ singlet that plays little role in the phenomenology) as

$$\Phi = \exp\left(\frac{i}{f}\Pi\right) \begin{pmatrix} 0 \\ 0 \\ f \end{pmatrix} \quad (4.54)$$

with

$$\Pi = \left(\begin{array}{cc|c} 0 & 0 & h_1 \\ 0 & 0 & h_2 \\ \hline h_1^* & h_2^* & 0 \end{array} \right). \quad (4.55)$$

Employing the symbol \mathbf{h} for the $SU(2)_W$ doublet of h_1 and h_2 we find

$$\Phi = \left(\begin{array}{c} \mathbf{h} \frac{if}{\sqrt{\mathbf{h}^\dagger \mathbf{h}}} \sin \left(\frac{\sqrt{\mathbf{h}^\dagger \mathbf{h}}}{f} \right) \\ f \cos \left(\frac{\sqrt{\mathbf{h}^\dagger \mathbf{h}}}{f} \right) \end{array} \right). \quad (4.56)$$

The top sector Yukawa interaction takes the form

$$-i \frac{\lambda_t f}{\sqrt{\mathbf{h}^\dagger \mathbf{h}}} \sin \left(\frac{\sqrt{\mathbf{h}^\dagger \mathbf{h}}}{f} \right) \mathbf{h}^\dagger t^c q + \lambda_t f \cos \left(\frac{\sqrt{\mathbf{h}^\dagger \mathbf{h}}}{f} \right) TT^c. \quad (4.57)$$

After moving to the unitary gauge $h_1 = 0$, $h_2 = (v + \rho)/\sqrt{2}$ this becomes

$$\lambda_t \left[-if \sin \left(\frac{v + \rho}{\sqrt{2}f} \right) t_L t^c + f \cos \left(\frac{v + \rho}{\sqrt{2}f} \right) TT^c \right] \quad (4.58)$$

with t_L and t^c transforming under $SU(3)_A$ and T and T^c transforming under $SU(3)_B$.

Expanding to first order in ρ and defining $\vartheta \equiv v/(\sqrt{2}f)$ we find

$$\lambda_t \left[-i \frac{v_{EW}}{\sqrt{2}} t_L t_R \left(1 + \frac{\rho}{v_{EW}} \cos \vartheta + \dots \right) + f \cos \vartheta TT^c \left(1 - \frac{\rho}{v_{EW}} \tan \vartheta \sin \vartheta + \dots \right) \right] \quad (4.59)$$

with $v_{EW} = \sqrt{2}f \sin \vartheta$. We see from this that the mass of the top and the mass of the top partner are related by $m_t = m_T \tan \vartheta$. The gauge sector analysis is very similar to that of the A sector in MTH models. We expand the gauge kinetic term $|D_\mu \Phi|^2$ in the unitary gauge to find the couplings between ρ and the gauge bosons:

$$\left[m_W^2 W_\mu^+ W^{\mu-} + \frac{m_Z^2}{2} Z_\mu Z^\mu \right] \left(1 + 2 \frac{\rho}{v_{EW}} \cos \vartheta + \dots \right). \quad (4.60)$$

We see from this that all zero mode quark and gauge boson couplings are suppressed by a universal factor of $\cos\vartheta$ relative to the SM.

The fact that all the Higgs couplings are corrected by the same factor implies that all the production modes are also suppressed by a common factor relative to the SM,

$$\sigma(pp \rightarrow \rho) = \cos^2\vartheta \sigma_{\text{SM}}(pp \rightarrow h). \quad (4.61)$$

A similar relation holds for all decay modes of the Higgs $\Gamma(\rho \rightarrow A_i)$, with the exception of $\Gamma(\rho \rightarrow \gamma\gamma)$, which receives new contributions from loops involving the top partners. The sign of the coupling of the top partner to the Higgs is opposite to that of the top. This causes their contributions to partially cancel, leading to an enhancement in the $\gamma\gamma$ rate. Using Eq. (4.40) we find

$$\Gamma(\rho \rightarrow \gamma\gamma) = \frac{\alpha^2 m_\rho^3}{1024\pi^3} \left| \frac{2}{v_{\text{EW}}} \cos\vartheta A_V \left(\frac{4m_W^2}{m_\rho^2} \right) + \frac{2}{v_{\text{EW}}} \cos\vartheta \frac{4}{3} A_F \left(\frac{4m_t^2}{m_\rho^2} \right) - \frac{2}{\sqrt{2}f} \tan\vartheta \frac{4}{3} A_F \left(\frac{4m_T^2}{m_\rho^2} \right) \right|^2. \quad (4.62)$$

We conclude that for all decay modes except the diphoton,

$$\frac{\sigma(pp \rightarrow \rho)\Gamma_{\text{BR}}(\rho \rightarrow A_i)}{\sigma_{\text{SM}}(pp \rightarrow h)\Gamma_{\text{BR}}^{\text{SM}}(h \rightarrow A_i)} = \frac{1}{1 + \frac{m_t^2}{m_T^2}}, \quad (4.63)$$

where we have neglected tiny effects of order $\Gamma(\rho \rightarrow \gamma\gamma)/\Gamma_{\text{SM}}(h)$. For diphoton decays

$$\frac{\sigma(pp \rightarrow \rho)\Gamma_{\text{BR}}(\rho \rightarrow \gamma\gamma)}{\sigma_{\text{SM}}(pp \rightarrow h)\Gamma_{\text{BR}}^{\text{SM}}(h \rightarrow \gamma\gamma)} = \frac{\Gamma(\rho \rightarrow \gamma\gamma)}{\Gamma_{\text{SM}}(h \rightarrow \gamma\gamma)}. \quad (4.64)$$

These functions are plotted in Fig. 4.4. The solid blue line denotes the rates for all final states other than diphoton and the dashed red line denotes the rate to

diphotons. Note that even though the rate into two photons is enhanced because of the top partner loop, the universal suppression factor more than compensates for this, leading to a net suppression.

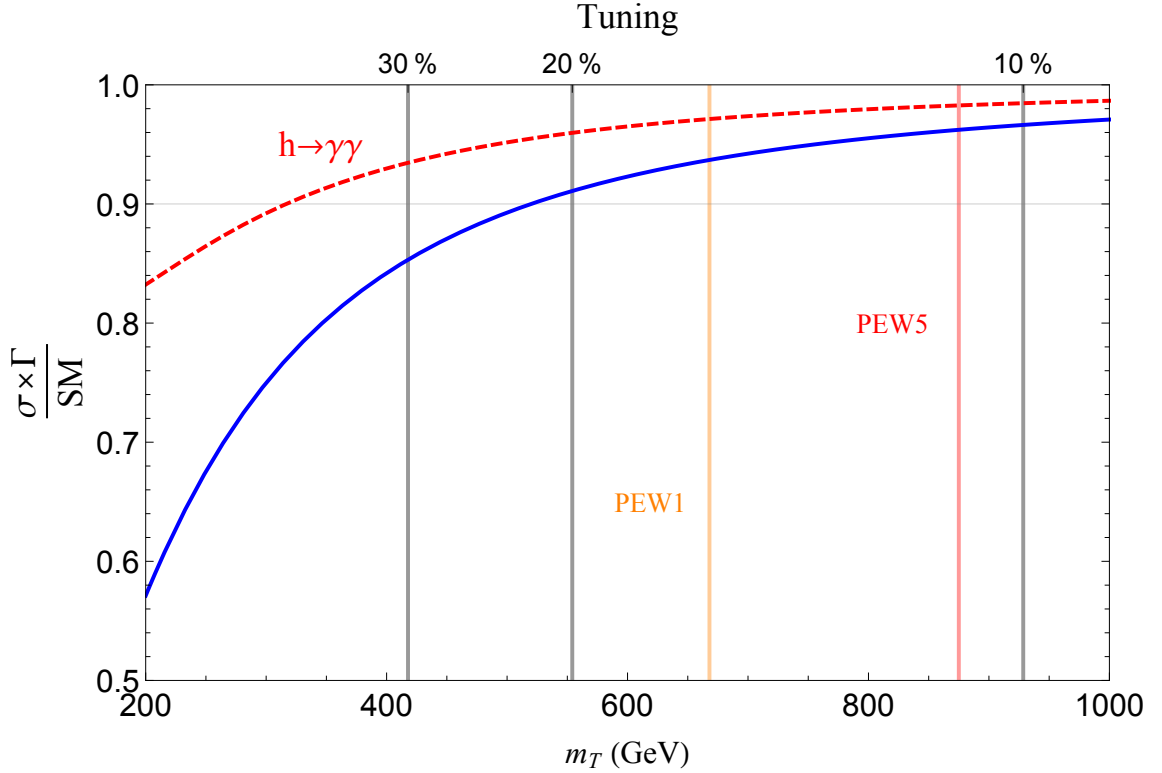


Figure 4.4: Ratios of the rate of Higgs events into a given final state in the QLH model normalized to the SM. The solid blue line denotes the rates for all final states other than diphoton and the dashed red line denotes the diphoton final state. The vertical orange and red lines represent the 95% confidence bound from precision electroweak (PEW) constraints at 1 and 5 TeV respectively.

As with the MTH model, modification of Higgs couplings in the QLH model relative to the SM is constrained by precision electroweak measurements. The analysis of the MCHM4 model in [314] also applies to the QLH. Their bound on ϵ , where $\sqrt{1 - \epsilon^2} = \cos \vartheta$, can be translated into a bound on the top partner mass. This analysis was carried out assuming a cutoff $\Lambda = 3$ TeV. As in the MTH case, we

can translate this bound on ϵ at Λ to a bound on ϵ' at Λ' ; see Eq. (4.21). The 2σ bound on ϵ' can be translated into a limit on the top partner mass. In Fig. 4.4 we denote the bound corresponding to a 1 and 5 TeV cutoff by the vertical orange and red lines respectively.

Finally, we estimate the tuning Δ_m of the Higgs mass parameter m^2 as a function of the top partner mass as a measure of the naturalness of the QLH model. We continue to estimate the tuning by

$$\Delta_m = \left| \frac{2\delta m^2}{m_h^2} \right|^{-1}, \quad (4.65)$$

where we have denoted the quantum corrections to the Higgs mass parameter as δm^2 and the physical Higgs mass as $m_h = 125$ GeV.

The diagrams in Fig. 3.5, with $\lambda_1 = \lambda_2 = \lambda_t$ lead to

$$|\delta m^2| = \frac{3\lambda_t^2 m_T^2}{8\pi^2} \ln \left(\frac{\Lambda^2}{m_T^2} \right), \quad (4.66)$$

up to finite corrections. We take $\Lambda = 5$ TeV as the cutoff of the theory. In Fig. 4.4 we have labeled the top partner masses corresponding to 30%, 20%, and 10% tuning. We see again that even at the 5% branching fraction precision expected at full luminosity, the LHC will not be able to probe tunings at the 10% level. Studies of the direct collider limits on quirky top partners are thus well motivated.

We have seen in this chapter modifications to Higgs couplings in NN theories. In frameworks like the Twin Higgs (TH) and QLH, both with fermionic top partners, the Higgs couplings to SM states are reduced. However, in FSUY the coupling variations are likely to be quite small. This motivates finding additional ways to

probe FSUSY. As the next chapter demonstrates, we may use another property of the Higgs, its exotic decays, to effectively probe FSUSY.

Chapter 5: Exotic Higgs Decays

Partner particles in NN models can interact with the SM through the Higgs. Therefore, the Higgs can decay into sufficiently light hidden sector particles. If the lightest states in the hidden sector are heavier than light SM states, they can decay back, through the Higgs, to SM states. These exotic decays of the Higgs have great power to discover many NN models.

In FSUSY the mass of the Higgs is protected by an accidental low-energy SUSY limit, with the SM fields and their superpartners charged under different $SU(3)$ gauge groups. The couplings of the superpartners to the SUSY Higgs fields requires them to carry EW charge. Therefore, such top partners are EW charged scalars.

These models, and related constructions like QLH, include a mirror sector with its own strong force $SU(3)_B$ under which the top partners are charged.¹ This leads to either mirror baryons or, in the absence of light $SU(3)_B$ -charged matter, glueballs (see [317–319]) at the bottom of the mirror sector spectrum, connecting Hidden Valley phenomenology [320–325] to naturalness. Future high-energy colliders, dark matter experiments, and cosmological observations might explore this rich

¹We use the terms ‘mirror sector’ and ‘mirror particles’ to refer to the new sectors and particles in theories with colorless top partner.

new world, but what can the LHC teach us now?

A few phenomenological studies of NN exist [167, 311], but these were not focused on the vital third generation partners. Recently, the authors of [137] pointed out the exciting connection between exotic Higgs decays and colorless top partner models. In this chapter we explore this direction further, and place it in the broader context of what experimental signals NN “requires.”

All known theories with fermionic top partners assume the Higgs is a pNGB. As shown in chapter 4, this leads to unavoidable Higgs coupling shifts relative to the SM. They occur at tree-level and are of the same order as the tuning in the theory. The LHC will only be sensitive to $\mathcal{O}(10\%)$ deviations, but future lepton colliders like the ILC, TLEP or CEPC will constrain these coupling at the sub-percent level [273, 311]. Therefore, natural fermionic-top-partner solutions to the hierarchy problem should produce measurable deviations. While diagnosing the details of the theory might be challenging, possibly requiring access to the UV completion with a 100 TeV collider, these couplings serve as a smoking-gun for the discovery of TH-type theories. (Higgs coupling deviations are, of course, also generated at loop-level if the mirror sector has any SM charge. However, chapter 4 showed that the small size of these deviations make them an unlikely discovery channel for partner masses above a few 100 GeV, see also [311].)

A more declarative signature is mirror glueballs. Our understanding of confining pure gauge theories has advanced significantly since the first uncolored naturalness theories were proposed [317–319]. The FTH setup, without light first and second generation partners [137], can have glueballs at the bottom of the mirror

sector spectrum. These glueballs couple to the visible-sector Higgs through a top partner loop, leading to glueball production by exotic Higgs decays. The glueballs then decay to two SM fermions via an off-shell Higgs. While the quantitative phenomenological details of this signature were not fully explored, it is clear that the corresponding decay lifetimes can be in the observable range, leading to striking LHC signatures.

As exciting as this experimental signature is, it is not required by generic TH models—the SM-singlet sector can easily have relatively light quarks, making the hadron spectrum similar to the visible sector. On the other hand, mirror glueballs, and their associated signals, are required for NN theories with EW-charged mirror sectors, like FSUSY or QLH. This is due to LEP limits that forbid EW charged BSM particles lighter than about 100 GeV [326]. Therefore, the mirror sector cannot contain very light strongly interacting matter, leaving glueballs at the bottom of the mirror-QCD spectrum. Consequently, mirror glueballs provide the smoking-gun discovery signal for NN frameworks with EW charged top partners.

It is interesting to think about, as yet unconstructed, theories with SM-singlet scalar top partners. If such theories exist, and require no SM-charged states near the weak scale, discovery could be quite difficult. A FSUSY like spectrum with weak-scale soft masses implies mirror glueballs and their accompanying experimental signatures. If, however, the mirror sector contains light matter or mirror-QCD is broken, discovery must proceed through Higgs-portal observables: invisible direct top partner production $h^* \rightarrow \tilde{t}\tilde{t}$ [327, 328], Higgs cubic coupling shifts [176, 327] at a 100 TeV collider, or sub-percent σ_{Zh} shifts at a lepton collider [175]. In each

case, the currently understood sensitivity extends only to singlet stop masses of about 300 GeV for the considered future machines (depending on the number and coupling structure of the partners). If the partners are heavier, we must rely on probing the UV completion for discovery channels.

This picture assumes the mirror sector is charged under a mirror QCD. This ensures similar running of the visible and hidden sector Yukawa couplings to protect the one-loop cancellation (see [137] for a recent discussion), but depending on the UV completion scale this is not technically essential.² We also focus on signatures due to the 3rd generation partners, because of their direct link to the hierarchy problem. Other signatures (like EW precision tests, or direct production of the first two generations and subsequent quirky annihilation [167, 311]) are certainly possible. Finally, it is likely possible to engineer theories that avoid these smoking-gun signatures. Nevertheless, this generic expectation gives an instructive overview of the experimental potential for probing NN.

Given the importance of mirror glueball signatures, we study their phenomenology in detail. We find that, for representative mirror sectors, the lightest glueball is favored to have a mass in the $\sim 10 - 60$ GeV range, which permits production via exotic Higgs decays. There are still uncertainties in our understanding of pure glue dynamics, most importantly possible mixing effects between glueballs and the Higgs and details of hadronization. We outline how to effectively account for these unknowns in a collider study, and demonstrate that concrete sensitivity predictions

²There are uncolored top partner theories without mirror color [163], but the scale of the UV-completion, defined broadly as the scale where additional states appear, is only a few TeV in the fully natural case.

can still be made.

In our collider analyses we make use of efficiency tables for the reconstruction of displaced vertices (DVs) supplied by the ATLAS studies [329,330]. We hope that this simple method for estimating signal yield can serve as a template for future theory studies of scenarios involving long-lived particles.³

We estimate the sensitivity of the LHC to discover these mirror glueballs, and find sensitivity to \sim TeV top partners (scalar or fermion) across the entire mass range with 3000 fb^{-1} of luminosity. This assumes present-day detector capabilities, which may be conservative. New searches are required to achieve this coverage, so our results provide strong motivation to implement the required experimental analyses, some of which require the reconstruction of displaced vertices $50 \mu\text{m}$ from the interaction point.⁴

We also estimate the reach of a 100 TeV collider by scaling the same searches to higher energy. As the triggering and reconstruction capabilities of new colliders are likely to greatly exceed the LHC, these estimates are very pessimistic. Even so, they demonstrate the impressive reach of such machines.

There is potential for an exciting complementarity between the experimental signatures of NN. Top partner direct pair production and annihilation could not only produce another detectable glueball signal [172], but also allow hidden sector masses and couplings to be determined, testing the solution to the hierarchy problem. Higgs coupling measurements would independently hint at the mass of

³The data driven techniques employed by [331,332] may also aid in further studies.

⁴The issue of how to trigger on exotic Higgs decays is a pressing one (see e.g. [137,333]), but we show that standard trigger strategies give significant reach to NN models.

fermionic top partners. Finally, the mirror sector’s connections to cosmology might also be probed: the existence of glueballs implies an absence of light quark flavors, which gives rise to a strong first-order chiral phase transition in the early universe. In that case there may be detectable gravitational-wave signals [154]. Correlating cosmological and LHC signals would serve as a powerful diagnostic of the mirror sector dynamics.

In this chapter we describe, in Sec. 5.1, the expected spectrum and properties of the mirror glueballs associated with the models defined in Chapter 3. In Sec. 5.2 we find the expected experimental reach for these models from exotic decays of the Higgs into mirror glueballs.

5.1 Mirror Glueballs

As outlined above, the mirror sector of many NN theories is pure gauge $SU(3)_B$ at low energies. In this section, we briefly review the resulting mirror glueball spectrum and derive the range of glueball masses favored by RGE evolution for a range of mirror sectors. We find that mirror glueballs, if they exist, are likely to have masses in the $\sim 10 - 60$ GeV range. We also show the form of the effective mirror-gluon coupling to the visible SM-like Higgs through a top partner loop, and discuss the resulting mirror glueball and Higgs decays.

5.1.1 Spectrum

The low-energy spectrum of a pure SU(3) gauge theory has been computed on the lattice by [317, 334]. There are 12 stable (in the absence of other interactions) J^{PC} eigenstates, shown in Fig. 5.1. Masses are given as multiples of m_0 , the mass of the 0^{++} scalar glueball state at the bottom of the spectrum. In terms of the familiar $\overline{\text{MS}}$ QCD confinement scale, $m_0 \approx 7\Lambda_{\text{QCD}}$ to a precision of about 5%. The other glueball masses, as a multiple of m_0 , are known to \sim few % or better. Above $\sim 2 - 3 m_0$ there is a continuum of glueball states that decay down to the 12 stable states shown in Fig. 5.1. Hadronization will be discussed in Sec. 5.1.4.

The mass of the mirror glueballs is entirely determined by the running of the B sector strong coupling constant $\alpha_s^B(\mu)$. Given the mirror sector matter content we can compute the running $\alpha_s^B(\mu)$ using the standard one-loop beta function. Define μ_{pole}^B as the scale satisfying $\alpha_s^B(\mu_{\text{pole}}^B)^{-1} = 0$, and similarly μ_{pole}^A for the visible sector. The A -sector beta function is also computed at one-loop and matched to the measured value of $\alpha_s(m_Z)$. The mirror glueball mass can then be obtained using the lattice result [334]:

$$m_0 = a_0 \cdot r_0^{-1}, \quad a_0 = 4.16 \pm 0.12, \quad (5.1)$$

where r_0^{-1} is the hadronic scale, with $(r_0^{\text{SM}})^{-1} = 410 \pm 20$ MeV. Rather than computing r_0 in the mirror sector directly from the running gauge coupling, which requires a more sophisticated treatment than one-loop RGEs, we estimate it by a simple

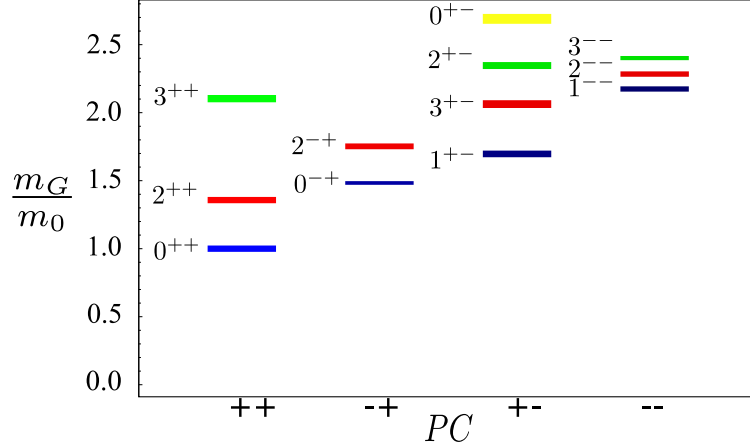


Figure 5.1: Spectrum of glueballs in pure SU(3) theory [317], arranged by J^{PC} quantum numbers. Plot taken from [319]. Masses given in units of $m_{0^{++}} = m_0 \approx 7\Lambda_{\text{QCD}}$.

rescaling of the one-loop Landau poles,

$$m_0 = a_0 \cdot (r_0^{\text{SM}})^{-1} \frac{\mu_{\text{pole}}^B}{\mu_{\text{pole}}^A} . \quad (5.2)$$

We then compute the well-motivated range of m_0 in several representative NN theories, showing that glueball masses below half the Higgs mass are strongly theoretically favored. We take a_0 and r_0^{SM} at their central value for these estimates.

Folded SUSY

In FSUSY without soft masses or Yukawa terms, the Kaluza-Klein (KK) - states of A -quarks (B -squarks) have masses $\{0, 1/R, 2/R, \dots\}$, while the A -squarks (B -quarks) have masses of $\{1/(2R), 3/(2R), \dots\}$. Both sectors have identical gauge-KK-towers, with no zero-mode gauginos. At each threshold $n/(2R)$ the A - and B -states have different spin but identical gauge quantum numbers and multiplicities. Their contributions to the $\alpha_s^{A,B}$ beta-functions are identical, so the two $SU(3)_{A,B}$

strong interactions have identical couplings.⁵

The introduction of soft masses and Yukawa terms results in very small shifts to the KK-towers, assuming $m_{\text{KK}}^2 \gg m_{\text{soft}}^2, m_{\text{Yukawa}}^2$. The most significant effect is the lifting of zero modes. Assuming the largest B -squark soft mass is larger than the A -sector top mass, the two strong couplings track each other from some UV-completion scale $\mu = \Lambda_{\text{UV}}$ down to $\mu = m_{\mathbb{Z}_2}$, which we designate as the scale (near the largest B -squark soft mass) where the \mathbb{Z}_2 symmetry between the two strong couplings is broken.

Without knowing the soft mass spectrum of the theory it is impossible to predict the mirror glueball mass m_0 precisely. However, it is possible to highlight the range m_0 can take. Heavier mirror sector soft masses lead to heavier glueballs, since less light matter causes the mirror-QCD to confine more quickly in the IR. Therefore, we find the most probable range of glueball masses by considering the opposite extremes of possible particle masses.

Without loss of generality, \tilde{t}_1^B can be designated as the lightest B -squark zero mode. Its mass, $m_{\tilde{t}_1}$, sets the bottom of the mirror sector matter spectrum. For a given $m_{\mathbb{Z}_2}$ where $\alpha_s^A(m_{\mathbb{Z}_2}) = \alpha_s^B(m_{\mathbb{Z}_2})$, we compute $\alpha_s^B(\mu)$ at one-loop order for two scenarios: one where all the B -squarks except \tilde{t}_1 have mass $m_{\mathbb{Z}_2}$, and one where all B -squarks are degenerate with \tilde{t}_1 . The resulting minimum and maximum values of m_0 for different $m_{\mathbb{Z}_2}$ are shown in Fig. 5.2. For values of $m_{\mathbb{Z}_2}$ up to 20 TeV, which is very high considering the Higgs mass is only protected at one-loop, the glueball mass

⁵Small differences are introduced at two-loop [335], but this should not affect our estimate of m_0 in a significant way.

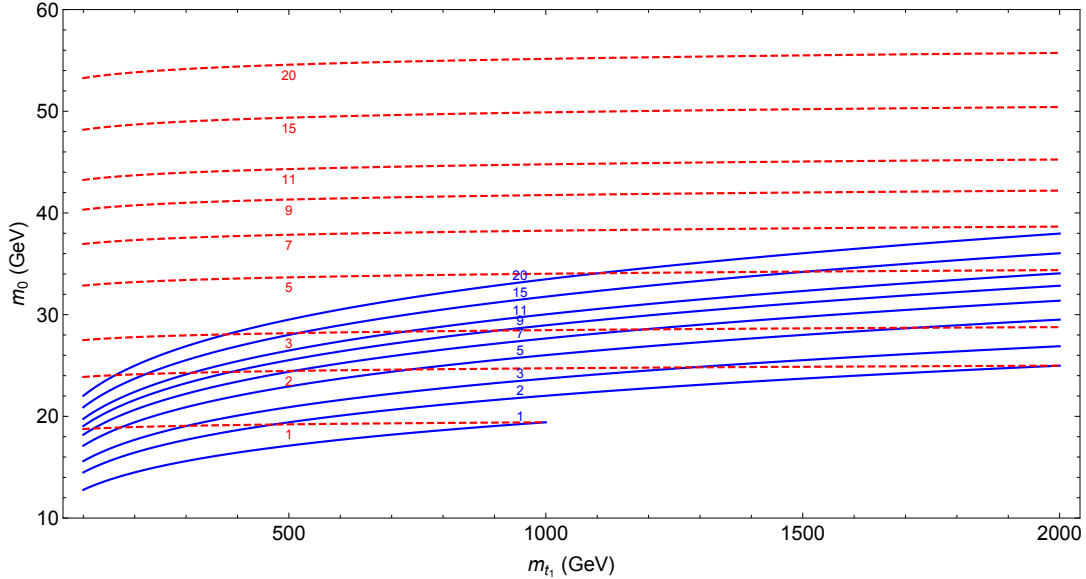


Figure 5.2: The minimum (blue) and maximum (red dashed) glueball mass m_0 as a function of the lightest B -squark mass in FSUSY. Different contours correspond to m_{Z_2} varying from 1 to 20 TeV. For the minimum glueball mass, all squarks were taken to have mass m_{t_1} . For the maximum glueball mass, all squarks except \tilde{t}_1 were taken to have mass m_{Z_2} .

ranges from $\sim 12 - 55$ GeV. While these extremes do not represent the most natural realizations of the framework, they span the lightest to heaviest glueball possibilities, with the more motivated models lying within these boundaries. For instance, if we keep the entire third generation at the light stop mass (a “Natural SUSY”-like construction [336]) then the upper glueball mass bound is lowered slightly to 50 GeV.

Twin Higgs

In the MTH model, the entire SM fermion spectrum is duplicated in the B sector. In that case there are no mirror glueballs, because the u_B, d_B, s_B and possibly

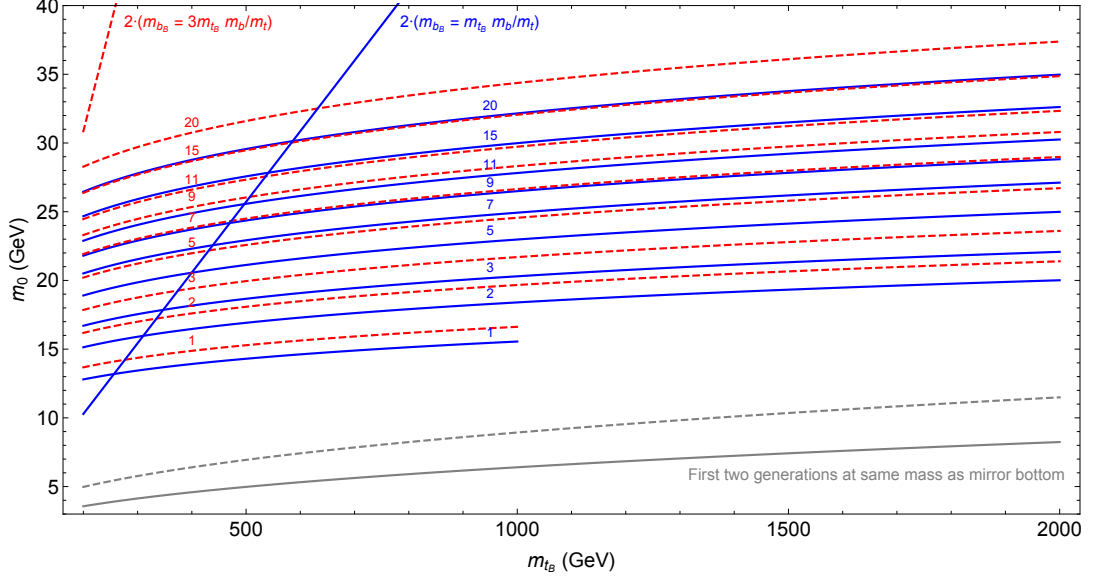


Figure 5.3: Glueball masses in TH models where the mirror symmetry is broken for the first two quark generations and optionally also the bottom quark, as a function of $m_{\mathbb{Z}_2}$ (contour labels) and the mirror top mass m_{t_B} . Blue (dashed red): for $m_{Q_{B_{1,2}}} = m_{\mathbb{Z}_2}$ and $m_{b_B} = r \cdot m_{t_B} \frac{m_b}{m_t}$, with $r = 1$ (3). Gray (dashed gray): for $m_{Q_{B_{1,2}}} = m_{b_B} = r \cdot m_{t_B} \frac{m_b}{m_t}$, with $r = 1$ (3). (In this case, there is no dependency on $m_{\mathbb{Z}_2}$ since all mirror states are light.) Note that glueball states only exist if they are lighter than approximately twice the lightest hidden sector quark (straight lines).

also the c_B quarks are lighter than m_0 .

Departing from the exact mirror symmetry assumption, a variety of hidden sector spectra are possible. This makes it impossible to predict, without additional information, whether mirror glueballs are realized in the TH framework, and at what masses. Even so, we can demonstrate that glueballs below half the Higgs mass are a plausible and well-motivated possibility.

For example, the FTH model [137] contains only third-generation b_B, t_B quarks in the mirror sector, which is sufficient to preserve the TH mechanism. Assuming

the two QCD forces unify $\alpha_s^A(m_{\mathbb{Z}_2}) = \alpha_s^B(m_{\mathbb{Z}_2})$, we can then calculate the glueball mass as a function of m_{t_B} and the scale $m_{\mathbb{Z}_2}$ as for FSUSY above. This is shown as the blue contours in Fig. 5.3, and motivates glueballs in the $\sim 12 - 35$ GeV range.

The glueball mass has to be below approximately twice the mirror bottom mass $m_{b_B} = m_{t_B} \frac{m_b}{m_t}$ for glueball states to form.⁶ Therefore, in the above scenario, there are no glueballs for mirror tops lighter than about 400 GeV. As we saw in chapter 4, however, TH top partners of such low masses lead to Higgs coupling deviations greater than 20%, which will be effectively probed by LHC run 2, see also [311].

It is possible to break the mirror symmetry even further and allow the mirror b -quark to depart from the \mathbb{Z}_2 prediction by a modest amount. The red dashed contours in Fig. 5.3 show the glueball mass if the mirror bottom mass is enhanced by a factor of 3. The effect on the glueball mass is minor, but glueballs can now exist for mirror tops as light as 200 GeV. Similarly, the mirror b -quark can be lighter than expected, which would decrease the parameter space with glueballs at the bottom of the spectrum.

Another possible scenario is a non-maximally broken mirror symmetry for the first two quark generations — rather than completely removing them from the spectrum (pushed to $m_{\mathbb{Z}_2}$), they could merely be significantly heavier than expected by the $\cot \vartheta$ scaling of the B sector masses, Eq. (4.8). The glueball mass for this scenario, where $m_{Q_b} = r \cdot m_{t_B} \frac{m_b}{m_t}$ with $r = 1$ or 3 , is shown as gray lines in Fig. 5.3.

⁶See [137] for a careful discussion of the relative importance of mirror bottomonium and glueballs in the FTH model. We avoid these complications here and focus on the regime where glueball states dominate the low-energy mirror sector.

This leads to glueballs with a mass of a few to 10 GeV, with no dependence on $m_{\mathbb{Z}_2}$.

Finally, it is possible that the \mathbb{Z}_2 symmetry is only approximate at $m_{\mathbb{Z}_2}$ (possibly due to threshold effects at even higher scale). A 10% difference between g_3^A and g_3^B can change the glueball masses by about an order of magnitude in either direction compared to the above predictions [137]. That being said, if the deviations are the typical size of threshold corrections at $m_{\mathbb{Z}_2}$, then the range of possible glueball masses is similar to that obtained in FSUSY.

In summary, while the TH framework makes it difficult to predict the existence or mass of mirror glueballs, there are many scenarios, including the FTH, where glueballs in the $\sim 10 - 60$ GeV mass range arise. This motivates our close examination of glueballs in this window.

Quirky Little Higgs

The mirror sector spectrum of the QLH [167] framework is similar to FSUSY, but containing a fermionic partner for each SM quark. All except the top partner, however, are given bulk masses to remove them from the low energy spectrum. This is phenomenologically motivated by LEP limits and the EW charge of the B sector partners. This results in approximately the same range of preferred m_0 values as the FSUSY setup described above.

5.1.2 Mirror Gluon Coupling to a SM-like Higgs Boson

The visible SM-like Higgs couples to mirror gluons through a top partner loop, in exact analogy to its coupling to visible gluons through a top loop. Assuming the top partner is significantly heavier than $m_h/2$, this interaction is described by an effective dimension-6 operator:

$$\begin{aligned}\delta\mathcal{L}^{(6)} &= \frac{\alpha_s^B}{3\pi} \left[\frac{y^2}{M^2} \right] |H|^2 G_{\mu\nu}^{(B)} G^{(B)\mu\nu} \\ &= \frac{\alpha_s^B}{3\pi} \left[\frac{y^2}{M^2} \right] v h G_{\mu\nu}^{(B)} G^{(B)\mu\nu} + \dots\end{aligned}\tag{5.3}$$

where H is the SM-like Higgs doublet, $G_{\mu\nu}^{(B)}$ is the mirror gluon field strength, and the second line arises from the substitution $H \rightarrow (0, (v+h)/\sqrt{2})^T$. We adopt the notation of [319] and use $[y^2/M^2]$ as a coefficient that is independently set for each theory.

Dimension-8 operators coupling two gluons to two visible or mirror sector EW gauge bosons can also be generated, depending on the top partner quantum numbers. This can open additional decay channels, but for top partners above ~ 100 GeV they do not significantly contribute to the 0^{++} decay width [319], which is our primary focus.

Folded SUSY

The B -sector squark zero modes in FSUSY have a standard MSSM spectrum, with stop mass matrix

$$M_{\tilde{t}\tilde{t}}^2 = \begin{pmatrix} \hat{M}_{\tilde{t}_L}^2 + m_t^2 & m_t X_t \\ m_t X_t & \hat{M}_{\tilde{t}_R}^2 + m_t^2 \end{pmatrix}, \quad (5.4)$$

where

$$\hat{M}_{\tilde{t}_L}^2 = m_{Q_3}^2 + \frac{1}{6} \cos 2\beta (1 + 2 \cos 2\theta_w) m_Z^2, \quad \hat{M}_{\tilde{t}_R}^2 = m_{U_3}^2 + \frac{2}{3} \cos 2\beta \sin^2 \theta_w m_Z^2 \quad (5.5)$$

are dominated by the Higgs independent soft masses.⁷ On the other hand, the terms depending on

$$m_t = \frac{1}{\sqrt{2}} \lambda_t \sin \beta v, \quad X_t = A_t - \mu \cot \beta, \quad (5.6)$$

arise from the B -stops' interaction with the Higgs field. The leading contributions to the hGG operator in Eq. 5.3 are therefore (see e.g. [337])

$$\frac{y^2}{M^2} = \frac{1}{16} \frac{1}{v^2} \left[\frac{m_t^2}{m_{\tilde{t}_1}^2} + \frac{m_t^2}{m_{\tilde{t}_2}^2} - \frac{m_t^2 X_t^2}{m_{\tilde{t}_1}^2 m_{\tilde{t}_2}^2} \right]. \quad (\text{Folded SUSY}) \quad (5.7)$$

A useful benchmark point is to assume $X_t = 0$ and $m_{\tilde{t}_1} = m_{\tilde{t}_2} = m_{\tilde{t}}$. In that case,

$$\frac{y^2}{M^2} = \frac{1}{8v^2} \frac{m_t^2}{m_{\tilde{t}}^2}. \quad (5.8)$$

We use the parameter $m_{\tilde{t}}$ to represent both stop masses in FSUSY.

⁷We are being agnostic about how the correct Higgs mass is achieved. In the case of new D -terms given in chapter 4 the variation to our analysis is very subleading.

Twin Higgs

In the TH model each Higgs doublet couples to the gluons in its sector:

$$\delta\mathcal{L}^{(6)} = \frac{\alpha_s^A}{24\pi} \frac{y_t^{A^2}}{m_t^2} |H_A|^2 G_{\mu\nu}^{(A)} G^{(A)\mu\nu} + \frac{\alpha_s^B}{24\pi} \frac{y_t^{B^2}}{m_T^2} |H_B|^2 G_{\mu\nu}^{(B)} G^{(B)\mu\nu}. \quad (5.9)$$

Cancellation of the quadratically divergent contributions to the light Higgs mass from the A - and B -top quarks requires $y_t^A = y_t^B$, which we assume from now on. The SU(2) doublet pNGB h field can be described in a non-linear model (see chapter 4):

$$\begin{aligned} |H_B|^2 &= \frac{f^2}{2} - |H_A|^2 \\ |H_A|^2 &= \frac{f^2}{2} \sin^2 \left(\frac{v+h}{f} \right) = \frac{v_{\text{EW}}^2}{2} + h v_{\text{EW}} \cos \vartheta + \dots \end{aligned} \quad (5.10)$$

where we have used the definitions in Eq. (4.5), up to a factor of $\sqrt{2}$, in the definition of f . The relevant dimension-6 operator coupling the visible SM-like Higgs to both visible and mirror gluons is therefore

$$\delta\mathcal{L}^{(6)} = |H_A|^2 \left[\frac{\alpha_s^A}{24\pi} \frac{y_t^2}{m_t^2} G_{\mu\nu}^{(A)} G^{(A)\mu\nu} - \frac{\alpha_s^B}{24\pi} \frac{y_t^2}{m_T^2} G_{\mu\nu}^{(B)} G^{(B)\mu\nu} \right]. \quad (5.11)$$

The $[y/M]$ coefficient in Eq. (5.3) is read off the second term:

$$\frac{y^2}{M^2} = \frac{1}{8} \frac{y_t^2}{m_T^2} \cos \vartheta = \frac{1}{4v_{\text{EW}}^2} \frac{m_t^2}{m_T^2} \cos \vartheta. \quad (\text{Twin Higgs}) \quad (5.12)$$

Quirky Little Higgs

The nonlinear low energy parameterization of the QLH model is nearly identical to the TH. While there is not a complete copy of the SM, recall from chapter

3 that the B -sector contains a scalar $SU(2)_L$ singlet Φ whose VEV is related to the EW VEV by $v_{\text{EW}}^2 + v_{\Phi}^2 = f^2$, just like TH. The induced coupling of Φ to mirror gluons is then related to the coupling of the Higgs to mirror gluons as above. In short, y/M is identical for the TH and QLH models.

5.1.3 Mirror Glueball Lifetime

The dimension-6 operator Eq. (5.3) allows glueballs to decay to SM particles through an off-shell Higgs. The corresponding decay widths were computed in [319]. For the lightest glueball decaying to two SM particles we have

$$\Gamma(0^{++} \rightarrow \xi\xi) = \left(\frac{1}{12\pi^2} \left[\frac{y^2}{M^2} \right] \frac{v}{m_h^2 - m_0^2} \right)^2 (4\pi\alpha_s^B \mathbf{F}_{0^{++}}^S)^2 \Gamma_{h \rightarrow \xi\xi}^{\text{SM}}(m_0^2), \quad (5.13)$$

where $\mathbf{F}_{0^{++}}^S = \langle 0 | \text{Tr} G_{\mu\nu}^{(B)} G^{(B)\mu\nu} | 0^{++} \rangle$ is the annihilation matrix element of the glueball through the scalar operator composed of gluon field strengths, and $\Gamma_{h \rightarrow \xi\xi}^{\text{SM}}(m_0^2)$ is the partial decay width of a SM-like Higgs with mass m_0 , computed to high precision using HDECAY 6.42 [338]. Mirror glueballs therefore have the same SM branching ratios as a SM-like Higgs of the same mass.

The hadronic matrix element can be extracted from lattice studies [334, 339].

We use the more recent result [339]:

$$4\pi\alpha_s^B \mathbf{F}_{0^{++}}^S = f_0 \cdot r_0^{-3} \quad , \quad f_0 = 167 \pm 16 \quad . \quad (5.14)$$

The main observable of mirror-QCD is the glueball mass, so we express the matrix element in terms of m_0 , see Eq. (5.1):

$$4\pi\alpha_s^B \mathbf{F}_{0^{++}}^S = \left(\frac{f_0}{a_0^3} \right) \cdot m_0^3 \approx (2.3) m_0^3 \quad . \quad (5.15)$$

Since $\Gamma_{h \rightarrow \xi\xi}^{\text{SM}}(m_0^2) \sim m_0$, this gives the familiar scaling $\Gamma_{0^{++}} \sim m_0^7/(M^4 m_h^2)$. We take m_0 as an input in our collider study. For this strategy, the main uncertainty in the total width is given by the uncertainty of the dimensionless number f_0^2/a_0^6 , which is about 25%.

The resulting decay length is shown, as a function of m_0 and top partner mass in FSUSY Eq. (5.8) and TH Eq. (5.12) theories, in Fig. 5.4. The 25% lifetime uncertainty on the contours is indicated with blue bands.

Clearly, discovering very light glueballs would be challenging. However, the situation is more promising for the preferred 12 – 60 GeV regime, with decay lengths ranging from microns to kilometers.

The heavier glueball states have lifetimes that are several orders of magnitude longer than 0^{++} . Since that state already decays on macroscopic scales, we will focus exclusively on detecting 0^{++} decays as a probe of NN.

5.1.4 Exotic Higgs Decays

For $m_0 \ll m_h/2$, the inclusive exotic branching ratio of the Higgs to mirror-gluons can be obtained from the SM branching ratio to gluons via a simple rescaling:

$$\text{Br}(h \rightarrow g_B g_B) \approx \text{Br}(h \rightarrow gg)_{\text{SM}} \cdot \left(\frac{\alpha_s^B(m_h)}{\alpha_s^A(m_h)} 4v^2 \left[\frac{y^2}{M^2} \right] \right)^2 \quad (5.16)$$

where $\text{Br}(h \rightarrow gg)_{\text{SM}} \approx 8.6\%$.

The coupling ratio $\alpha_s^B(m_h)/\alpha_s^A(m_h)$ depends on the mirror sector spectrum between m_0 and m_h . Ignoring threshold effects below m_h , it can be estimated by

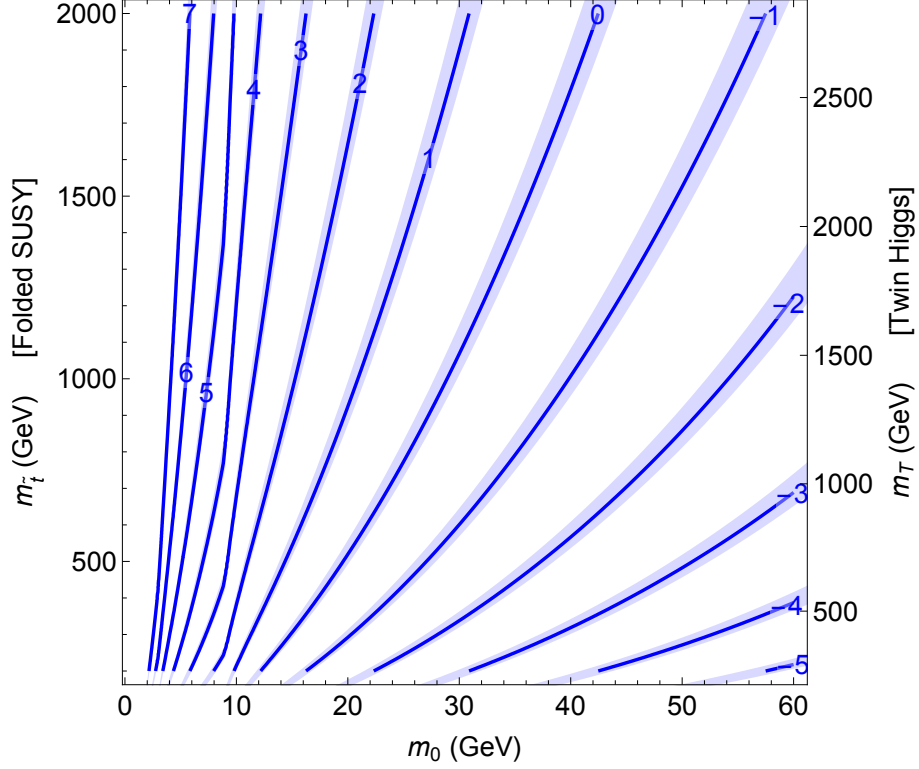


Figure 5.4: Contours show $\log_{10} c\tau/(\text{meters})$, where $c\tau$ is the mean decay length of the lightest glueball state 0^{++} . Computed with Eq. (5.13) in FSUSY Eq. (5.8) and TH Eq. (5.12) theories. The blue bands correspond to the shift of the contours resulting from the 25% uncertainty in the total 0^{++} width.

solving Eq. (5.2) for μ_{pole}^B and evolving to $\mu = m_h$:

$$\alpha_s^B(m_h)^{-1} = \frac{b}{2\pi} \log \frac{m_h}{\mu_{\text{pole}}^B}, \quad \text{where} \quad \mu_{\text{pole}}^B = \mu_{\text{pole}}^A \cdot \frac{m_0}{a_0(r_0^{\text{SM}})^{-1}}. \quad (5.17)$$

The minimal assumption, $b = 11$, corresponds to no mirror sector matter below m_h , which is almost required by LEP limits for FSUSY and QLH. The resulting coupling ratio $(\alpha_s^B(m_h)/\alpha_s^A(m_h))^2$ is shown as the green band in Fig. 5.5 (left), ranging from about 1 to 2.5 for m_0 from 10 to 60 GeV. For a likely FTH scenario, with a single mirror bottom below m_h (assumed for illustrative purposes to be close to m_0 in mass), the ratio is only about 10% higher due to the negative contribution

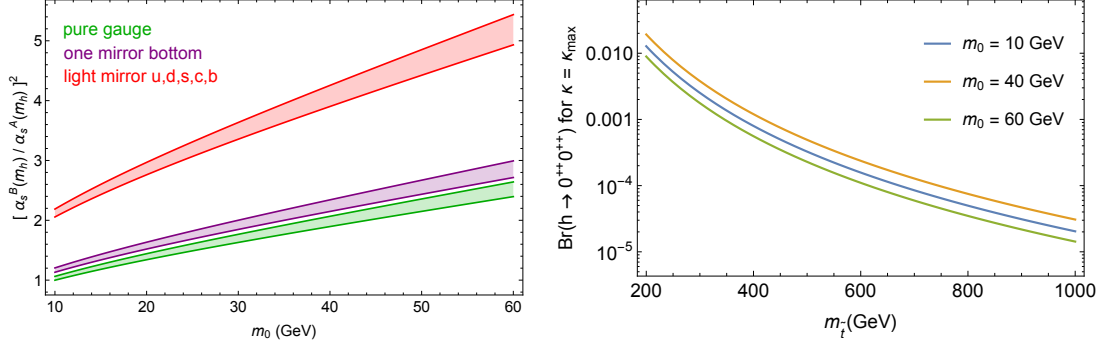


Figure 5.5: *Left:* The overall $(\alpha_s^B(m_h)/\alpha_s^A(m_h))^2$ factor in Eq. (5.16), using one-loop RGE extrapolation from m_0 , assuming either pure gauge (green, $b = 11$), one mirror bottom (purple, $b = 31/3$) or five light mirror quarks (red, $b = 23/3$). The pure gauge and one mirror bottom case closely resemble typical FSUSY and FTH scenarios, respectively. The width of the band represents the range obtained by letting a_0 and r_0^{SM} vary independently within their uncertainties. *Right:* Estimate of $\text{Br}(h \rightarrow 0^{++}0^{++})$ for $\kappa = \kappa_{\text{max}} = 1$ from Eq. (5.18) for FSUSY Eq. (5.8).

to b , as indicated by the purple band. If much more matter is present there can be significant enhancement, as shown by the red band for all mirror quarks being close in mass to m_0 except the mirror top. However, as illustrated by Fig. 5.3, in TH scenarios this is only compatible with glueball masses below about 10 GeV.

5.1.5 Estimating 0^{++} production

Owing to the vastly different lifetimes of the glueball states, we need to estimate the exclusive production rate of 0^{++} from exotic Higgs decays, as it is likely to be the only glueball state that decays observably (though there can be exceptions). This requires detailed knowledge of pure-gluon hadronization, which is not available. However, by parameterizing our ignorance and being pessimistic about signal rates

we can make a conservative sensitivity analysis.

First, we assume 0^{++} glueballs are only produced in symmetric two-body Higgs decays. For very light glueballs ($m_0 \ll m_h/2$) this might seem to be a poor approximation, since mirror hadronization is likely to result in more than two glueballs. Nevertheless, the two-body assumption is suitable for a conservative signal estimate in DV searches. Compared to a realistic modeling of mirror hadronization, which would be challenging to do reliably, it underestimates glueball multiplicity and overestimates the p_T of the resulting glueballs. The former trivially reduces the derived signal, but so does the latter, because the larger boost makes the glueballs more likely to escape the detector in this low-mass long-lifetime regime (see Fig. 5.4). We can then bootstrap an estimate for the exclusive Higgs branching fraction:

$$\text{BR}(h \rightarrow 0^{++}0^{++}) \approx \text{BR}(h \rightarrow gg)_{\text{SM}} \left(\frac{\alpha_s^B(m_h)}{\alpha_s^A(m_h)} 4v^2 \left[\frac{y^2}{M^2} \right] \right)^2 \sqrt{1 - \frac{4m_0^2}{m_h^2}} \cdot \kappa(m_0). \quad (5.18)$$

For our benchmark models of FSUSY and FTH we use the lower green curve in Fig. 5.5 (left) to conservatively estimate $\alpha_s^B(m_h)/\alpha_s^A(m_h)$. The phase-space factor in Eq. (5.18) ensures the branching ratio approaches zero at the kinematic threshold. Finally, $\kappa(m_0)$ is a nuisance parameter which encapsulates our ignorance about glueball hadronization, as well as non-perturbative mixing effects between excited 0^{++*} states and the Higgs. Fig. 5.5 (right) shows the branching ratio for $\kappa = 1$. For a given $[y/M]$ and m_0 , $\text{BR}(h \rightarrow 0^{++}0^{++})$ is completely fixed up to the overall factor κ . A search which is sensitive to these exotic Higgs decays will therefore set an upper bound on κ .

Thermal partition functions with $T \sim \Lambda_{\text{QCD}}$ give one estimate of the relative abundances of the different glueballs [340]. Since the glueball masses are almost an order of magnitude higher than the confinement scale, Boltzmann suppression significantly favors the lightest state 0^{++} relative to the other species, despite the small relative mass difference. These arguments suggest $\kappa \sim 0.5$, but this estimate is unlikely to be correct in detail. For glueball production in exotic Higgs decays, some or all of the heavier glueball final states are forbidden if $m_0 \gtrsim 20$ GeV, further complicating the picture. To span the range of expected possibilities we choose two benchmark functions $\kappa_{\text{min,max}}(m_0)$ that roughly take the decreasing number of available final states with increasing m_0 into account.

With some exceptions (discussed below) it seems unlikely that κ be bigger than unity. Therefore, we define

$$\kappa_{\text{max}} = 1, \tag{5.19}$$

as a maximally optimistic signal estimate. A more pessimistic assumption (given the thermal expectation of $\kappa \sim 0.5$) is that only $\sim 10\%$ of glueballs end up in the 0^{++} state if all two-gluon final states are kinematically allowed. This pessimistic estimate should approach the optimistic one as the glueball mass is increased to the point where only 0^{++} is allowed. We therefore choose the ad-hoc ratio of phase space factors

$$\kappa_{\text{min}}(m_0) = \frac{\sqrt{1 - \frac{4m_0^2}{m_h^2}}}{\sum_i \sqrt{1 - \frac{4m_i^2}{m_h^2}}}, \tag{5.20}$$

where i runs over stable glueball states with $m_i < m_h/2$. (Note the absence of

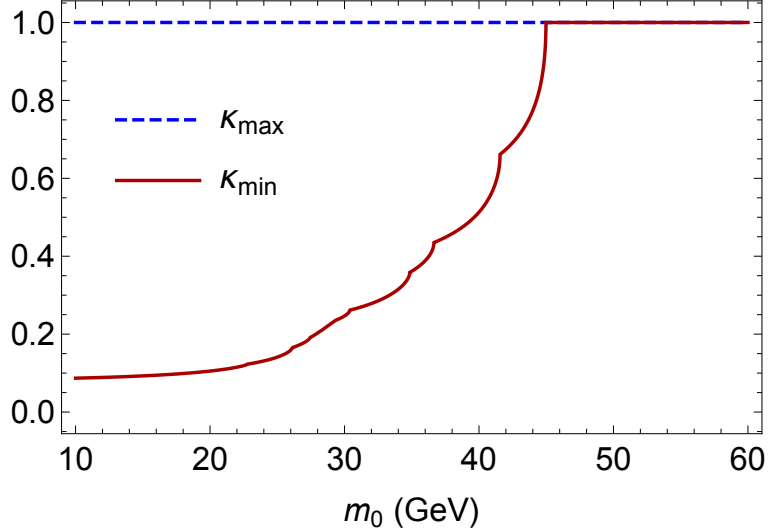


Figure 5.6: The high and low benchmark values for $\kappa(m_0)$, representing optimistic and pessimistic estimates of exclusive $h \rightarrow 0^{++}0^{++}$ production.

spin multiplicities.) This factor ranges from about $1/12$ for $m_0 \sim 10$ GeV to 1 for $m_0 \gtrsim 45$ GeV, see Fig. 5.6. These two assumptions represent optimistic and pessimistic estimates of hadronization effects on the 0^{++} signal rate. Our projections show explicit exclusion regions using $\kappa = \kappa_{\min}, \kappa_{\max}$ to illustrate the potential reach of the LHC and a future 100 TeV collider.

There are also non-perturbative effects which could, for some values of m_0 , modify κ [137]. The 0^{++} glueball, which has the same quantum numbers as the physical Higgs boson, has a tower of excited resonances $0_{(n)}^{++*}$. There is evidence [317] for the first excited resonance $0_{(1)}^{++}$ around mass $m_{0_{(1)}^{++*}} \approx 1.5m_0$. Going up in energy, there are likely to be a few more excited states before they get lost in the glueball continuum. These excited states could mix with the Higgs if $m_{0_{(n)}^{++*}} \approx m_h$, leading to enhancements in $\text{Br}(h \rightarrow 0^{++}0^{++})$, since the glueballs have $\mathcal{O}(1)$ couplings amongst themselves. Similarly, if m_h lies between two such resonances, $\text{Br}(h \rightarrow 0^{++}0^{++})$

could be suppressed. These non-perturbative enhancements and suppressions can be significant, though very likely smaller than a factor of 10.

We interpret these non-perturbative effects as possible enhancements or suppressions of $\kappa(m_0)$ for some glueball masses. To understand when this could be significant, consider a toy-model of four $0_{(n)}^{++*}$ states, with $m_{0_{(n)}^{++*}}/m_0 = 1.5, 2, 2.5, 3$. In that case,

$$m_0 \sim 50, 42 \text{ GeV} \quad (\kappa\text{-enhancement}), \quad (5.21)$$

would enhance κ due to the Higgs mixing with $0_{(4)}^{++*}$ and $0_{(3)}^{++*}$ respectively. On the other hand,

$$m_0 \sim 56, 46 \text{ GeV} \quad (\kappa\text{-suppression}), \quad (5.22)$$

could lead to κ -suppression. The above values of m_0 are indicated in our limit projection plots, to indicate where κ may be significantly different from κ_{\min} or κ_{\max} .

5.2 Sensitivity of Exotic Higgs Decays

The enormous number of Higgs bosons already produced at the LHC, and the fact that mirror glueballs are likely to be in the $\sim 10 - 60$ GeV mass range, make Higgs decays to mirror glueballs an excellent discovery channel for NN. Displaced decay searches are expected to be very sensitive to mirror glueballs.

The HL-LHC will produce about 10^8 Higgs bosons. With $\text{Br}(h \rightarrow 0^{++}0^{++}) \sim 10^{-5} - 10^{-2}$ for Folded SUSY stops in the 200 - 1000 GeV mass range (see Fig. 5.5), the number of produced mirror glueballs could be in the thousands or millions. This

should result in several detectable glueball decays even for kilometer decay lengths.

In this section we estimate the total number of exotic Higgs decay events where, under the assumptions outlined in Sec. 5.1.5, one or more glueballs decay in various subsystems of the ATLAS detector. (The results would be qualitatively similar for CMS.)

These events form the ‘raw material’ for displaced searches. We then apply estimated reconstruction efficiencies and trigger requirements to estimate the actual discovery potential of the LHC, as well as a hypothetical future 100 TeV collider. The HL-LHC could be sensitive to uncolored top partners with TeV scale masses. Achieving full coverage requires several new search strategies, some of which involve the reconstruction of DVs within $50\mu\text{m}$ of the interaction point.

5.2.1 Geometrical Signal Estimates

We start with a purely geometrical signal estimate for the three detector volumes defined in Table 5.1. This gives an intuition for the amount of ‘raw material’ available for DV searches of NN. In the next section, we include triggers and reconstruction efficiencies.

The number of expected glueball decays in these detector volumes is estimated as follows. The HAHM MADGRAPH model [341] is used to simulate the kinematics of Higgs bosons produced via gluon-fusion and vector-boson-fusion. These decay into two scalars s , which each decay dominantly into two b -quarks. This can be used to model the kinematics of $h \rightarrow 0^{++}0^{++}$, $0^{++} \rightarrow \bar{f}f$. The hard matrix element

for $h \rightarrow ss$ is different from the hard matrix element for $h \rightarrow g_B g_B$, but since the Higgs is a scalar the distribution of the final glueballs is isotropic in the Higgs rest frame, which is the case for either matrix element. Glueball decay, on the other hand, occurs long after mirror hadronization, when the glueball is a genuine scalar. This is correctly modeled by having the scalar s decay to $\bar{f}f$.

Matched samples with 0 or 1 extra jet are generated in MADGRAPH 5 and showered in Pythia 6 [342, 343]. The total signal cross section is computed by using the Higgs working group cross sections [344] for gluon fusion or vector boson fusion. These are multiplied by the Higgs to Glueballs branching ratio Eq. (5.18) with $\kappa = \kappa_{\max}$ (κ_{\min}) giving optimistic (pessimistic) signal estimates assuming that the Higgs to glueball decays are dominantly two-body.⁸

Displaced glueball decays are analyzed by extracting the decayed scalars s (the glueballs) from each event, and using their boosted decay length $|\vec{p}_3|/m_0 \cdot c\tau$ and angle θ to the beam axis to compute their probability of decaying within each detector volume in Table 5.1. This allows us to estimate the number of events with (a) at least one glueball decaying in the tracker, and (b) two glueballs decaying in the barrel HCAL or Muon System (MS).

Fig. 5.7 shows the estimated event rates for LHC run 1, the 14 TeV LHC with 3000 fb^{-1} of data, and a hypothetical future 100 TeV pp collider with 3000 fb^{-1} of data. The numbers for the 100 TeV collider should be seen as suggestive, since we

⁸Assuming SM Higgs production is not exactly correct for the TH, where the cross sections are reduced by a factor of $\cos^2 \vartheta$ due to mixing with the mirror Higgs. However, this effect is negligible (compared to other uncertainties) for top partner masses near the edges of sensitivity that we derive. Since we are interested in the top partner mass reach of different searches we neglect this effect to preserve the easy comparison of FSUSY and TH.

	r (m)	$ z $ (m)	$ \eta $
Tracker	(0, 1)	(0, 2.7)	< 2.4
HCAL (barrel)	(2.25, 4.25)	(0, 4.3)	—
Muon System (barrel)	(5, 10)	—	< 1.1

Table 5.1: Extent of detector volumes for geometrical signal estimates, modeled on the ATLAS detector.

use the ATLAS detector geometry to estimate signal yield, and the future detector layout will be different.

Clearly, reconstructing DVs in the tracker is crucial for detecting glueballs above ~ 30 GeV. In principle, the 14 TeV run of the LHC may access top partners as heavy as a TeV, with the potential reach exceeding 3 TeV for the HL-LHC. However, as shown below, triggering and DV reconstruction significantly reduce that sensitivity. Even so, the reach is very relevant for constraining NN models.

5.2.2 Estimated Sensitivity of Searches

The purely geometrical signal estimate of the previous section suggests that the LHC might have very promising reach for NN. However, arriving at a realistic sensitivity estimate is challenging. A detailed collider study involving DVs, and including backgrounds, is far beyond our scope and would be very difficult to validate.

Fortunately, the ATLAS collaboration recently released two experimental searches [329, 330] for exotic Higgs decays of the form $h \rightarrow XX \rightarrow 4f$, where X is long-lived and decays with SM-Higgs-like branching ratios to SM-fermions. This is identical

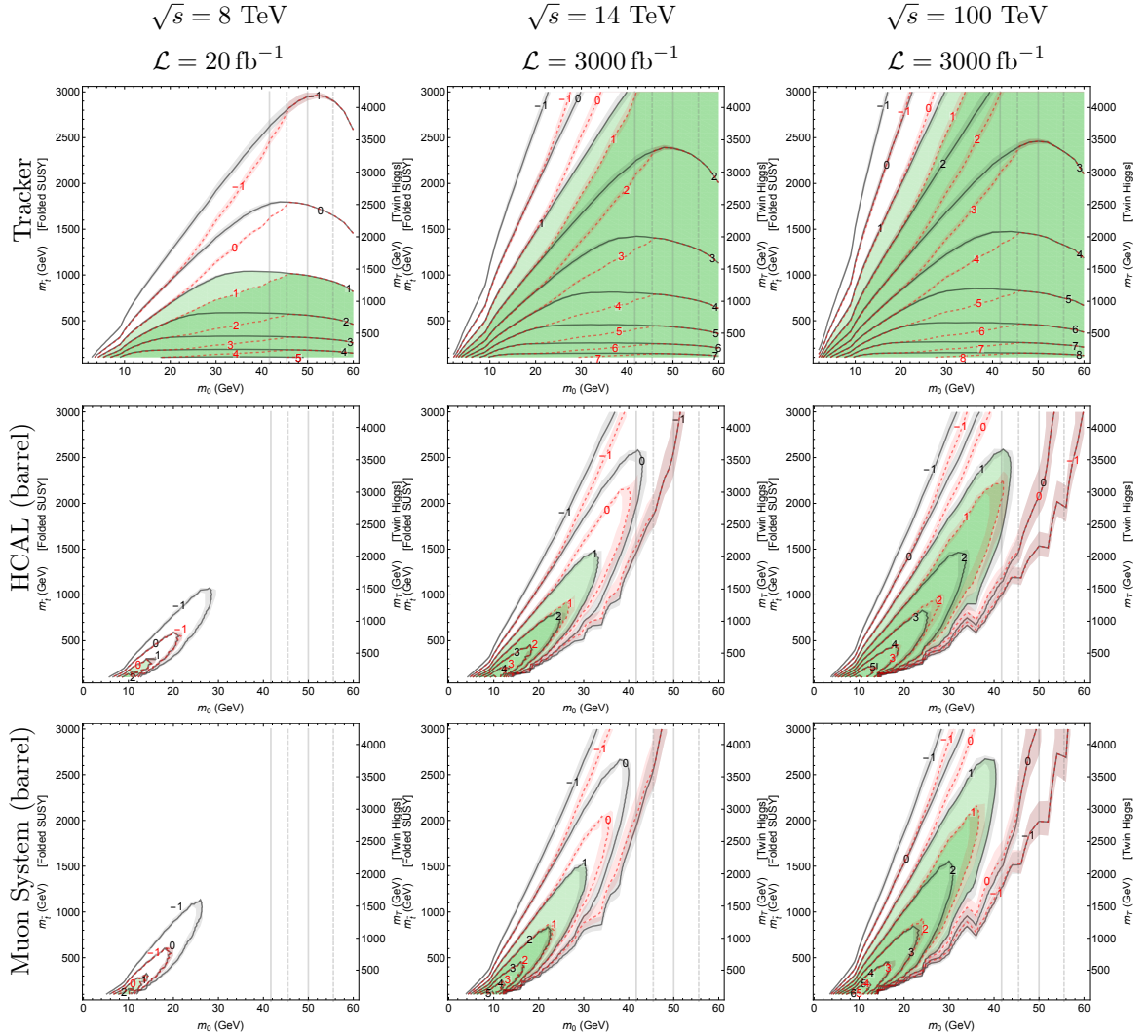


Figure 5.7: Geometrical signal estimates of the number N of Higgs production and decay to gluballs of mass m_0 as defined in Table 5.1. Left, center, and right columns correspond to LHC run 1, HL-LHC, and a hypothetical 100 TeV collider. The vertical axes correspond top partner masses in FSUSY and TH. Black (dashed red) contours show $\log_{10} N$ for $\kappa = \kappa_{\max}$ (κ_{\min}), giving an optimistic (pessimistic) signal estimate assuming h decays dominantly to two glueballs. Shaded bands around contours indicate effects of the 25% uncertainty in 0^{++} lifetime. Vertical solid (dashed) lines show where κ might be enhanced (suppressed) due to non-perturbative mixing effects. Light (dark) green shaded regions have more than 10 events for $\kappa = \kappa_{\max}$ (κ_{\min})

to the $h \rightarrow 0^{++}0^{++}$ signature we are focusing on, and the ATLAS analyses contain important lessons that we can use to estimate LHC reach, both beyond run 1 and beyond these two particular searches.

The first search [329] used specialized triggers to look for a single displaced decay in the HCAL. A second decay in the HCAL was then required to reduce the background to a very low level, about 20 events. The second search [330] followed a similar strategy, using a specialized trigger for displaced decays in the muon system (MS). Two separate offline analyses were performed, which required (a) one DV in the MS and another DV in either the MS or the inner tracker (IT), or (b) one DV in the MS, and at least 4 jets passing stringent p_T cuts. The requirement of one fully reconstructed displaced vertex in addition to either another DV or a hard kinematic cut resulted in, effectively, zero background.

Displaced vertices are a very distinctive signature. The two ATLAS searches suggest (and CMS agrees [347]) that searches for DVs could be regarded as background-free, provided they look for

- (a) two DVs, or
- (b) one DV, in addition to a stringent non-DV requirement, such as high jet activity or leptons.

We suspect these guidelines to be particularly applicable for fully reconstructed DVs in the MS or IT. The absence of track reconstruction in the calorimeters is likely one factor leading to higher (though still very low) background levels in the HCAL search.

Trigger	8 TeV	14 TeV
1 jet	$p_T^{j_1} > 180 \text{ GeV}$	$p_T^{j_1} > 290 \text{ GeV}$
inclusive VBF	$ \eta_{j_1, j_2} > 2$ $\eta_{j_1} \eta_{j_2} < 0$ $ \eta_{j_1} - \eta_{j_2} > 3.6$ $m_{j_1 j_2} > 600 \text{ GeV}$	<p style="text-align: center;">same</p> $m_{j_1 j_2} > 1000 \text{ GeV}$
VBF $h \rightarrow \bar{b}b$	$p_T^{j_{1,2,3}} > (70, 50, 35) \text{ GeV}$ $ \eta_{j_{1,2,3}} < (5.2, 5.2, 2.6)$ $ \eta_{j_1} \text{ or } \eta_{j_2} < 2.6$	$p_T^{j_{1,2,3}} > (112, 80, 56) \text{ GeV}$ <p style="text-align: center;">same</p>
single lepton	<p style="text-align: center;">one lepton with</p> $p_T > 25 \text{ GeV}, \eta < 2.4$	same

Table 5.2: Triggers explored for DV searches of exotic Higgs decays to mirror glueballs. *Top three rows:* three representative jet triggers. The VBF $h \rightarrow \bar{b}b$ trigger is modeled on [345], the others are representative generic triggers [346]. The 14 TeV thresholds are derived from the 8 TeV thresholds by a 60% upscaling, and for illustrative purposes the 100 TeV thresholds are assumed identical to 14 TeV. *Bottom row:* single lepton trigger [346] for DV searches in the $Wh, Zh, t\bar{t}h$ production channels.

The two ATLAS searches looked for particles with about meter decay lengths. However, the geometrical signal estimate demonstrated that sensitivity to much shorter decay lengths is required to cover the whole (m_0, m_{TP}) parameter space of NN theories with long-lived glueballs (where m_{TP} stands for the top partner mass). This forces us to utilize strategy (b), since at present there is no way to trigger on only displaced decays in the tracker without other requirements like high H_T [347]. Therefore, we explore the sensitivity of several possible searches that require one DV in the tracker, and additional hadronic or leptonic activity in the event to trigger on.

A list of prompt trigger candidates, modeled on existing experimental searches,

Search	Displaced Vertex requirements	Conventional Trigger
(IT, $r > 50 \mu\text{m}$) \times (1L)	one DV in IT with $r > 50 \mu\text{m}$	single lepton
(IT, $r > 4 \text{ cm}$) \times (VBF $h \rightarrow bb$)	1 DV in IT with $r > 4 \text{ cm}$	VBF $h \rightarrow \bar{b}b$
(HCAL) \times (HCAL)	2 DVs in HCAL barrel/endcap	—
(MS) \times (MS or IT)	1 DV in MS barrel/endcap and an additional DV in either MS or IT ($r > 4 \text{ cm}$)	—

Table 5.3: Summary of explored DV searches for exotic Higgs decays to mirror glueballs. The (IT) \times (non-DV-trigger) searches in the first two rows are newly suggested searches. (HCAL) \times (HCAL) and (MS) \times (MS or IT) are recasts of [329] and [330]. DV reconstruction efficiencies and trigger information are listed in Tables 5.2 and 5.4.

is presented in Table 5.2. To be conservative we require glueballs to decay to $\bar{b}b$ in order to pass the VBF $h \rightarrow \bar{b}b$ trigger. The multijet trigger from [330] is not included, since it has very low efficiency for Higgs decays. For jet triggers, we follow [330] and assume DV reconstruction down to a minimal impact parameter of $r_{\min} = 4 \text{ cm}$. We find the VBF $h \rightarrow \bar{b}b$ trigger to be the most useful above the $\bar{b}b$ threshold, but other triggers can perform comparably, as we outline in more detail below. Probing parameter regions with relatively heavy glueballs requires sensitivity to even shorter decay lengths, down to $\mathcal{O}(10\mu\text{m})$. Such DV reconstruction might be possible with a clean enough dataset [346]. We test this by requiring exotic Higgs decays from $Wh, Zh, \bar{t}th$ production to pass a single lepton trigger, and assume that DVs can be reconstructed down to $r_{\min} = 50 \mu\text{m}$ with the same efficiency as for $r_{\min} = 4 \text{ cm}$. Such an analysis would, no doubt, be challenging, but our work serves as powerful motivation to pursue this search.

	r (m)	$ z $ (m)	$ \eta $	ϵ_{trig}	offline
Inner Tracker	$(r_{\text{min}}, 0.3)$	$(0, 2.7)$	< 2.4	—	$\epsilon_{\text{DV}} = 0.10$
HCAL (barrel)	$(2.1, 3.5)$	$(0, 4.3)$	—	0.22	$\epsilon_{\text{offline}} = 0.4$
HCAL (endcap)	$(2.25, 3.5)$	$(4.3, 5.0)$	< 3.2	0.07	
Muon System (barrel)	$(4, 6.5)$	—	< 1.1	0.40	$\epsilon_{\text{DV}} = 0.25$
Muon System (endcap)	—	$(7, 12)$	$(1.1, 2.4)$	0.25	$\epsilon_{\text{DV}} = 0.5$

Table 5.4: ATLAS detector regions with sensitivity to DVs. ϵ_{trig} is the efficiency to trigger on a single displaced decay in that detector region. In the tracker and MS, each displaced decay has offline reconstruction efficiency ϵ_{DV} . The overall reconstruction efficiency of an event with two decays in the HCAL that already passed triggers is $\epsilon_{\text{offline}}$. Geometrical definition and approximate efficiencies for displaced $h \rightarrow XX \rightarrow 4f$ decay based on [329] (HCAL) and [330] (Muon System and tracker). For the tracker, [330] gives about $r_{\text{min}} = 4$ cm, which we use as well. However, for a clean final state recorded via the lepton trigger we consider $r_{\text{min}} = 50 \mu\text{m}$ [346].

The four searches we investigate are summarized in Table 5.3: one search of the form (jet activity) \times (DV in IT), another of (lepton) \times (DV in IT), and the two existing searches (HCAL) \times (HCAL) and (MS) \times (MS or IT). We assume these searches have close to zero background and estimate sensitivities accordingly. As explained above, this assumption is likely too optimistic for the HCAL search.

To arrive at approximately realistic signal estimates, it is necessary to understand triggering and offline reconstruction efficiencies for displaced decays. Fortunately, the two ATLAS searches supply these efficiencies either directly, or in the form of final event yields, see Table 5.4. The displaced decay triggers in the HCAL and MS have triggering efficiencies ϵ_{trig} per decay that can be taken to be approximately constant and (for our purposes) independent of glueball mass in the relevant

detector volume. A full DV in the IT or MS can be reconstructed with an offline efficiency ϵ_{DV} per vertex [330]. For displaced decays in the HCAL, an overall offline efficiency $\epsilon_{\text{offline}}$ is applied to the event, which reproduces the ~ 500 signal events predicted for this search at run 1 of the LHC with $\text{Br}(h \rightarrow XX) = 1$ [329].

For the prompt lepton trigger, a flat lepton reconstruction efficiency of 85% is applied. For jet triggers, PGS is used for hadronic object reconstruction. This might not, at first, appear sufficient, since PGS assumes prompt decay. However, when glueball final states are used for triggering the prompt assumption under-estimates trigger efficiency, since it does not take into account collimation of glueball final states decaying on the edge of the tracker, which increases the likelihood of surpassing jet thresholds. Therefore, our simple pipeline is sufficient for a conservative signal estimate.

Our results can be easily rescaled for different DV reconstruction efficiencies. This is especially salient since projecting HL-LHC limits using current ATLAS capabilities may be very conservative. First, even though the CMS displaced dijet search [347] has no sensitivity to exotic Higgs decays due to a large H_T requirement, it does suggest that CMS may be able to reconstruct DVs in the tracker with significantly higher than 10% efficiency. Second, both detectors will undergo upgrades as part of the HL-LHC program, which should greatly improve tracking and triggering capabilities [232, 348]. As a result, the 3000 fb^{-1} signal may be larger than what we project by an $\mathcal{O}(1)$ factor, but this does not affect our main conclusions.⁹

⁹It should be noted that our DV + (lepton or jets) searches are robust at the $\mathcal{O}(1)$ level, even under the pessimistic assumption that most of the unstable glueballs are produced in asymmetric $h \rightarrow 0^{++} + X$ decays. The searches requiring two DV's would have to be modified, but in that

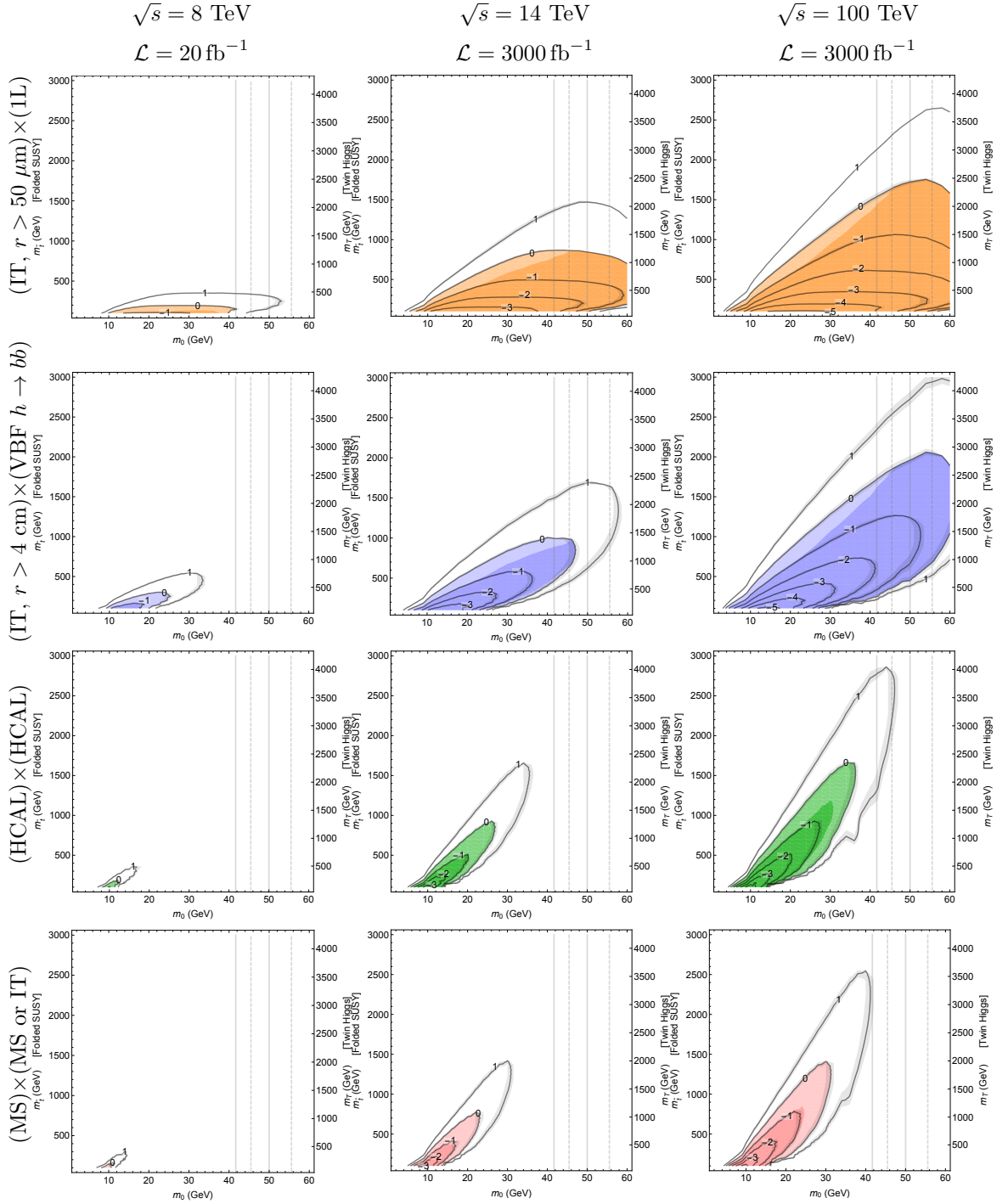


Figure 5.8: Contours of excludable (discoverable) values of $\log_{10} \kappa$, for $\text{Br}(h \rightarrow 0^{++}0^{++})$, if $N = 10$ events can be excluded (discovered) in the four searches of Table 5.3. All formatting same as Fig. 5.7.

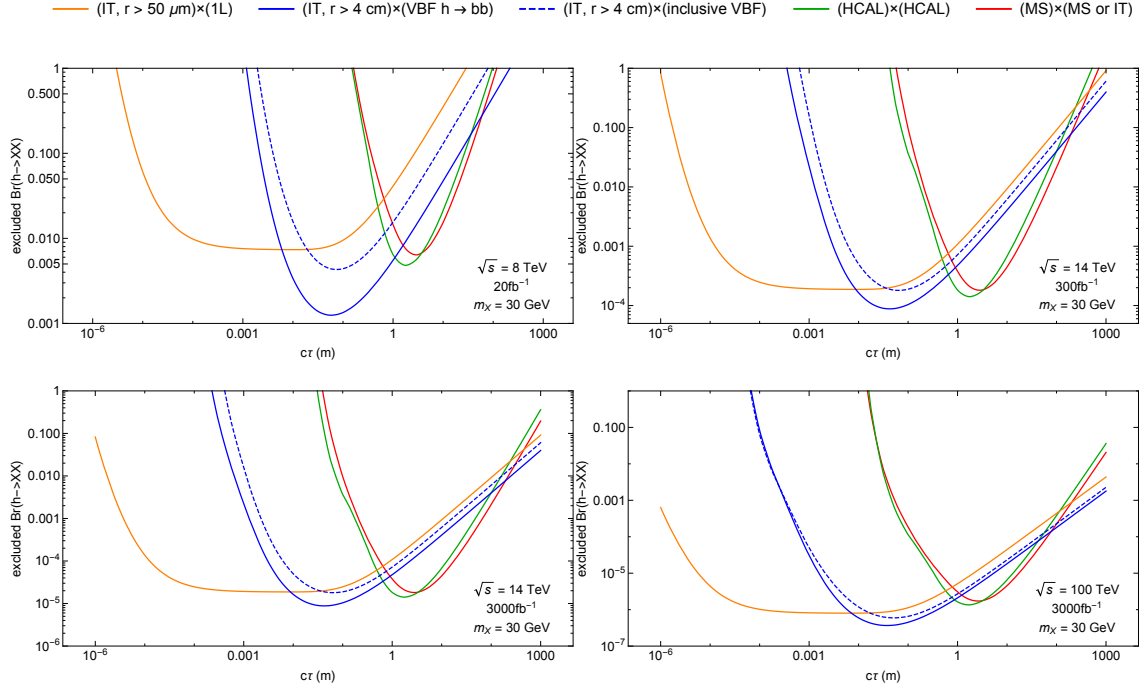


Figure 5.9: Projected sensitivities of the displaced decay searches listed in Table 5.3, expressed model-independently as limits on the exotic Higgs decay branching ratio $\text{Br}(h \rightarrow XX)$ as a function of the proper lifetime $c\tau$ of X , for $m_X = 30$ GeV. Zero background is assumed, which is not likely to be realistic for the HCAL search. Decreasing (increasing) m_X shifts the curves slightly to the left (right).

The results are presented in Fig. 5.8. The dark (light) shaded colored regions indicate which regions of the (m_0, m_{TP}) parameter space give more than $N = 10$ detected signal events for $\kappa = \kappa_{\text{min}} (\kappa_{\text{max}})$, which for a relatively background-free search approximates discovery or exclusion potential. The black contours indicate the value of κ required to give $N = 10$ across the whole parameter space. This allows for an easy rescaling of the actual parameter space exclusions for different

case it should be possible to combine a single reconstructed vertex in the MS or HCAL with a lepton or jet requirement and recover a similar sensitivity to what we show for the MS and HCAL searches.

hypotheses of what $\kappa(m_0)$ might be. It also makes clear that our conclusions are robust even assuming $\mathcal{O}(1)$ uncertainties for our signal estimate (as might be the case if additional cuts are required to reduce background to zero in a realistic analysis). We also show the sensitivity of these searches in a model-independent way, as projected limits on the exotic Higgs decay branching ratio $\text{Br}(h \rightarrow XX)$ as a function of lifetime for $m_X = 30$ GeV in Fig. 5.9.

The 8 TeV (HCAL) \times (HCAL) and (MS) \times (MS or IT) searches have very little sensitivity to NN, and only probe a small part of parameter space with very light top partners.¹⁰ The MS limits in Fig. 5.9 agree well with the experimental exclusions [330], while our background-free assumption overestimates the sensitivity of the HCAL compared to the published limits [329], as expected. If the two new searches with a single DV in the IT were performed on the run 1 dataset, mirror glueballs lighter than about 40 GeV could be probed for top partner masses of about 100 – 300 GeV.

At the HL-LHC, the most coverage is achieved by looking for one DV in association with a lepton. For lighter glueballs, jets + one DV or two DVs in the muon system provide additional coverage. The jets + one DV search could cover much of the same parameter space as the lepton + one DV search if DV reconstruction down to $r_{\min} = 50 \mu\text{m}$ was possible for that search as well. Overall, the HL-LHC should be able to probe NN via Higgs to glueball decay with top partner masses up to about a TeV for a wide range of theoretically motivated glueball masses.

¹⁰This region is already probed by $h \rightarrow \gamma\gamma$ signal strength measurements and other Higgs coupling measurements for the case of FSUSY and TH respectively [311].

The reach at the 14 TeV LHC with only 300 fb^{-1} can be easily read off from Fig. 5.8 by shifting the exclusions one $\log_{10} \kappa$ contour inward, corresponding to a factor of 10 reduction in signal compared to the HL-LHC. Most of the glueball masses are covered, and top partners up to $500 - 700 \text{ GeV}$ can be probed, though the lepton + one DV search loses sensitivity for $m_0 \sim 60 \text{ GeV}$, $m_{\text{TP}} \sim 200 \text{ GeV}$.

The 100 TeV results are illustrative only, since our assumptions are driven by the limitations of present-day experiments. By the time the next collider is built, it is likely that full track reconstruction can be used for low-level triggering, if triggering is needed at all. DV reconstruction capabilities might be superior as well. That being said, new backgrounds, like those from B and D decays, which are not essential at current energies and luminosities, may play a role at 100 TeV. Even so, our estimates serve to demonstrate an enticing potential sensitivity to exotic Higgs decays with glueballs in the final state. This provides strong motivation to make sure such relatively soft signatures, which in this case give access to multi-TeV scale top partner masses, are not missed in the detector design of future machines.

We have used the VBF $h \rightarrow \bar{b}b$ and the inclusive VBF trigger for our example of a (jets) \times (IT) type search. In Fig. 5.10 we show how sensitivity depends on the type of jet trigger utilized for a search at the HL-LHC. All the jet triggers have roughly comparable performance.

Finally, it is possible that other glueball decays provide additional sensitivity in certain parts of parameter space. For example, the 2^{++} glueball has a mass of $\approx 1.4m_0$ and a lifetime several orders of magnitude longer than the 0^{++} state [319]. Depending on the details of mirror hadronization, $h \rightarrow 2^{++} + X$ decays may therefore

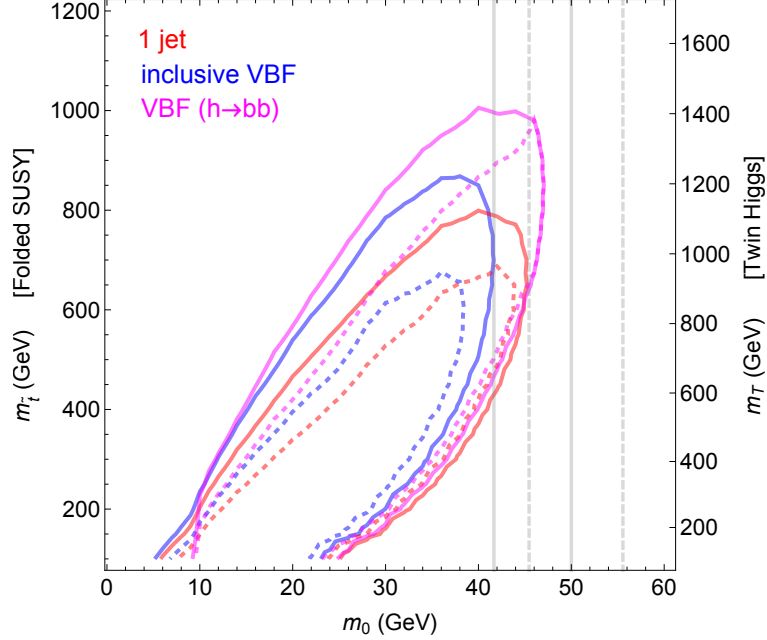


Figure 5.10: Comparison of different $(IT, r > 4 \text{ cm}) \times (\text{jet trigger})$ searches for $\sqrt{s} = 14 \text{ TeV}$ with 3000 fb^{-1} . The solid (dashed) lines bound regions with more than 10 signal events for $\kappa = \kappa_{\text{max}}$ (κ_{min}). For the purpose of this comparison, glueball lifetime uncertainties are not shown.

produce DV's in the tracker or MS for $30 - 40 \text{ GeV} \lesssim m_0 < 52 \text{ GeV}$, when decays to 2^{++} are kinematically allowed, and 0^{++} is relatively short-lived.

The overall lesson of our investigation is clear. The LHC has great potential to probe NN. Exotic Higgs decays to mirror glueballs, with reconstruction of the subsequent displaced decay down to $50 \mu\text{m}$ from the interaction point, give sensitivity to glueballs across the theoretically preferred $12 - 60 \text{ GeV}$ range, with uncolored top partner masses up to around a TeV.

In this chapter we present the first detailed phenomenological analysis of these exotic Higgs decays to mirror glueballs. RG arguments suggest that the lightest and most unstable glueball, which is a prediction of FSUSY and QLH models and a

possible outcome of the TH scenario, has a mass in the $\sim 10 - 60$ GeV range, which makes the discovered 125 GeV SM-like Higgs a powerful probe of NN. A careful treatment of hadronization and non-perturbative uncertainties of the mirror sector allows us to perform an explicit signal estimate for the 8 and 14 TeV LHC, as well as a hypothetical 100 TeV machine. This is greatly aided by efficiency tables for DV reconstruction released by the ATLAS collaboration [329, 330]. We suggest several new searches requiring one DV in the IT along with jet or lepton triggers. This approach is vital to probe glueballs with $\gtrsim 30$ GeV masses, and strongly motivates the reconstruction of DVs with decay lengths $\sim 50 \mu\text{m}$.

The discovery potential of various searches is summarized in Fig. 5.11. Our approach for estimating signal has been conservative, both by assuming only two-body production of 0^{++} from Higgs decays and by assuming present-day ATLAS detector capabilities for all future projections. Even so, the achievable reach at the LHC across the whole range of considered glueball masses is impressive. Folded-stops could be discovered with masses up to 600 (1100) GeV at the LHC with 300 (3000) fb^{-1} of data, while TH top partners could be accessible with masses up to 900 (1500) GeV. At a 100 TeV collider, top partner masses in excess of 2 TeV are easily probed. This allows for an exciting complementarity between measuring the low-energy consequences of NN and directly probing details of the UV completion required by such theories.

Fig. 5.11 also shows the TLEP limit [273] on $\text{Br}(h \rightarrow \text{invisible})$, as applied to the perturbative prediction for $\text{Br}(h \rightarrow \text{all glueballs})$. However, lepton colliders could also set powerful limits by directly looking for prompt or displaced $h \rightarrow 4b$

decays. This channel deserves future study. Indirect constraints on FSUSY from Higgs coupling measurements will only constrain for top partner masses $\lesssim 350$ GeV [311]. Direct production of first and second generation FSUSY mirror squarks would be a distinctive signal, but their mass is not tied directly to the little hierarchy problem and they could easily escape detection in a natural theory [311]. In the TH and QLH models, precision Higgs measurements with 3000 fb^{-1} of data may probe top partners up to $\lesssim 800$ GeV (depending on the cutoff). Exotic Higgs decay searches could easily surpass this sensitivity.

All the searches we examine lose sensitivity if the glueball mass is below the $\bar{b}b$ threshold. This leads to very long glueball lifetimes and very few decays in the detector. While theories with EW top partners (FSUSY, QLH) motivate glueballs heavier than 12 GeV, such light and long-lived glueballs can easily be realized in TH models, and developing searches with sensitivity to these scenarios is highly motivated.

It has long been understood that future lepton colliders allow for the detection of all known natural TH scenarios through precision Higgs coupling measurements. We demonstrated that the LHC has sensitivity to TeV-scale top partners through exotic Higgs decays to mirror glueballs, which covers FSUSY and QLH theories. This makes clear once again the special role of the Higgs in probing naturalness. This complementarity puts all known uncolored top partner theories within our reach, and might allow us to eventually probe naturalness in all its forms.

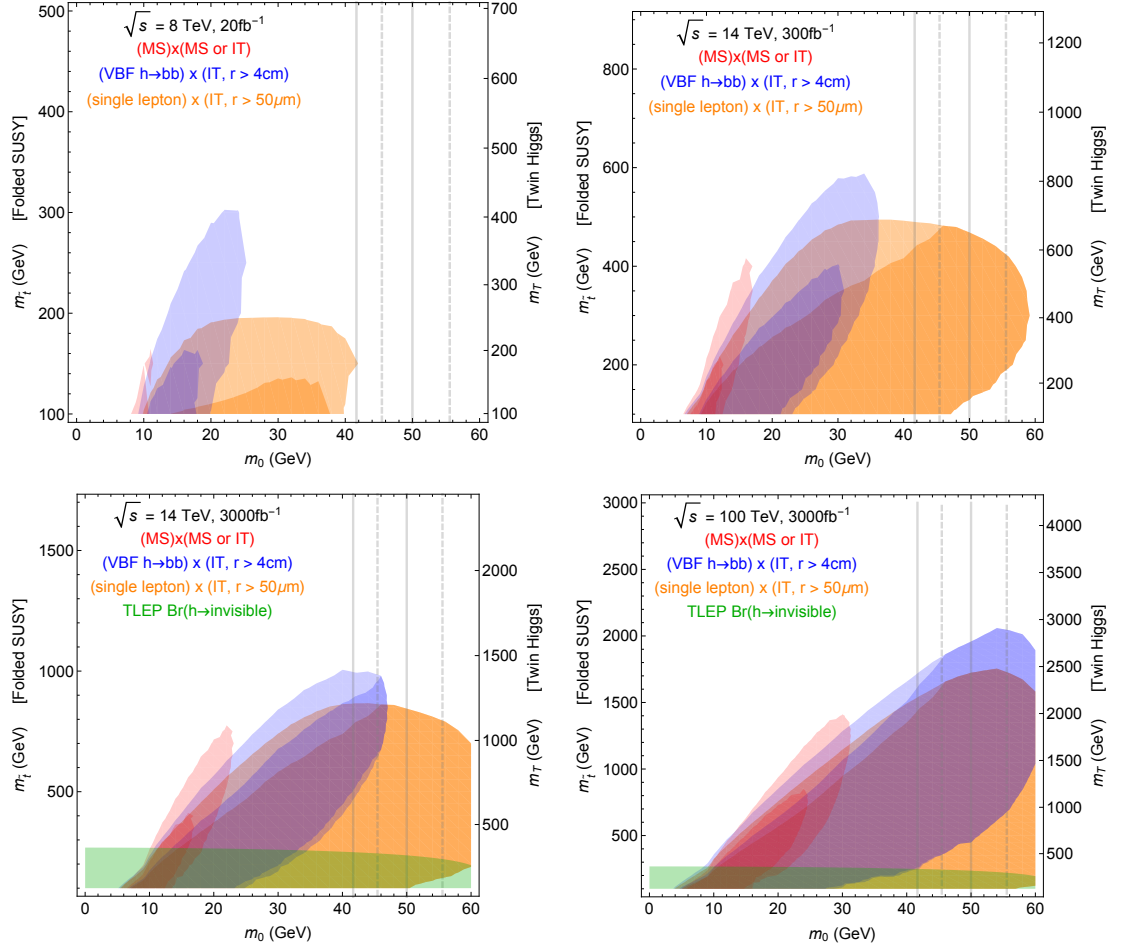


Figure 5.11: Summary of discovery potential at LHC run 1, LHC14 with 300 fb^{-1} , HL-LHC and 100 TeV if searches like those in Table 5.3 are approximately background-free, and ~ 10 events allow discovery. Note different scaling of vertical axes. The inclusive TLEP $h \rightarrow \text{invisible}$ limit, as applied to the perturbative prediction for $\text{Br}(h \rightarrow \text{all glueballs})$, is shown for future searches. Lighter (darker) shading corresponds to optimistic (pessimistic) signal estimates $\kappa = \kappa_{\text{max}}$ (κ_{min}), assuming h decays dominantly to two glueballs of mass m_0 . The vertical axes correspond to top partner mass in FSUSY and TH or QLH. Vertical solid (dashed) lines show where κ might be enhanced (suppressed) due to non-perturbative mixing effects.

Chapter 6: Conclusion

The discovery of the Higgs has been rightly recognized as a triumph for the SM. However, there must be particles and interactions beyond the SM to explain dark matter and the matter-antimatter asymmetry. Other puzzles, like flavor structure and the lack of CP violation in QCD, point outside the SM for their solutions. In short, the SM must be an EFT, albeit an remarkably successful one. Still, the enticement of leaving the SM for unknown waters drive theory and experiment to carefully examine every possible point of departure. Because the Higgs mass is tied to the EFT cutoff, the Higgs is a window onto whatever lies beyond.

With its extensively planned and precisely executed program, the LHC is poised to make great discoveries during its second run. In fact, hints of something beyond the standard model are already in the air [349–354]. These results are very preliminary, but they have the potential to address at least one of the outstanding mysteries in particle physics. If they signal a new particle, then its mass is about right to connect it to a natural Higgs mass. While this is very far from compelling evidence, it is consistent with naturalness. Time and testing will tell if they are linked.

If this signal fades into the background as more data is collected, then much of

the second run of the LHC will focus on the properties of the Higgs. This is in part due to its potential to first reveal how the SM breaks down. The most natural ways to keep the Higgs light and remain consistent with experiment either involve colored top partners that happen to be difficult to discover, or colorless top partners, which are difficult to produce. In the former case, indirect probes are a valuable diagnostic tool in finding the top partners. Probes that are tied to the Higgs have particular utility in addressing naturalness, making the di-Higgs rate, discussed in Chapter 2, especially interesting.

However, we showed that the non-resonant di-Higgs rate is anti-correlated with single Higgs production, which is close to the SM prediction. This implies that heavy top partners will be probed more effectively by single Higgs production. However, if the top partners are light, di-Higgs production is sensitive to top partners that single Higgs production misses, making it a useful complementary probe of light top partners.

Our analysis also showed how to make smaller deviations more apparent. The SM rate experiences a cancellation close to threshold, which generic new states are likely to spoil. Therefore, looking at the invariant mass spectrum near threshold can reveal large deviations from the SM, even when the total rate is quite similar. This gives extra discriminating strength to searches at the LHC and at future hadron machines.

Discovering colorless top partners requires different search strategies, but the Higgs remains a powerful probe. As shown in Chapters 4 and 5 both the Higgs couplings to SM states and its exotic decays can give valuable information about

colorless top partners. Using the models defined in Chapter 3, we determined how top partners affect Higgs production and decay rates. This allowed us to place limits on the top partner masses, and therefore on naturalness. In some cases, like the Mirror Twin Higgs, these coupling shifts are the only required LHC signals. For these models, even with 3000 fb^{-1} at 14 TeV, the LHC Higgs studies will not be able to strongly disfavor naturalness. We also saw that Folded SUSY predicted coupling shifts far below what the LHC can find. This led us to consider other methods of detecting such frameworks.

Chapter 5 presented the first detailed phenomenological analysis of exotic Higgs decays to mirror glueballs. Such decays are guaranteed in NN models, like FSUSY, that share the EW force between SM and mirror sectors, and may occur in when the mirror sector is completely neutral to SM forces. Using RGEs to estimate the range of glueball masses, we set discovery limits both for the LHC and a future 100 TeV collider for the case study models of Chapter 3.

Exploring these scenarios made clear that new experimental searches are needed to maximize reach. We outlined these new strategies and determined their potential to discover NN. We found sensitivity to top partners of nearly TeV masses at the LHC and multi-TeV at future colliders. Unexpectedly, the displaced nature of these exotic decays leads to reach comparable to colored top partner searches. This gives an additional way to pursue naturalness at the LHC.

All these processes underscore the great utility of using the Higgs to investigate its own naturalness. Gluon fusion, the leading Higgs (and multi-Higgs) production mechanism, is a loop process, so new colored states affect the rate, if they are not too

heavy. Frameworks in which the Higgs is the pNGB of a broken symmetry predict variations in the tree level Higgs couplings, even if the new states are completely neutral to SM forces. If the couplings are not shifted, as can occur in SUSY, the symmetry partners can mediate decays into mirror states, like glueballs. These new decay channels have the potential to yield displaced vertices at the LHC. Such a conspicuous sign of new physics allows these searches to probe much of the natural parameter space.

In short, when a symmetry protects the Higgs' mass in some degree, the Higgs is necessarily tied to the symmetry partner particles. This allows for many natural frameworks to be probed by a limited number of tests. This efficiency in testing comes from being closer to the source. When we want the direct answer about Higgs naturalness, we should ask the Higgs.

Bibliography

- [1] Douglas Adams. *Dirk Gently's Holistic Detective Agency*. William Heinemann Ltd, 1987.
- [2] John Dalton. On the Absorption of Gases by Water and other Liquids. *Manchester Mem.*, 1:271–287, 1805.
- [3] John Dalton. *A New System of Chemical Philosophy, Part I*. Manchester, 1808.
- [4] John Dalton. *A New System of Chemical Philosophy, Part II*. Manchester, 1810.
- [5] Rudolf Clausius. Ueber die Art der Bewegung, welche wir Wärme nennen. *Ann. d. Physik*, 100:353–380, 1857.
- [6] Rudolf Clausius. Ueber die mittlere Länge der Wege, welche bei der Molecularbewegung gasförmiger Körper von den einzelnen Molecülen zurückgelegt werden; nebst einigen anderen Bemerkungen über die mechanische Wärmetheorie. *Ann. d. Physik*, 105:339–258, 1858.
- [7] James Clerk Maxwell. Illustrations of the Dynamical Theory of Gases. Part I. On the motions and collisions of perfectly elastic spheres. *Phil. Mag.*, 19:19–32, 1860.
- [8] James Clerk Maxwell. Illustrations of the Dynamical Theory of Gases. Part II. On the Process of Diffusion of two or more kinds of moving particles among one another. *Phil. Mag.*, 20:21–37, 1860.
- [9] James Clerk Maxwell. On the Dynamical Theory of Gases. *Phil. Trans. Roy. Soc.*, 157:49–88, 1867.
- [10] James Clerk Maxwell. On the Dynamical Evidence of the Molecular Constitution of Bodies. *Nature*, 11:357–359, 1875.

- [11] Ludwig Boltzmann. Ueber die mechanische Bedeutung des zweiten Hauptsatzes der Wärmetheorie. *Wiener Berichte*, 53:195–220, 1866.
- [12] Ludwig Boltzmann. Weitere Studien über das Wärmegleichgewicht unter Gasmolekülen. *Wiener Berichte*, 66:275–370, 1872.
- [13] Ludwig Boltzmann. Über die beziehung dem zweiten Haubtsatze der mechanischen Wärmetheorie und der Wahrscheinlichkeitsrechnung respektive den Sätzen über das Wärmegleichgewicht. *Wiener Berichte*, 76:373–435, 1877.
- [14] Ernst Mach. *Compendium der Physick für Mediciner*. Vienna, 1863.
- [15] Bohuslav Brauner. Einstein and Mach. *Nature*, 113:927, 1933.
- [16] Wilhelm Ostwald. *Abhandlungen und Vorträge allgemeinen Inhaltes*. Leipzig, 1904.
- [17] Wilhelm Ostwald. Elements and Compounds. *J. Chem. Soc.*, 85:506–522, 1904.
- [18] Albert Einstein. Über die von der molekularkinetischen Theorie der Wärme geforderte Bewegung von in ruhenden Flüssigkeiten suspendierten Teilchen. *Ann. d. Physik*, 12:549–560, 1905.
- [19] John T. Blackmore. *Ernst Mach: His Work, Life, and Influence*. University of California Press, 1972.
- [20] Joseph John Thomson. Cathode rays. *Phil. Mag.*, 44(269):293–316, 1897.
- [21] Joseph John Thomson. On the structure of the atom: an investigation of the stability and periods of oscillation of a number of corpuscles arranged at equal intervals around the circumference of a circle; with application of the results to the theory of atomic structure. *Phil. Mag.*, 7(39):237–265, 1904.
- [22] Hans Geiger and Ernest Marsden. On a Diffuse Reflection of the α -Particles. *Proc. Roy. Soc. Lond.*, A82:495–500, 1909.
- [23] Ernest Rutherford. The scattering of α and β particles by matter and the structure of the atom. *Phil. Mag.*, 21(125):669–688, 1911.
- [24] Niels Bohr. On the Constitution of Atoms and Molecules. *Phil. Mag.*, 26:1–24, 1913.
- [25] Niels Bohr. On the Constitution of Atoms and Molecules. 2. Systems containing only a Single Nucleus. *Phil. Mag.*, 26:476, 1913.
- [26] Niels Bohr. On the Constitution of Atoms and Molecules. 3. Systems containing Several Nuclei. *Phil. Mag.*, 26:857, 1913.

- [27] Max Planck. Ueber das Gesetz der Energieverteilung im Normalspectrum . *Ann. d. Physik*, 4:553, 1901.
- [28] Albert Einstein. Über einen die Erzeugung und Verwandlung des Lichtes betreffenden heuristischen Gesichtspunkt. *Ann. d. Physik*, 17:132–148, 1905.
- [29] J. J. Balmer. Notiz über die Spektrallinien des Wasserstoffs. *Verh. Naturf. Ges. Basel*, 7:548–560, 1885.
- [30] J. R. Rydberg. Recherches sur la constitution des spectres d'émission des éléments chimiques. *Kongl. Svenska Vetenskaps Akademiens Handlingar*, 23, 1890.
- [31] Werner Heisenberg. Über quantentheoretische Umdeutung kinematischer und mechanischer Beziehungen. *Z. f. Physik*, 33:879, 1925.
- [32] Erwin Schrödinger. Quantisierung als Eigenwertproblem. *Ann. d. Physik*, 79:361, 1926.
- [33] Erwin Schrödinger. Quantisierung als Eigenwertproblem, II. *Ann. d. Physik*, 79:489, 1926.
- [34] Erwin Schrödinger. Quantisierung als Eigenwertproblem, III: Störungstheorie mit Anwendung auf den Starkeffekt der Balmerlinien. *Ann. d. Physik*, 80:437, 1926.
- [35] Erwin Schrödinger. Quantisierung als Eigenwertproblem, IV. *Ann. d. Physik*, 81:109, 1926.
- [36] Wolfgang Pauli. Zur Quantenmechanik des magnetischen Elektrons. *Z. f. Physik*, 43:601, 1927.
- [37] Oskar Klein. Quantentheorie und fünfdimensionale Relativitätstheorie. *Z. f. Physik*, 37:895, 1926.
- [38] Walter Gordon. Der Comptoneffekt nach der Schrödingerschen Theorie. *Z. f. Physik*, 40:117, 1926.
- [39] Paul A. M. Dirac. The quantum theory of the electron. *Proc. Roy. Soc. Lond.*, A117:610–624, 1928.
- [40] Willis E. Lamb and Robert C. Retherford. Fine Structure of the Hydrogen Atom by a Microwave Method. *Phys. Rev.*, 72:241–243, 1947.
- [41] Robert. E. Marshak and E. C. George. Sudarshan. The Nature of the Four-Fermion Interaction. Padua-Venice, September 1957. Proceedings of the Conference on Mesons and Newly-Discovered Particles.
- [42] R. P. Feynman and Murray Gell-Mann. Theory of Fermi interaction. *Phys. Rev.*, 109:193–198, 1958.

- [43] Chen-Ning Yang and Robert L. Mills. Conservation of Isotopic Spin and Isotopic Gauge Invariance. *Phys. Rev.*, 96:191–195, 1954.
- [44] Robert Shaw. *The Problem of Particle Types and Other Contributions to the Theory of Elementary Particles*. PhD thesis, Cambridge, 1955.
- [45] Julian S. Schwinger. A Theory of the Fundamental Interactions. *Annals Phys.*, 2:407–434, 1957.
- [46] Sidney A. Bludman. On the universal Fermi interaction. *Nuovo Cim.*, 9:433–445, 1958.
- [47] S. L. Glashow. Partial Symmetries of Weak Interactions. *Nucl. Phys.*, 22:579–588, 1961.
- [48] Peter W. Higgs. Broken symmetries, massless particles and gauge fields. *Phys. Lett.*, 12:132–133, 1964.
- [49] F. Englert and R. Brout. Broken Symmetry and the Mass of Gauge Vector Mesons. *Phys. Rev. Lett.*, 13:321–323, 1964.
- [50] Peter W. Higgs. Broken Symmetries and the Masses of Gauge Bosons. *Phys. Rev. Lett.*, 13:508–509, 1964.
- [51] G. S. Guralnik, C. R. Hagen, and T. W. B. Kibble. Global Conservation Laws and Massless Particles. *Phys. Rev. Lett.*, 13:585–587, 1964.
- [52] Steven Weinberg. A Model of Leptons. *Phys. Rev. Lett.*, 19:1264–1266, 1967.
- [53] Abdus Salam. Weak and Electromagnetic Interactions. *Conf. Proc.*, C680519:367–377, 1968.
- [54] Thorsten Ohl. Drawing Feynman diagrams with Latex and Metafont. *Comput. Phys. Commun.*, 90:340–354, 1995, hep-ph/9505351.
- [55] Eldad Gildener. Gauge Symmetry Hierarchies. *Phys. Rev.*, D14:1667, 1976.
- [56] Steven Weinberg. Gauge Hierarchies. *Phys. Lett.*, B82:387–391, 1979.
- [57] Georges Aad et al. Observation of a new particle in the search for the Standard Model Higgs boson with the ATLAS detector at the LHC. *Phys.Lett.*, B716:1–29, 2012, 1207.7214.
- [58] Serguei Chatrchyan et al. Observation of a new boson at a mass of 125 GeV with the CMS experiment at the LHC. *Phys.Lett.*, B716:30–61, 2012, 1207.7235.
- [59] Georges Aad et al. Combined Measurement of the Higgs Boson Mass in pp Collisions at $\sqrt{s} = 7$ and 8 TeV with the ATLAS and CMS Experiments. *Phys. Rev. Lett.*, 114:191803, 2015, 1503.07589.

- [60] Leonard Susskind. Dynamics of Spontaneous Symmetry Breaking in the Weinberg-Salam Theory. *Phys. Rev.*, D20:2619–2625, 1979.
- [61] Arthur Conan Doyle. *The Sign of the Four*. Lippincott’s Monthly Magazine, 1890.
- [62] Arthur Conan Doyle. The Adventure of the Beryl Coronet. *The Strand*, 05, 1892.
- [63] Arthur Conan Doyle. The Adventure of the Bruce-Partington Plans. *The Strand*, 12, 1908.
- [64] Arthur Conan Doyle. The Adventure of the Blanched Soldier. *The Strand*, 11, 1926.
- [65] Douglas Adams. *The Long Dark Tea-Time of the Soul*. William Heinemann Ltd, 1988.
- [66] Gerard 't Hooft, C. Itzykson, A. Jaffe, H. Lehmann, P. K. Mitter, I. M. Singer, and R. Stora. Recent Developments in Gauge Theories. Proceedings, Nato Advanced Study Institute, Cargese, France, August 26 - September 8, 1979. *NATO Sci. Ser. B*, 59:pp.1–438, 1980.
- [67] Gian Francesco Giudice. Naturally Speaking: The Naturalness Criterion and Physics at the LHC. 2008, 0801.2562.
- [68] V. F. Weisskopf. On the Self-Energy and the Electromagnetic Field of the Electron. *Phys. Rev.*, 56:72–85, 1939.
- [69] Hitoshi Murayama. Supersymmetry phenomenology. In *Particle physics. Proceedings, Summer School, Trieste, Italy, June 21-July 9, 1999*, pages 296–335, 2000, hep-ph/0002232.
- [70] T. Das, G. S. Guralnik, V. S. Mathur, F. E. Low, and J. E. Young. Electromagnetic mass difference of pions. *Phys. Rev. Lett.*, 18:759–761, 1967.
- [71] M. K. Gaillard and Benjamin W. Lee. Rare Decay Modes of the K-Mesons in Gauge Theories. *Phys. Rev.*, D10:897, 1974.
- [72] S. L. Glashow, J. Iliopoulos, and L. Maiani. Weak Interactions with Lepton-Hadron Symmetry. *Phys. Rev.*, D2:1285–1292, 1970.
- [73] Steven Weinberg. Implications of Dynamical Symmetry Breaking. *Phys. Rev.*, D13:974–996, 1976.
- [74] Steven Weinberg. Implications of Dynamical Symmetry Breaking: An Addendum. *Phys. Rev.*, D19:1277–1280, 1979.
- [75] Stephen P. Martin. A Supersymmetry primer. *Adv.Ser.Direct.High Energy Phys.*, 21:1–153, 2010, hep-ph/9709356.

- [76] Nima Arkani-Hamed, Andrew G. Cohen, and Howard Georgi. Electroweak symmetry breaking from dimensional deconstruction. *Phys.Lett.*, B513:232–240, 2001, hep-ph/0105239.
- [77] N. Arkani-Hamed, A.G. Cohen, E. Katz, A.E. Nelson, T. Gregoire, et al. The Minimal moose for a little Higgs. *JHEP*, 0208:021, 2002, hep-ph/0206020.
- [78] N. Arkani-Hamed, A.G. Cohen, E. Katz, and A.E. Nelson. The Littlest Higgs. *JHEP*, 0207:034, 2002, hep-ph/0206021.
- [79] Martin Schmaltz. The Simplest little Higgs. *JHEP*, 0408:056, 2004, hep-ph/0407143.
- [80] Brando Bellazzini, Csaba Csáki, and Javi Serra. Composite Higgses. *Eur. Phys. J.*, C74(5):2766, 2014, 1401.2457.
- [81] Roberto Contino, Yasunori Nomura, and Alex Pomarol. Higgs as a holographic pseudoGoldstone boson. *Nucl.Phys.*, B671:148–174, 2003, hep-ph/0306259.
- [82] Kaustubh Agashe, Roberto Contino, and Alex Pomarol. The Minimal composite Higgs model. *Nucl.Phys.*, B719:165–187, 2005, hep-ph/0412089.
- [83] Roberto Contino, Leandro Da Rold, and Alex Pomarol. Light custodians in natural composite Higgs models. *Phys.Rev.*, D75:055014, 2007, hep-ph/0612048.
- [84] Juan Martin Maldacena. The Large N limit of superconformal field theories and supergravity. *Int. J. Theor. Phys.*, 38:1113–1133, 1999, hep-th/9711200. [Adv. Theor. Math. Phys.2,231(1998)].
- [85] S. S. Gubser, Igor R. Klebanov, and Alexander M. Polyakov. Gauge theory correlators from noncritical string theory. *Phys. Lett.*, B428:105–114, 1998, hep-th/9802109.
- [86] Edward Witten. Anti-de Sitter space and holography. *Adv. Theor. Math. Phys.*, 2:253–291, 1998, hep-th/9802150.
- [87] Lisa Randall and Raman Sundrum. A Large mass hierarchy from a small extra dimension. *Phys. Rev. Lett.*, 83:3370–3373, 1999, hep-ph/9905221.
- [88] Lisa Randall and Raman Sundrum. An Alternative to compactification. *Phys. Rev. Lett.*, 83:4690–4693, 1999, hep-th/9906064.
- [89] JiJi Fan, Matthew Reece, and Joshua T. Ruderman. Stealth Supersymmetry. *JHEP*, 1111:012, 2011, 1105.5135.
- [90] JiJi Fan, Matthew Reece, and Joshua T. Ruderman. A Stealth Supersymmetry Sampler. *JHEP*, 1207:196, 2012, 1201.4875.

- [91] Csaba Csaki, Lisa Randall, and John Terning. Light Stops from Seiberg Duality. *Phys.Rev.*, D86:075009, 2012, 1201.1293.
- [92] Zhenyu Han, Andrey Katz, David Krohn, and Matthew Reece. (Light) Stop Signs. *JHEP*, 1208:083, 2012, 1205.5808.
- [93] Can Kilic and Brock Tweedie. Cornering Light Stops with Dileptonic mT2. *JHEP*, 1304:110, 2013, 1211.6106.
- [94] Michal Czakon, Alexander Mitov, Michele Papucci, Joshua T. Ruderman, and Andreas Weiler. Closing the stop gap. *Phys.Rev.Lett.*, 113(20):201803, 2014, 1407.1043.
- [95] Stephen P. Martin. Compressed supersymmetry and natural neutralino dark matter from top squark-mediated annihilation to top quarks. *Phys.Rev.*, D75:115005, 2007, hep-ph/0703097.
- [96] Thomas J. LeCompte and Stephen P. Martin. Compressed supersymmetry after 1/fb at the Large Hadron Collider. *Phys.Rev.*, D85:035023, 2012, 1111.6897.
- [97] Thomas J. LeCompte and Stephen P. Martin. Large Hadron Collider reach for supersymmetric models with compressed mass spectra. *Phys.Rev.*, D84:015004, 2011, 1105.4304.
- [98] Herbi K. Dreiner, Michael Kramer, and Jamie Tattersall. How low can SUSY go? Matching, monojets and compressed spectra. *Europhys.Lett.*, 99:61001, 2012, 1207.1613.
- [99] Biplob Bhattacharjee and Kirtiman Ghosh. Degenerate SUSY search at the 8 TeV LHC. 2012, 1207.6289.
- [100] Manuel Drees, M. Hanussek, and Jong Soo Kim. Light Stop Searches at the LHC with Monojet Events. *Phys.Rev.*, D86:035024, 2012, 1201.5714.
- [101] Genevieve Belanger, Matti Heikinheimo, and Veronica Sanz. Model-Independent Bounds on Squarks from Monophoton Searches. *JHEP*, 1208:151, 2012, 1205.1463.
- [102] Daniele S.M. Alves, Matthew R. Buckley, Patrick J. Fox, Joseph D. Lykken, and Chiu-Tien Yu. Stops and \cancel{E}_T : The shape of things to come. *Phys.Rev.*, D87(3):035016, 2013, 1205.5805.
- [103] Karol Krizka, Abhishek Kumar, and David E. Morrissey. Very Light Scalar Top Quarks at the LHC. *Phys.Rev.*, D87(9):095016, 2013, 1212.4856.
- [104] Stephen P. Martin. Diphoton decays of stoponium at the Large Hadron Collider. *Phys.Rev.*, D77:075002, 2008, 0801.0237.

- [105] Krzysztof Rolbiecki and Kazuki Sakurai. Constraining compressed supersymmetry using leptonic signatures. *JHEP*, 1210:071, 2012, 1206.6767.
- [106] David Curtin, Patrick Meade, and Pin-Ju Tien. Natural SUSY in Plain Sight. *Phys.Rev.*, D90(11):115012, 2014, 1406.0848.
- [107] Jong Soo Kim, Krzysztof Rolbiecki, Kazuki Sakurai, and Jamie Tattersall. ‘Stop’ that ambulance! New physics at the LHC? *JHEP*, 1412:010, 2014, 1406.0858.
- [108] V. Khachatryan et al. Search for stealth supersymmetry in events with jets, either photons or leptons, and low missing transverse momentum in pp collisions at 8 TeV. *Phys.Lett.*, B743:503–525, 2015, 1411.7255.
- [109] Krzysztof Rolbiecki and Jamie Tattersall. Refining light stop exclusion limits with W^+W^- cross sections. *Phys. Lett.*, B750:247–251, 2015, 1505.05523.
- [110] Haipeng An and Lian-Tao Wang. Opening up the compressed region of top squark searches at 13 TeV LHC. *Phys. Rev. Lett.*, 115:181602, 2015, 1506.00653.
- [111] Marcela Carena, Stefania Gori, Nausheen R. Shah, Carlos E. M. Wagner, and Lian-Tao Wang. Light Stau Phenomenology and the Higgs $\gamma\gamma$ Rate. *JHEP*, 07:175, 2012, 1205.5842.
- [112] Marcela Carena, Stefania Gori, Nausheen R. Shah, Carlos E. M. Wagner, and Lian-Tao Wang. Light Stops, Light Staus and the 125 GeV Higgs. *JHEP*, 08:087, 2013, 1303.4414.
- [113] Christopher Brust, Andrey Katz, and Raman Sundrum. SUSY Stops at a Bump. *JHEP*, 1208:059, 2012, 1206.2353.
- [114] Jared A. Evans and Yevgeny Kats. LHC Coverage of RPV MSSM with Light Stops. *JHEP*, 1304:028, 2013, 1209.0764.
- [115] Yang Bai, Andrey Katz, and Brock Tweedie. Pulling Out All the Stops: Searching for RPV SUSY with Stop-Jets. *JHEP*, 1401:040, 2014, 1309.6631.
- [116] Search for RPV supersymmetry with three or more leptons and b-tags. 2012, CMS-PAS-SUS-12-027.
- [117] Serguei Chatrchyan et al. Search for top squarks in R -parity-violating supersymmetry using three or more leptons and b-tagged jets. *Phys. Rev. Lett.*, 111(22):221801, 2013, 1306.6643.
- [118] Vardan Khachatryan et al. Search for pair-produced resonances decaying to jet pairs in protonproton collisions at $\sqrt{s}=8$ TeV. *Phys. Lett.*, B747:98–119, 2015, 1412.7706.

- [119] The ATLAS collaboration. A search for $B-L$ R -Parity violating scalar top decays in $\sqrt{s} = 8$ TeV pp collisions with the ATLAS experiment. 2015, ATLAS-CONF-2015-015.
- [120] Georges Aad et al. A search for top squarks with R -parity-violating decays to all-hadronic final states with the ATLAS detector in $\sqrt{s} = 8$ TeV proton-proton collisions. *JHEP*, 06:067, 2016, 1601.07453.
- [121] Vardan Khachatryan et al. Precise determination of the mass of the Higgs boson and tests of compatibility of its couplings with the standard model predictions using proton collisions at 7 and 8 TeV. *Eur. Phys. J.*, C75(5):212, 2015, 1412.8662.
- [122] The ATLAS collaboration. Measurements of the Higgs boson production and decay rates and coupling strengths using pp collision data at $\sqrt{s} = 7$ and 8 TeV in the ATLAS experiment. 2015, ATLAS-CONF-2015-007.
- [123] Brian Batell, Matthew McCullough, Daniel Stolarski, and Christopher B. Verhaaren. Putting a Stop to di-Higgs Modifications. *JHEP*, 09:216, 2015, 1508.01208.
- [124] Michael Dine. Naturalness Under Stress. *Ann. Rev. Nucl. Part. Sci.*, 65:43–62, 2015, 1501.01035.
- [125] Arthur Conan Doyle. The Adventure of the Silver Blaze. *The Strand*, 12, 1892.
- [126] Peter W. Graham, David E. Kaplan, and Surjeet Rajendran. Cosmological Relaxation of the Electroweak Scale. *Phys. Rev. Lett.*, 115(22):221801, 2015, 1504.07551.
- [127] Brian Batell, Gian F. Giudice, and Matthew McCullough. Natural Heavy Supersymmetry. *JHEP*, 12:162, 2015, 1509.00834.
- [128] Nikita Blinov and Anson Hook. Solving the Wrong Hierarchy Problem. 2016, 1605.03178.
- [129] Z. Chacko, Hock-Seng Goh, and Roni Harnik. The Twin Higgs: Natural electroweak breaking from mirror symmetry. *Phys.Rev.Lett.*, 96:231802, 2006, hep-ph/0506256.
- [130] Gustavo Burdman, Z. Chacko, Hock-Seng Goh, and Roni Harnik. Folded supersymmetry and the LEP paradox. *JHEP*, 0702:009, 2007, hep-ph/0609152.
- [131] Z. Chacko, Hock-Seng Goh, and Roni Harnik. A Twin Higgs model from left-right symmetry. *JHEP*, 01:108, 2006, hep-ph/0512088.
- [132] Riccardo Barbieri, Thomas Gregoire, and Lawrence J. Hall. Mirror world at the large hadron collider. 2005, hep-ph/0509242.

- [133] Z. Chacko, Yasunori Nomura, Michele Papucci, and Gilad Perez. Natural little hierarchy from a partially goldstone twin Higgs. *JHEP*, 01:126, 2006, hep-ph/0510273.
- [134] Hock-Seng Goh and Christopher A. Krenke. A Little Twin Higgs Model. *Phys. Rev.*, D76:115018, 2007, 0707.3650.
- [135] Hugues Beauchesne, Kevin Earl, and Thomas Grégoire. The spontaneous \mathbb{Z}_2 breaking Twin Higgs. *JHEP*, 01:130, 2016, 1510.06069.
- [136] Nathaniel Craig, Simon Knapen, Pietro Longhi, and Matthew Strassler. The Vector-like Twin Higgs. 2016, 1601.07181.
- [137] Nathaniel Craig, Andrey Katz, Matt Strassler, and Raman Sundrum. Naturalness in the Dark at the LHC. *JHEP*, 07:105, 2015, 1501.05310.
- [138] Nathaniel Craig, Simon Knapen, and Pietro Longhi. Neutral Naturalness from Orbifold Higgs Models. *Phys.Rev.Lett.*, 114(6):061803, 2015, 1410.6808.
- [139] Nathaniel Craig, Simon Knapen, and Pietro Longhi. The Orbifold Higgs. *JHEP*, 1503:106, 2015, 1411.7393.
- [140] Spencer Chang, Lawrence J. Hall, and Neal Weiner. A Supersymmetric twin Higgs. *Phys. Rev.*, D75:035009, 2007, hep-ph/0604076.
- [141] Adam Falkowski, Stefan Pokorski, and Martin Schmaltz. Twin SUSY. *Phys. Rev.*, D74:035003, 2006, hep-ph/0604066.
- [142] Nathaniel Craig and Kiel Howe. Doubling down on naturalness with a supersymmetric twin Higgs. *JHEP*, 1403:140, 2014, 1312.1341.
- [143] Michael Geller and Ofri Telem. A Holographic Twin Higgs Model. *Phys.Rev.Lett.*, 114(19):191801, 2015, 1411.2974.
- [144] Puneet Batra and Z. Chacko. A Composite Twin Higgs Model. *Phys.Rev.*, D79:095012, 2009, 0811.0394.
- [145] Riccardo Barbieri, Davide Greco, Riccardo Rattazzi, and Andrea Wulzer. The Composite Twin Higgs scenario. *JHEP*, 08:161, 2015, 1501.07803.
- [146] Matthew Low, Andrea Tesi, and Lian-Tao Wang. Twin Higgs mechanism and a composite Higgs boson. *Phys.Rev.*, D91(9):095012, 2015, 1501.07890.
- [147] Hsin-Chia Cheng, Sunghoon Jung, Ennio Salvioni, and Yuhsin Tsai. Exotic Quarks in Twin Higgs Models. *JHEP*, 03:074, 2016, 1512.02647.
- [148] Csaba Csaki, Michael Geller, Ofri Telem, and Andreas Weiler. The Flavor of the Composite Twin Higgs. 2015, 1512.03427.

- [149] Isabel García García, Robert Lasenby, and John March-Russell. Twin Higgs WIMP Dark Matter. *Phys. Rev.*, D92(5):055034, 2015, 1505.07109.
- [150] Nathaniel Craig and Andrey Katz. The Fraternal WIMP Miracle. *JCAP*, 1510(10):054, 2015, 1505.07113.
- [151] Isabel García García, Robert Lasenby, and John March-Russell. Twin Higgs Asymmetric Dark Matter. *Phys. Rev. Lett.*, 115(12):121801, 2015, 1505.07410.
- [152] Marco Farina. Asymmetric Twin Dark Matter. *JCAP*, 1511(11):017, 2015, 1506.03520.
- [153] Marat Freytsis, Simon Knapen, Dean J. Robinson, and Yuhsin Tsai. Gamma-rays from Dark Showers with Twin Higgs Models. *JHEP*, 05:018, 2016, 1601.07556.
- [154] Pedro Schwaller. Gravitational Waves from a Dark Phase Transition. *Phys. Rev. Lett.*, 115(18):181101, 2015, 1504.07263.
- [155] Gian F. Giudice, Matthew McCullough, and Alfredo Urbano. Hunting for Dark Particles with Gravitational Waves. 2016, 1605.01209.
- [156] Brian Batell and Matthew McCullough. Neutrino Masses from Neutral Top Partners. *Phys. Rev.*, D92(7):073018, 2015, 1504.04016.
- [157] Yang Bai, Ran Lu, Sida Lu, Jordi Salvado, and Ben A. Stefanek. Three Twin Neutrinos: Evidence from LSND and MiniBooNE. *Phys. Rev.*, D93(7):073004, 2016, 1512.05357.
- [158] Can Kilic and Sivaramakrishnan Swaminathan. Can A Pseudo-Nambu-Goldstone Higgs Lead To Symmetry Non-Restoration? *JHEP*, 01:002, 2016, 1508.05121.
- [159] Marco Farina, Angelo Monteux, and Chang Sub Shin. Twin Baryogenesis. 2016, 1604.08211.
- [160] Nathaniel Craig and Hou Keong Lou. Scherk-Schwarz Supersymmetry Breaking in 4D. *JHEP*, 12:184, 2014, 1406.4880.
- [161] Timothy Cohen, Nathaniel Craig, Hou Keong Lou, and David Pinner. Folded Supersymmetry with a Twist. *JHEP*, 03:196, 2016, 1508.05396.
- [162] Haiying Cai, Hsin-Chia Cheng, and John Terning. A Quirky Little Higgs Model. *JHEP*, 0905:045, 2009, 0812.0843.
- [163] David Poland and Jesse Thaler. The Dark Top. *JHEP*, 0811:083, 2008, 0808.1290.
- [164] L. B. Okun. Thetons. *JETP Lett.*, 31:144–147, 1980. [Pisma Zh. Eksp. Teor. Fiz.31,156(1979)].

- [165] L. B. Okun. Theta Particles. *Nucl. Phys.*, B173:1, 1980.
- [166] Junhai Kang and Markus A. Luty. Macroscopic Strings and ‘Quirks’ at Colliders. *JHEP*, 0911:065, 2009, 0805.4642.
- [167] Gustavo Burdman, Z. Chacko, Hock-Seng Goh, Roni Harnik, and Christopher A. Krenke. The Quirky Collider Signals of Folded Supersymmetry. *Phys.Rev.*, D78:075028, 2008, 0805.4667.
- [168] Kingman Cheung, Wai-Yee Keung, and Tzu-Chiang Yuan. Phenomenology of iquarkonium. *Nucl. Phys.*, B811:274–287, 2009, 0810.1524.
- [169] Roni Harnik and Tommer Wizansky. Signals of New Physics in the Underlying Event. *Phys.Rev.*, D80:075015, 2009, 0810.3948.
- [170] Roni Harnik, Graham D. Kribs, and Adam Martin. Quirks at the Tevatron and Beyond. *Phys. Rev.*, D84:035029, 2011, 1106.2569.
- [171] R. Fok and Graham D. Kribs. Chiral Quirkonium Decays. *Phys. Rev.*, D84:035001, 2011, 1106.3101.
- [172] Zackaria Chacko, David Curtin, and Christopher B. Verhaaren. A Quirky Probe of Neutral Naturalness. 2015, 1512.05782.
- [173] Gustavo Burdman and Raffaele Tito D’Agnolo. Scalar Leptons in Folded Supersymmetry. 2015, 1512.00040.
- [174] David Curtin and Christopher B. Verhaaren. Discovering Uncolored Naturalness in Exotic Higgs Decays. *JHEP*, 12:072, 2015, 1506.06141.
- [175] Nathaniel Craig, Christoph Englert, and Matthew McCullough. New Probe of Naturalness. *Phys.Rev.Lett.*, 111(12):121803, 2013, 1305.5251.
- [176] David Curtin and Prashant Saraswat. Towards a No-Lose Theorem for Naturalness. *Phys. Rev.*, D93(5):055044, 2016, 1509.04284.
- [177] Xin Li and M.B. Voloshin. Remarks on double Higgs boson production by gluon fusion at threshold. *Phys.Rev.*, D89(1):013012, 2014, 1311.5156.
- [178] Duane A. Dicus, Chung Kao, and Wayne W. Repko. Interference effects and the use of Higgs boson pair production to study the Higgs trilinear self coupling. *Phys. Rev.*, D92(9):093003, 2015, 1504.02334.
- [179] S. Dawson, A. Ismail, and Ian Low. Whats in the loop? The anatomy of double Higgs production. *Phys. Rev.*, D91(11):115008, 2015, 1504.05596.
- [180] Serguei Chatrchyan et al. Search for top-squark pair production in the single-lepton final state in pp collisions at $\sqrt{s} = 8$ TeV. *Eur.Phys.J.*, C73(12):2677, 2013, 1308.1586.

- [181] Georges Aad et al. Search for top squark pair production in final states with one isolated lepton, jets, and missing transverse momentum in $\sqrt{s} = 8$ TeV pp collisions with the ATLAS detector. *JHEP*, 1411:118, 2014, 1407.0583.
- [182] Georges Aad et al. Search for direct pair production of the top squark in all-hadronic final states in proton-proton collisions at $\sqrt{s} = 8$ TeV with the ATLAS detector. *JHEP*, 1409:015, 2014, 1406.1122.
- [183] CMS Collaboration. Exclusion limits on gluino and top-squark pair production in natural SUSY scenarios with inclusive razor and exclusive single-lepton searches at 8 TeV. 2014, CMS-PAS-SUS-14-011.
- [184] Daniel Stolarski. Reach in All Hadronic Stop Decays: A Snowmass White Paper. 2013, 1309.1514.
- [185] Y. Gershtein, M. Luty, M. Narain, L. T. Wang, D. Whiteson, et al. Working Group Report: New Particles, Forces, and Dimensions. 2013, 1311.0299.
- [186] Vernon Barger, Peisi Huang, Muneyuki Ishida, and Wai-Yee Keung. Scalar-Top Masses from SUSY Loops with 125 GeV mh and Precise Mw. *Phys.Lett.*, B718:1024–1030, 2013, 1206.1777.
- [187] Sven Heinemeyer, W. Hollik, Georg Weiglein, and Lisa Zeune. Implications of LHC search results on the W boson mass prediction in the MSSM. *JHEP*, 1312:084, 2013, 1311.1663.
- [188] Jose R. Espinosa, Christophe Grojean, Veronica Sanz, and Michael Trott. NSUSY fits. *JHEP*, 1212:077, 2012, 1207.7355.
- [189] JiJi Fan and Matthew Reece. A New Look at Higgs Constraints on Stops. *JHEP*, 1406:031, 2014, 1401.7671.
- [190] Christophe Grojean, Ennio Salvioni, Matthias Schlaffer, and Andreas Weiler. Very boosted Higgs in gluon fusion. *JHEP*, 1405:022, 2014, 1312.3317.
- [191] Matthias Schlaffer, Michael Spannowsky, Michihisa Takeuchi, Andreas Weiler, and Chris Wymant. Boosted Higgs Shapes. *Eur.Phys.J.*, C74(10):3120, 2014, 1405.4295.
- [192] Stefania Gori and Ian Low. Precision Higgs Measurements: Constraints from New Oblique Corrections. *JHEP*, 1309:151, 2013, 1307.0496.
- [193] Stephen P. Martin and James E. Younkin. Radiative corrections to stoponium annihilation decays. *Phys.Rev.*, D80:035026, 2009, 0901.4318.
- [194] James E. Younkin and Stephen P. Martin. QCD corrections to stoponium production at hadron colliders. *Phys.Rev.*, D81:055006, 2010, 0912.4813.
- [195] Brian Batell and Sunghoon Jung. Probing Light Stops with Stoponium. *JHEP*, 07:061, 2015, 1504.01740.

- [196] Nathaniel Craig, Marco Farina, Matthew McCullough, and Maxim Perelstein. Precision Higgsstrahlung as a Probe of New Physics. *JHEP*, 1503:146, 2015, 1411.0676.
- [197] JiJi Fan, Matthew Reece, and Lian-Tao Wang. Precision Natural SUSY at CEPC, FCC-ee, and ILC. *JHEP*, 08:152, 2015, 1412.3107.
- [198] T. Plehn, M. Spira, and P.M. Zerwas. Pair production of neutral Higgs particles in gluon-gluon collisions. *Nucl.Phys.*, B479:46–64, 1996, hep-ph/9603205.
- [199] A. Djouadi, W. Kilian, M. Muhlleitner, and P.M. Zerwas. Production of neutral Higgs boson pairs at LHC. *Eur.Phys.J.*, C10:45–49, 1999, hep-ph/9904287.
- [200] A. Belyaev, Manuel Drees, Oscar J.P. Eboli, J.K. Mizukoshi, and S.F. Novaes. Supersymmetric Higgs pair production at hadron colliders. *Phys.Rev.*, D60:075008, 1999, hep-ph/9905266.
- [201] A.A. Barrientos Bendezu and Bernd A. Kniehl. Pair production of neutral Higgs bosons at the CERN large hadron collider. *Phys.Rev.*, D64:035006, 2001, hep-ph/0103018.
- [202] Mikhail A. Shifman, A.I. Vainshtein, M.B. Voloshin, and Valentin I. Zakharov. Low-Energy Theorems for Higgs Boson Couplings to Photons. *Sov.J.Nucl.Phys.*, 30:711–716, 1979.
- [203] Bernd A. Kniehl and Michael Spira. Low-energy theorems in Higgs physics. *Z.Phys.*, C69:77–88, 1995, hep-ph/9505225.
- [204] M. Gillioz, R. Grober, C. Grojean, M. Muhlleitner, and E. Salvioni. Higgs Low-Energy Theorem (and its corrections) in Composite Models. *JHEP*, 1210:004, 2012, 1206.7120.
- [205] Graham D. Kribs and Adam Martin. Enhanced di-Higgs Production through Light Colored Scalars. *Phys.Rev.*, D86:095023, 2012, 1207.4496.
- [206] Duane A. Dicus, Kalpana J. Kallianpur, and Scott S.D. Willenbrock. Higgs Boson Pair Production in the Effective W Approximation. *Phys.Lett.*, B200:187, 1988.
- [207] Oscar J.P. Eboli, G.C. Marques, S.F. Novaes, and A.A. Natale. Twin Higgs Boson Production. *Phys.Lett.*, B197:269, 1987.
- [208] E.W. Nigel Glover and J.J. van der Bij. Higgs Boson Pair Production via Gluon Fusion. *Nucl.Phys.*, B309:282, 1988.
- [209] S. Dawson, S. Dittmaier, and M. Spira. Neutral Higgs boson pair production at hadron colliders: QCD corrections. *Phys.Rev.*, D58:115012, 1998, hep-ph/9805244.

- [210] Jonathan Grigo, Jens Hoff, Kirill Melnikov, and Matthias Steinhauser. On the Higgs boson pair production at the LHC. *Nucl.Phys.*, B875:1–17, 2013, 1305.7340.
- [211] Daniel de Florian and Javier Mazzitelli. Higgs Boson Pair Production at Next-to-Next-to-Leading Order in QCD. *Phys.Rev.Lett.*, 111:201801, 2013, 1309.6594.
- [212] F. Maltoni, E. Vryonidou, and M. Zaro. Top-quark mass effects in double and triple Higgs production in gluon-gluon fusion at NLO. *JHEP*, 1411:079, 2014, 1408.6542.
- [213] R. Frederix, S. Frixione, V. Hirschi, F. Maltoni, O. Mattelaer, et al. Higgs pair production at the LHC with NLO and parton-shower effects. *Phys.Lett.*, B732:142–149, 2014, 1401.7340.
- [214] Jonathan Grigo, Kirill Melnikov, and Matthias Steinhauser. Virtual corrections to Higgs boson pair production in the large top quark mass limit. *Nucl.Phys.*, B888:17–29, 2014, 1408.2422.
- [215] Matthew J. Dolan, Christoph Englert, and Michael Spannowsky. Higgs self-coupling measurements at the LHC. *JHEP*, 1210:112, 2012, 1206.5001.
- [216] Qiang Li, Qi-Shu Yan, and Xiaoran Zhao. Higgs Pair Production: Improved Description by Matrix Element Matching. *Phys.Rev.*, D89(3):033015, 2014, 1312.3830.
- [217] Philipp Maierhofer and Andreas Papaefstathiou. Higgs Boson pair production merged to one jet. *JHEP*, 1403:126, 2014, 1401.0007.
- [218] Matthew J. Dolan, Christoph Englert, Nicolas Greiner, and Michael Spannowsky. Further on up the road: $hhjj$ production at the LHC. *Phys.Rev.Lett.*, 112:101802, 2014, 1310.1084.
- [219] G. Aad et al. Search For Higgs Boson Pair Production in the $\gamma\gamma b\bar{b}$ Final State using pp Collision Data at $\sqrt{s} = 8$ TeV from the ATLAS Detector. *Phys.Rev.Lett.*, 114(8):081802, 2015, 1406.5053.
- [220] CMS Collaboration. Search for di-Higgs resonances decaying to 4 bottom quarks. 2014, CMS-PAS-HIG-14-013.
- [221] Vardan Khachatryan et al. Search for resonant pair production of Higgs bosons decaying to two bottom quarkantiquark pairs in protonproton collisions at 8 TeV. *Phys. Lett.*, B749:560–582, 2015, 1503.04114.
- [222] The ATLAS collaboration. A search for resonant Higgs-pair production in the $b\bar{b}b\bar{b}$ final state in pp collisions at $\sqrt{s} = 8$ TeV. 2014, ATLAS-CONF-2014-005.

- [223] Georges Aad et al. Search for Higgs boson pair production in the $b\bar{b}b\bar{b}$ final state from pp collisions at $\sqrt{s} = 8$ TeV with the ATLAS detector. *Eur. Phys. J.*, C75(9):412, 2015, 1506.00285.
- [224] CMS Collaboration. Search for the resonant production of two Higgs bosons in the final state with two photons and two bottom quarks. 2014, CMS-PAS-HIG-13-032.
- [225] CMS Collaboration. Search for extended Higgs sectors in the H to hh and A to Zh channels in $\sqrt{s} = 8$ TeV pp collisions with multileptons and photons final states. 2013, CMS-PAS-HIG-13-025.
- [226] Georges Aad et al. Searches for Higgs boson pair production in the $hh \rightarrow bb\tau\tau, \gamma\gamma WW^*, \gamma\gamma bb, bbbb$ channels with the ATLAS detector. *Phys. Rev.*, D92:092004, 2015, 1509.04670.
- [227] The ATLAS collaboration. Search for Higgs boson pair production in the $b\bar{b}\gamma\gamma$ final state using pp collision data at $\sqrt{s} = 13$ TeV with the ATLAS detector. 2016, ATLAS-CONF-2016-004.
- [228] The ATLAS collaboration. Search for pair production of Higgs bosons in the $b\bar{b}b\bar{b}$ final state using proton-proton collisions at $\sqrt{s} = 13$ TeV with the ATLAS detector. 2016, ATLAS-CONF-2016-017.
- [229] CMS Collaboration. Search for resonant Higgs boson pair production in the $b\bar{b}\tau^+\tau^-$ final state. 2016.
- [230] CMS Collaboration. Search for resonant pair production of Higgs bosons decaying to two bottom quark-antiquark pairs in proton-proton collisions at 13 TeV. 2016, CMS-PAS-HIG-16-002.
- [231] Prospects for measuring Higgs pair production in the channel $H(\rightarrow \gamma\gamma)H(\rightarrow b\bar{b})$ using the ATLAS detector at the HL-LHC. Technical Report ATL-PHYS-PUB-2014-019, CERN, Geneva, Oct 2014.
- [232] J Butler, D Contardo, M Klute, J Mans, and L Silvestris. Technical Proposal for the Phase-II Upgrade of the CMS Detector. Technical Report CERN-LHCC-2015-010. LHCC-P-008, CERN, Geneva. Geneva, Jun 2015. Upgrade Project Leader Deputies: Lucia Silvestris (INFN-Bari), Jeremy Mans (University of Minnesota) Additional contacts: Lucia.Silvestris@cern.ch, Jeremy.Mans@cern.ch.
- [233] Souvik Das. Searches for Higgs pair production using the CMS detector. <https://indico.mitp.uni-mainz.de/getFile.py/access?contribId=3&sessionId=2&resId=0&materialId=slides&confId=31>.
- [234] U. Baur, T. Plehn, and David L. Rainwater. Probing the Higgs selfcoupling at hadron colliders using rare decays. *Phys.Rev.*, D69:053004, 2004, hep-ph/0310056.

- [235] J. Baglio, A. Djouadi, R. Grber, M.M. Mhlleitner, J. Quevillon, et al. The measurement of the Higgs self-coupling at the LHC: theoretical status. *JHEP*, 1304:151, 2013, 1212.5581.
- [236] Weiming Yao. Studies of measuring Higgs self-coupling with $HH \rightarrow b\bar{b}\gamma\gamma$ at the future hadron colliders. 2013, 1308.6302.
- [237] Vernon Barger, Lisa L. Everett, C.B. Jackson, and Gabe Shaughnessy. Higgs-Pair Production and Measurement of the Triscalar Coupling at LHC(8,14). *Phys.Lett.*, B728:433–436, 2014, 1311.2931.
- [238] Aleksandr Azatov, Roberto Contino, Giuliano Panico, and Minho Son. Effective field theory analysis of double Higgs boson production via gluon fusion. *Phys. Rev.*, D92(3):035001, 2015, 1502.00539.
- [239] Hong-Jian He, Jing Ren, and Weiming Yao. Probing new physics of cubic Higgs boson interaction via Higgs pair production at hadron colliders. *Phys. Rev.*, D93(1):015003, 2016, 1506.03302.
- [240] Alan J. Barr, Matthew J. Dolan, Christoph Englert, and Michael Spannowsky. Di-Higgs final states augMT2ed – selecting hh events at the high luminosity LHC. *Phys.Lett.*, B728:308–313, 2014, 1309.6318.
- [241] Andreas Papaefstathiou, Li Lin Yang, and Jose Zurita. Higgs boson pair production at the LHC in the $b\bar{b}W^+W^-$ channel. *Phys.Rev.*, D87(1):011301, 2013, 1209.1489.
- [242] Danilo Enoque Ferreira de Lima, Andreas Papaefstathiou, and Michael Spannowsky. Standard model Higgs boson pair production in the $(b\bar{b})(b\bar{b})$ final state. *JHEP*, 1408:030, 2014, 1404.7139.
- [243] David Wardrope, Eric Jansen, Nikos Konstantinidis, Ben Cooper, Rebecca Falla, and Nurfikri Norjoharuddeen. Non-resonant Higgs-pair production in the $b\bar{b}b\bar{b}$ final state at the LHC. *Eur. Phys. J.*, C75(5):219, 2015, 1410.2794.
- [244] Roberto Contino, Christophe Grojean, Mauro Moretti, Fulvio Piccinini, and Riccardo Rattazzi. Strong Double Higgs Production at the LHC. *JHEP*, 1005:089, 2010, 1002.1011.
- [245] Christoph Englert, Frank Krauss, Michael Spannowsky, and Jennifer Thompson. Di-Higgs phenomenology in $t\bar{t}hh$: The forgotten channel. *Phys.Lett.*, B743:93–97, 2015, 1409.8074.
- [246] Ning Liu, Yanming Zhang, Jinzhong Han, and Bingfang Yang. Enhancing $t\bar{t}hh$ production through CP-violating top-Higgs interaction at the LHC and future colliders. *JHEP*, 09:008, 2015, 1503.08537.

- [247] Aaron Pierce, Jesse Thaler, and Lian-Tao Wang. Disentangling Dimension Six Operators through Di-Higgs Boson Production. *JHEP*, 0705:070, 2007, hep-ph/0609049.
- [248] Florian Goertz, Andreas Papaefstathiou, Li Lin Yang, and Jos Zurita. Higgs boson pair production in the D=6 extension of the SM. *JHEP*, 04:167, 2015, 1410.3471.
- [249] Ramona Grober, Margarete Muhlleitner, Michael Spira, and Juraj Streicher. NLO QCD Corrections to Higgs Pair Production including Dimension-6 Operators. *JHEP*, 09:092, 2015, 1504.06577.
- [250] Chih-Ting Lu, Jung Chang, Kingman Cheung, and Jae Sik Lee. An exploratory study of Higgs-boson pair production. *JHEP*, 08:133, 2015, 1505.00957.
- [251] Abdesslam Arhrib, Rachid Benbrik, Chuan-Hung Chen, Renato Guedes, and Rui Santos. Double Neutral Higgs production in the Two-Higgs doublet model at the LHC. *JHEP*, 0908:035, 2009, 0906.0387.
- [252] Eri Asakawa, Daisuke Harada, Shinya Kanemura, Yasuhiro Okada, and Koji Tsumura. Higgs boson pair production in new physics models at hadron, lepton, and photon colliders. *Phys.Rev.*, D82:115002, 2010, 1009.4670.
- [253] Sally Dawson, Elisabetta Furlan, and Ian Lewis. Unravelling an extended quark sector through multiple Higgs production? *Phys.Rev.*, D87(1):014007, 2013, 1210.6663.
- [254] Matthew J. Dolan, Christoph Englert, and Michael Spannowsky. New Physics in LHC Higgs boson pair production. *Phys.Rev.*, D87(5):055002, 2013, 1210.8166.
- [255] Junjie Cao, Zhaoxia Heng, Liangliang Shang, Peihua Wan, and Jin Min Yang. Pair Production of a 125 GeV Higgs Boson in MSSM and NMSSM at the LHC. *JHEP*, 1304:134, 2013, 1301.6437.
- [256] Chengcheng Han, Xuanting Ji, Lei Wu, Peiwen Wu, and Jin Min Yang. Higgs pair production with SUSY QCD correction: revisited under current experimental constraints. *JHEP*, 04:003, 2014, 1307.3790.
- [257] Kenji Nishiwaki, Saurabh Niyogi, and Ambresh Shivaji. ttH Anomalous Coupling in Double Higgs Production. *JHEP*, 1404:011, 2014, 1309.6907.
- [258] Naoyuki Haba, Kunio Kaneta, Yukihiro Mimura, and Enkhbat Tsedenbaljir. Higgs Pair Production at the LHC and ILC from general potential. *Phys.Rev.*, D89(1):015018, 2014, 1311.0067.
- [259] Tsedenbaljir Enkhbat. Scalar leptoquarks and Higgs pair production at the LHC. *JHEP*, 1401:158, 2014, 1311.4445.

- [260] Chuan-Ren Chen and Ian Low. Double take on new physics in double Higgs boson production. *Phys.Rev.*, D90(1):013018, 2014, 1405.7040.
- [261] Chien-Yi Chen, S. Dawson, and I. M. Lewis. Top Partners and Higgs Boson Production. *Phys. Rev.*, D90(3):035016, 2014, 1406.3349.
- [262] Junjie Cao, Dongwei Li, Liangliang Shang, Peiwen Wu, and Yang Zhang. Exploring the Higgs Sector of a Most Natural NMSSM and its Prediction on Higgs Pair Production at the LHC. *JHEP*, 12:026, 2014, 1409.8431.
- [263] Chien-Yi Chen, S. Dawson, and I. M. Lewis. Exploring resonant di-Higgs boson production in the Higgs singlet model. *Phys. Rev.*, D91(3):035015, 2015, 1410.5488.
- [264] Melissa van Beekveld, Wim Beenakker, Sascha Caron, Remco Castelijns, Marie Lanfermann, and Antonia Struebig. Higgs, di-Higgs and tri-Higgs production via SUSY processes at the LHC with 14 TeV. *JHEP*, 05:044, 2015, 1501.02145.
- [265] Lei Wu, Jin Min Yang, Chien-Peng Yuan, and Mengchao Zhang. Higgs self-coupling in the MSSM and NMSSM after the LHC Run 1. *Phys. Lett.*, B747:378–389, 2015, 1504.06932.
- [266] Tsedenbaljir Enkhbat. Higgs pair production from color octet scalars and vectors. 2015, 1504.08305.
- [267] Seyed Mohsen Etesami and Mojtaba Mohammadi Najafabadi. Double Higgs boson production with a jet substructure analysis to probe extra dimensions. *Phys. Rev.*, D92(7):073013, 2015, 1505.01028.
- [268] Martino Dall’Osso, Tommaso Dorigo, Carlo A. Gottardo, Alexandra Oliveira, Mia Tosi, and Florian Goertz. Higgs Pair Production: Choosing Benchmarks With Cluster Analysis. *JHEP*, 04:126, 2016, 1507.02245.
- [269] Lan-Chun Lü, Chun Du, Yaquan Fang, Hong-Jian He, and Huijun Zhang. Searching for Heavier Higgs Boson via Di-Higgs Production at LHC Run-2. *Phys. Lett.*, B755:509–522, 2016, 1507.02644.
- [270] Alan J. Barr, Matthew J. Dolan, Christoph Englert, Danilo Enoque Ferreira de Lima, and Michael Spannowsky. Higgs Self-Coupling Measurements at a 100 TeV Hadron Collider. *JHEP*, 1502:016, 2015, 1412.7154.
- [271] Qiang Li, Zhao Li, Qi-Shu Yan, and Xiaoran Zhao. Probe Higgs boson pair production via the $3\ell 2j + \cancel{E}$ mode. *Phys. Rev.*, D92(1):014015, 2015, 1503.07611.
- [272] Andreas Papaefstathiou. Discovering Higgs boson pair production through rare final states at a 100 TeV collider. *Phys. Rev.*, D91(11):113016, 2015, 1504.04621.

- [273] Sally Dawson, Andrei Gribsan, Heather Logan, Jianming Qian, Chris Tully, et al. Working Group Report: Higgs Boson. 2013, 1310.8361.
- [274] A.D. Martin, W.J. Stirling, R.S. Thorne, and G. Watt. Parton distributions for the LHC. *Eur.Phys.J.*, C63:189–285, 2009, 0901.0002.
- [275] A.D. Martin, W.J. Stirling, R.S. Thorne, and G. Watt. Uncertainties on $\alpha(S)$ in global PDF analyses and implications for predicted hadronic cross sections. *Eur.Phys.J.*, C64:653–680, 2009, 0905.3531.
- [276] A.D. Martin, W.J. Stirling, R.S. Thorne, and G. Watt. Heavy-quark mass dependence in global PDF analyses and 3- and 4-flavour parton distributions. *Eur.Phys.J.*, C70:51–72, 2010, 1007.2624.
- [277] M. Maniatis. The Next-to-Minimal Supersymmetric extension of the Standard Model reviewed. *Int.J.Mod.Phys.*, A25:3505–3602, 2010, 0906.0777.
- [278] Ulrich Ellwanger, Cyril Hugonie, and Ana M. Teixeira. The Next-to-Minimal Supersymmetric Standard Model. *Phys.Rept.*, 496:1–77, 2010, 0910.1785.
- [279] Puneet Batra, Antonio Delgado, David E. Kaplan, and Timothy M.P. Tait. The Higgs mass bound in gauge extensions of the minimal supersymmetric standard model. *JHEP*, 0402:043, 2004, hep-ph/0309149.
- [280] Alexander Maloney, Aaron Pierce, and Jay G. Wacker. D-terms, unification, and the Higgs mass. *JHEP*, 0606:034, 2006, hep-ph/0409127.
- [281] Thomas Hahn. Generating Feynman diagrams and amplitudes with FeynArts 3. *Comput.Phys.Commun.*, 140:418–431, 2001, hep-ph/0012260.
- [282] T. Hahn and M. Perez-Victoria. Automatized one loop calculations in four-dimensions and D-dimensions. *Comput.Phys.Commun.*, 118:153–165, 1999, hep-ph/9807565.
- [283] Hans Peter Nilles, M. Srednicki, and D. Wyler. Weak Interaction Breakdown Induced by Supergravity. *Phys.Lett.*, B120:346, 1983.
- [284] Luis Alvarez-Gaume, J. Polchinski, and Mark B. Wise. Minimal Low-Energy Supergravity. *Nucl.Phys.*, B221:495, 1983.
- [285] J.P. Derendinger and Carlos A. Savoy. Quantum Effects and $SU(2) \times U(1)$ Breaking in Supergravity Gauge Theories. *Nucl.Phys.*, B237:307, 1984.
- [286] Mark Claudson, Lawrence J. Hall, and Ian Hinchliffe. Low-Energy Supergravity: False Vacua and Vacuum Predictions. *Nucl.Phys.*, B228:501, 1983.
- [287] C. Kounnas, A.B. Lahanas, Dimitri V. Nanopoulos, and M. Quiros. Low-Energy Behavior of Realistic Locally Supersymmetric Grand Unified Theories. *Nucl.Phys.*, B236:438, 1984.

- [288] Manuel Drees, M. Gluck, and K. Grassie. A New Class of False Vacua in Low-energy $N = 1$ Supergravity Theories. *Phys.Lett.*, B157:164, 1985.
- [289] J.F. Gunion, H.E. Haber, and M. Sher. Charge / Color Breaking Minima and a -Parameter Bounds in Supersymmetric Models. *Nucl.Phys.*, B306:1, 1988.
- [290] H. Komatsu. New Constraints on Parameters in the Minimal Supersymmetric Model. *Phys.Lett.*, B215:323, 1988.
- [291] Paul Langacker and Nir Polonsky. Implications of Yukawa unification for the Higgs sector in supersymmetric grand unified models. *Phys.Rev.*, D50:2199–2217, 1994, hep-ph/9403306.
- [292] J.A. Casas, A. Lleyda, and C. Munoz. Strong constraints on the parameter space of the MSSM from charge and color breaking minima. *Nucl.Phys.*, B471:3–58, 1996, hep-ph/9507294.
- [293] J.A. Casas and S. Dimopoulos. Stability bounds on flavor violating trilinear soft terms in the MSSM. *Phys.Lett.*, B387:107–112, 1996, hep-ph/9606237.
- [294] Andrew J. Bordner. Parameter bounds in the supersymmetric standard model from charge / color breaking vacua. 1995, hep-ph/9506409.
- [295] P.M. Ferreira. A Full one loop charge and color breaking effective potential. *Phys.Lett.*, B509:120–130, 2001, hep-ph/0008115.
- [296] Antonio Riotto and Esteban Roulet. Vacuum decay along supersymmetric flat directions. *Phys.Lett.*, B377:60–66, 1996, hep-ph/9512401.
- [297] Alexander Kusenko, Paul Langacker, and Gino Segre. Phase transitions and vacuum tunneling into charge and color breaking minima in the MSSM. *Phys.Rev.*, D54:5824–5834, 1996, hep-ph/9602414.
- [298] Alexander Kusenko and Paul Langacker. Is the vacuum stable? *Phys.Lett.*, B391:29–33, 1997, hep-ph/9608340.
- [299] Toby Falk, Keith A. Olive, Leszek Roszkowski, Anupam Singh, and Mark Srednicki. Constraints from inflation and reheating on superpartner masses. *Phys.Lett.*, B396:50–57, 1997, hep-ph/9611325.
- [300] J.E. Camargo-Molina, B. O’Leary, W. Porod, and F. Staub. **Vevacious**: A Tool For Finding The Global Minima Of One-Loop Effective Potentials With Many Scalars. *Eur.Phys.J.*, C73(10):2588, 2013, 1307.1477.
- [301] J.E. Camargo-Molina, B. O’Leary, W. Porod, and F. Staub. Stability of the CMSSM against sfermion VEVs. *JHEP*, 1312:103, 2013, 1309.7212.
- [302] J.E. Camargo-Molina, B. Garbrecht, B. O’Leary, W. Porod, and F. Staub. Constraining the Natural MSSM through tunneling to color-breaking vacua at zero and non-zero temperature. *Phys.Lett.*, B737:156–161, 2014, 1405.7376.

- [303] N. Chamoun, H.K. Dreiner, F. Staub, and T. Stefaniak. Resurrecting light stops after the 125 GeV Higgs in the baryon number violating CMSSM. *JHEP*, 1408:142, 2014, 1407.2248.
- [304] Debtosh Chowdhury, Rohini M. Godbole, Kirtimaan A. Mohan, and Sudhir K. Vempati. Charge and Color Breaking Constraints in MSSM after the Higgs Discovery at LHC. *JHEP*, 02:110, 2014, 1310.1932.
- [305] Nikita Blinov and David E. Morrissey. Vacuum Stability and the MSSM Higgs Mass. *JHEP*, 1403:106, 2014, 1310.4174.
- [306] Markus Bobrowski, Guillaume Chalons, Wolfgang G. Hollik, and Ulrich Nierste. Vacuum stability of the effective Higgs potential in the Minimal Supersymmetric Standard Model. *Phys.Rev.*, D90(3):035025, 2014, 1407.2814.
- [307] Utpal Chattopadhyay and Abhishek Dey. Exploring MSSM for Charge and Color Breaking and Other Constraints in the Context of Higgs@125 GeV. *JHEP*, 1411:161, 2014, 1409.0611.
- [308] S. Heinemeyer, W. Hollik, and G. Weiglein. Electroweak precision observables in the minimal supersymmetric standard model. *Phys.Rept.*, 425:265–368, 2006, hep-ph/0412214.
- [309] Haiying Cai, Hsin-Chia Cheng, and John Terning. A Spin-1 Top Quark Superpartner. *Phys. Rev. Lett.*, 101:171805, 2008, 0806.0386.
- [310] Rachel Houtz, Kitran Colwell, and John Terning. Little Conformal Symmetry. 2016, 1603.00030.
- [311] Gustavo Burdman, Zackaria Chacko, Roni Harnik, Leonardo de Lima, and Christopher B. Verhaaren. Colorless Top Partners, a 125 GeV Higgs, and the Limits on Naturalness. *Phys.Rev.*, D91:055007, 2015, 1411.3310.
- [312] Abdelhak Djouadi. The Anatomy of electro-weak symmetry breaking. I: The Higgs boson in the standard model. *Phys. Rept.*, 457:1–216, 2008, hep-ph/0503172.
- [313] J R Andersen et al. Handbook of LHC Higgs Cross Sections: 3. Higgs Properties. 2013, 1307.1347.
- [314] Adam Falkowski, Francesco Riva, and Alfredo Urbano. Higgs at last. *JHEP*, 1311:111, 2013, 1303.1812.
- [315] Howard E. Haber. Introductory low-energy supersymmetry. In *Theoretical Advanced Study Institute (TASI 92): From Black Holes and Strings to Particles Boulder, Colorado, June 3-28, 1992*, 1993, hep-ph/9306207.
- [316] K.A. Olive et al. Review of Particle Physics. *Chin.Phys.*, C38:090001, 2014.

- [317] Colin J. Morningstar and Mike J. Peardon. The Glueball spectrum from an anisotropic lattice study. *Phys.Rev.*, D60:034509, 1999, hep-lat/9901004.
- [318] Jose E. Juknevich, Dmitry Melnikov, and Matthew J. Strassler. A Pure-Glue Hidden Valley I. States and Decays. *JHEP*, 0907:055, 2009, 0903.0883.
- [319] Jose E. Juknevich. Pure-gluon hidden valleys through the Higgs portal. *JHEP*, 1008:121, 2010, 0911.5616.
- [320] Matthew J. Strassler and Kathryn M. Zurek. Echoes of a hidden valley at hadron colliders. *Phys.Lett.*, B651:374–379, 2007, hep-ph/0604261.
- [321] Matthew J. Strassler and Kathryn M. Zurek. Discovering the Higgs through highly-displaced vertices. *Phys.Lett.*, B661:263–267, 2008, hep-ph/0605193.
- [322] Matthew J. Strassler. Possible effects of a hidden valley on supersymmetric phenomenology. 2006, hep-ph/0607160.
- [323] Tao Han, Zongguo Si, Kathryn M. Zurek, and Matthew J. Strassler. Phenomenology of hidden valleys at hadron colliders. *JHEP*, 0807:008, 2008, 0712.2041.
- [324] Matthew J. Strassler. Why Unparticle Models with Mass Gaps are Examples of Hidden Valleys. 2008, 0801.0629.
- [325] Matthew J. Strassler. On the Phenomenology of Hidden Valleys with Heavy Flavor. 2008, 0806.2385.
- [326] J. Beringer et al. Review of Particle Physics (RPP). *Phys.Rev.*, D86:010001, 2012.
- [327] David Curtin, Patrick Meade, and Chiu-Tien Yu. Testing Electroweak Baryogenesis with Future Colliders. *JHEP*, 1411:127, 2014, 1409.0005.
- [328] Nathaniel Craig, Hou Keong Lou, Matthew McCullough, and Arun Thalappilil. The Higgs Portal Above Threshold. *JHEP*, 02:127, 2016, 1412.0258.
- [329] Georges Aad et al. Search for pair-produced long-lived neutral particles decaying in the ATLAS hadronic calorimeter in pp collisions at $\sqrt{s} = 8$ TeV. *Phys.Lett.*, B743:15–34, 2015, 1501.04020.
- [330] Georges Aad et al. Search for long-lived, weakly interacting particles that decay to displaced hadronic jets in proton-proton collisions at $\sqrt{s} = 8$ TeV with the ATLAS detector. *Phys. Rev.*, D92(1):012010, 2015, 1504.03634.
- [331] Valerie Halyo, Hou Keong Lou, Paul Lujan, and Wenhan Zhu. Data driven search in the displaced $b\bar{b}$ pair channel for a Higgs boson decaying to long-lived neutral particles. *JHEP*, 01:140, 2014, 1308.6213.

- [332] Andrea Coccaro, David Curtin, H. J. Lubatti, Heather Russell, and Jessie Shelton. Data-driven Model-independent Searches for Long-lived Particles at the LHC. 2016, 1605.02742.
- [333] David Curtin, Rouven Essig, Stefania Gori, Prerit Jaiswal, Andrey Katz, et al. Exotic decays of the 125 GeV Higgs boson. *Phys.Rev.*, D90(7):075004, 2014, 1312.4992.
- [334] Y. Chen, A. Alexandru, S.J. Dong, Terrence Draper, I. Horvath, et al. Glueball spectrum and matrix elements on anisotropic lattices. *Phys.Rev.*, D73:014516, 2006, hep-lat/0510074.
- [335] Marie E. Machacek and Michael T. Vaughn. Two Loop Renormalization Group Equations in a General Quantum Field Theory. 1. Wave Function Renormalization. *Nucl. Phys.*, B222:83, 1983.
- [336] Michele Papucci, Joshua T. Ruderman, and Andreas Weiler. Natural SUSY Endures. *JHEP*, 09:035, 2012, 1110.6926.
- [337] Dean Carmi, Adam Falkowski, Eric Kuflik, and Tomer Volansky. Interpreting LHC Higgs Results from Natural New Physics Perspective. *JHEP*, 07:136, 2012, 1202.3144.
- [338] A. Djouadi, J. Kalinowski, and M. Spira. HDECAY: A Program for Higgs boson decays in the standard model and its supersymmetric extension. *Comput. Phys. Commun.*, 108:56–74, 1998, hep-ph/9704448.
- [339] Harvey B. Meyer. Glueball matrix elements: A Lattice calculation and applications. *JHEP*, 01:071, 2009, 0808.3151.
- [340] Jose Juknevich. *Phenomenology of pure-gauge hidden valleys at Hadron colliders*. PhD thesis, Rutgers U., Piscataway, 2010.
- [341] David Curtin, Rouven Essig, Stefania Gori, and Jessie Shelton. Illuminating Dark Photons with High-Energy Colliders. *JHEP*, 02:157, 2015, 1412.0018.
- [342] J. Alwall, R. Frederix, S. Frixione, V. Hirschi, F. Maltoni, O. Mattelaer, H. S. Shao, T. Stelzer, P. Torrielli, and M. Zaro. The automated computation of tree-level and next-to-leading order differential cross sections, and their matching to parton shower simulations. *JHEP*, 07:079, 2014, 1405.0301.
- [343] Torbjorn Sjostrand, Stephen Mrenna, and Peter Z. Skands. A Brief Introduction to PYTHIA 8.1. *Comput. Phys. Commun.*, 178:852–867, 2008, 0710.3820.
- [344] LHC Higgs Cross Section Working Group. <https://twiki.cern.ch/twiki/bin/view/LHCPhysics/HiggsEuropeanStrategy>, 2014.

- [345] CMS Collaboration. Higgs to bb in the VBF channel. 2013, CMS-PAS-HIG-13-011.
- [346] Andy Haas. Private Communication.
- [347] Vardan Khachatryan et al. Search for Long-Lived Neutral Particles Decaying to Quark-Antiquark Pairs in Proton-Proton Collisions at $\sqrt{s} = 8$ TeV. *Phys. Rev.*, D91(1):012007, 2015, 1411.6530.
- [348] D Cinca. ATLAS Upgrades Towards the High Luminosity LHC. Technical Report ATL-UPGRADE-PROC-2014-001, CERN, Geneva, Jun 2014.
- [349] The ATLAS collaboration. Search for resonances decaying to photon pairs in 3.2 fb^{-1} of pp collisions at $\sqrt{s} = 13$ TeV with the ATLAS detector. 2015, ATLAS-CONF-2015-081.
- [350] CMS Collaboration. Search for new physics in high mass diphoton events in proton-proton collisions at 13TeV. 2015, CMS-PAS-EXO-15-004.
- [351] The ATLAS collaboration. Search for resonances in diphoton events with the ATLAS detector at $\sqrt{s} = 13$ TeV. 2016, ATLAS-CONF-2016-018.
- [352] CMS Collaboration. Search for new physics in high mass diphoton events in 3.3 fb^{-1} of proton-proton collisions at $\sqrt{s} = 13$ TeV and combined interpretation of searches at 8 TeV and 13 TeV. 2016, CMS-PAS-EXO-16-018.
- [353] Morad Aaboud et al. Search for resonances in diphoton events at $\sqrt{s}=13$ TeV with the ATLAS detector. 2016, 1606.03833.
- [354] Vardan Khachatryan et al. Search for resonant production of high-mass photon pairs in proton-proton collisions at $\sqrt{s} = 8$ and 13 TeV. 2016, 1606.04093.